
Theses and Dissertations

Spring 2014

Proton NMR studies of functionalized nanoparticles in aqueous environments

Yulia Nikolaevna Tataurova
University of Iowa

Copyright 2014 Yulia Tataurova

This dissertation is available at Iowa Research Online: <http://ir.uiowa.edu/etd/4769>

Recommended Citation

Tataurova, Yulia Nikolaevna. "Proton NMR studies of functionalized nanoparticles in aqueous environments." PhD (Doctor of Philosophy) thesis, University of Iowa, 2014.
<http://ir.uiowa.edu/etd/4769>.

Follow this and additional works at: <http://ir.uiowa.edu/etd>

 Part of the [Chemistry Commons](#)

PROTON NMR STUDIES OF FUNCTIONALIZED NANOPARTICLES IN
AQUEOUS ENVIRONMENTS

by

Yulia Nikolaevna Tataurova

A thesis submitted in partial fulfillment
of the requirements for the Doctor of
Philosophy degree in Chemistry
in the Graduate College of
The University of Iowa

May 2014

Thesis Supervisor: Professor Sarah C. Larsen

Copyright by

YULIA NIKOLAEVNA TATAUROVA

2014

All Rights Reserved

Graduate College
The University of Iowa
Iowa City, Iowa

CERTIFICATE OF APPROVAL

PH.D. THESIS

This is to certify that the Ph.D. thesis of

Yulia Nikolaevna Tataurova

has been approved by the Examining Committee
for the thesis requirement for the Doctor of
Philosophy degree in Chemistry
at the May 2014 graduation.

Thesis Committee:

Sarah C. Larsen, Thesis Supervisor

Vicki H. Grassian

F. Christopher Pigge

Edward G. Gillan

David G. Rethwisch

To my beloved parents,
without whom I would never have come this far
and
my dearest husband Andrey
who stood by me through thick and thin

ACKNOWLEDGMENTS

During the course of my graduate studies, there are many amazing people who helped me to succeed. First of all, I am very grateful to my advisor, Professor Sarah C. Larsen for the inspiration, opportunities and the learning experiences provided to me. Without her support and guidance this dissertation would never be possible. She always demonstrated a great confidence in my ability, while encouraging me to do my best during my graduate career. She is a talented teacher and very passionate for teaching in the lab as well as in the classroom. It was a very positive experience to work with her. I also would like to thank her husband, Dr. Russell Larsen for providing advice and support during my studies.

I thank Professors Vicki H. Grassian, Christopher F. Pigge, Edward G. Gillan, and David G. Rethwisch for serving on my dissertation committee, and reading my thesis and giving me helpful advice.

I thank the past and present Larsen group members that I have worked with: Dr. Anton Petushkov, Dr. Nicholas Ndiege, Dr. Karna Barquist, Dr. Ashish Datt, Shani Egodawatte, Sean Lehman, and Paul Mueller. We have become friends and shared many remarkable moments together. I will always remember hospitality and generosity during our annual dinners at the Larsens's home.

I also thank Dr. Velupillai Santhana for all the experience I gathered from you while working with various NMR experiments. I am appreciative for his patience and advice.

I am grateful to my parents and my brother for their love and support. You constantly challenged me to “raise the bar” and made me believe in myself so that I can. I

thank my friends in the Iowa City Russian community for their encouragement and for being here with me through some of the toughest times in my life.

Then last but not least to my husband Andrey, who gave me the greatest gift anyone could give another person, he believed in me. His unconditional love and faith never ceased to amaze me and gave me the strength to be myself.

ABSTRACT

Nanoscience is an emerging field that can provide potential routes towards addressing critical issues such as clean and sustainable energy, environmental remediation and human health. Specifically, porous nanomaterials, such as zeolites and mesoporous silica, are found in a wide range of applications including catalysis, drug delivery, imaging, environmental protection, and sensing. The characterization of the physical and chemical properties of nanocrystalline materials is essential to the realization of these innovative applications. The great advantage of porous nanocrystals is their increased external surface area that can control their biological, chemical and catalytic activities. Specific functional groups synthesized on the surface of nanoparticles are able to absorb heavy metals from solution or target disease cells, such as cancer cells. In these studies, three main issues related to functionalized nanomaterials will be addressed through the application of nuclear magnetic resonance (NMR) techniques including: 1) surface composition and structure of functionalized nanocrystalline particles; 2) chemical properties of the guest molecules on the surface of nanomaterials, and 3) adsorption and reactivity of surface bound functional groups.

Nuclear magnetic resonance (NMR) is one of the major spectroscopic techniques available for the characterization of molecular structure and conformational dynamics with atomic level detail. This thesis deals with the application of ^1H solution state NMR to porous nanomaterials in an aqueous environment. Understanding the aqueous phase behavior of functionalized nanomaterials is a key factor in the design and development of safe nanomaterials because their interactions with living systems are always mediated through the aqueous phase. This is important for successful surface modifications to

obtain fundamental knowledge in interfacial chemical and physical phenomena that occur on the surface of nanoparticles. The use of solution NMR spectroscopy results in high-resolution NMR spectra. This technique is selective for protons on the surface organic functional groups due to their motional averaging in solution.

In this study, ^1H solution NMR spectroscopy was used to investigate the interface of the organic functional groups on mesoporous silica and silicalite-1 in D_2O . The pK_a for the functional groups covalently bound to the surface of nanoparticles was determined using an NMR–pH titration method based on the variation in the proton chemical shift for the alkyl group protons closest to the amine group with pH.

The adsorption of toxic contaminants (chromate and arsenate anions) on the surface of functionalized silicalite-1 and mesoporous silica nanoparticles has been studied by ^1H solution NMR spectroscopy. These studies demonstrate the sensitivity of solution NMR spectroscopy to the electronic environment and structure of the surface functional groups on porous nanomaterials.

TABLE OF CONTENTS

LIST OF TABLES	x
LIST OF FIGURES	xi
CHAPTER	
1. INTRODUCTION	1
1.1 Zeolites and Mesoporous Silica	1
1.2 Nuclear Magnetic Resonance (NMR) Spectroscopy	5
1.2.1 NMR Basics	5
1.2.2 NMR Instrumentation	17
1.2.3 Solid State NMR	18
1.2.4 Solution State NMR of Nanomaterials	22
1.3 Adsorption of Environmental Contaminants	25
1.3.1 Chromium (VI)	25
1.3.2 Arsenic (V)	26
1.4 Thesis Overview	27
2. SYNTHESIS AND FUNCTIONALIZATION OF SILICALITE-1 & MESOPOROUS SILICA.....	30
2.1 Introduction.....	30
2.2 Synthesis of Silicalite-1	33
2.2.1 APDMMS (APTES) Functionalization of Silicalite-1.....	33
2.2.2 MPTMS Functionalization of Silicalite-1.....	34
2.3 Synthesis of Mesoporous Silica Nanoparticles.....	34
2.3.1 APDMMS (APTES) Functionalization of Mesoporous Silica Nanoparticles	35
2.3.2 MPTMS Functionalization of Mesoporous Silica Nanoparticles	35
3. PHYSICOCHEMICAL CHARACTERIZATION OF SYNTHESIZED NANOMATERIALS	36
3.1 Nanoparticle Characterization	36
3.1.1 XRD	36
3.1.2 BET	40
3.1.3 SEM, TEM.....	42
3.1.4 ζ -Potential Measurements	47
3.1.5 TGA	49
3.1.6 FTIR.....	51

3.1.7	Solid State NMR (^1H , ^{29}Si , ^{13}C)	53
4.	pKa DETERMINATION FOR SURFACE BOUND FUNCTIONAL GROUPS AND FREE MOLECULES IN D_2O USING ^1H SOLUTION NMR TITRATIONS	59
4.1	Abstract	59
4.2	Introduction	59
4.3	Experimental Methods	61
4.4	Results and Discussion	63
4.4.1	Free Organic Molecules vs Surface Bound Functional Groups	63
4.4.2	T^1/T^2 Measurements.....	64
4.4.3	pKa Determination.....	69
4.5	Conclusions.....	83
5.	SURFACE SELECTIVE ^1H SOLUTION NMR STUDIES OF FUNCTIONALIZED NANOPARTICLES	84
5.1	Abstract	84
5.2	Introduction.....	85
5.3	Experimental Methods.....	87
5.3.1	Synthesis and Surface Modification of Nanoparticles	87
5.3.2	Sample Characterization	88
5.3.3	Solution NMR Experiments.....	88
5.3.4	Experimental Parameters for Pulse Field Gradient Spin-echo (PGSE) NMR experiments	89
5.3.5	Experimental Parameters for 2D NOESY NMR Spectroscopy	89
5.4	Results and Discussion	90
5.4.1	Proton Solution NMR Spectroscopy of Functionalized Silicalite and Mesoporous Silica.....	91
5.4.2	NMR/TGA Quantitative Analysis	93
5.4.3	NOESY Experiments	94
5.4.4	DOSY Experiments	96
5.4.5	DOSY NMR Data Processed by DECRA method	100
5.5	Conclusions.....	101
6.	PROTON NMR STUDIES OF THE ADSORPTION OF HEAVY METAL ENVIRONMENTAL CONTAMINANTS	104
6.1	Abstract	104
6.2	Introduction	104
6.3	Experimental Methods.....	107
6.3.1	Chromate Adsorption Experiments	107

6.3.2	Arsenate Adsorption Experiments.....	109
6.3.3	NMR Experiments.....	109
6.3.4	Experimental Parameters for Pulse Field Gradient Spin-echo (PGSE) NMR Experiments.....	110
6.3.5	Experimental Parameters for 2D NOESY NMR Spectroscopy	110
6.4	Results and Discussion	111
6.4.1	¹ H Solution NMR Studies	111
6.4.2	2D NOESY NMR spectroscopy.....	113
6.4.3	DOSY/Diffusion Coefficient Measurements	113
6.5	Conclusions.....	114
7.	CONCLUSIONS AND FUTURE DIRECTIONS	121
	REFERENCES	126

LIST OF TABLES

Table

1.1	Nuclear spins and the Gyromagnetic ratios of the nuclei routinely used in NMR spectroscopy	14
1.2	Resonance frequencies for the most important isotopes for the field strength of 11.7 T	16
3.1	Organic Loadings (mmol/g) ^b Calculated from TGA Data, Particle Size Estimated from TEM Image (nm) ^c and BET Specific Surface Area (m ² /g) ^a	41
4.1	The longitudinal relaxation time (T ¹) (in seconds) for APDMMS and APDMMS functionalized silicalite-1 sample.	66
4.2	Proton Chemical Shift Assignments for APDMMS at pH=7 in D ₂ O.	67
4.3	Proton Chemical Shift Assignments for APTES at pH=7 in D ₂ O	68
4.4	Proton Chemical Shift Assignments for MPTMS at pH=7 in D ₂ O.	69
4.5	pKa values calculated from fits to proton NMR data collected as a function of pH.	79
5.1	Proton Chemical Shift Assignments for APDMMS, APDMMS Functionalized silicalite-1 at pH=7 in D ₂ O.....	98
5.2	Diffusion Coefficients (m ² /s) obtained from DOSY Experiments. Proton NMR spectra (at pH=7) of silicalite-1 in D ₂ O, APDMMS-functionalized silicalite-1, and APDMMS in D ₂ O are shown in Figure 5.5 A, B, and C respectively.....	99
6.1	Diffusion Coefficients (m ² /s) obtained from DOSY experiments for Pure APDMMS, MSN-APDMMS, and chromate/APDMMS-functionalized MSN in D ₂ O at pH=11.6. Proton solution state NMR spectra for chromate/APDMMS-functionalized MSN in D ₂ O at various pH are shown in Figure 6.3	115

LIST OF FIGURES

Figure

1.1	Silica-based mesoporous material MCM-41 with methane and ethane inside one of the hexagonal pores.	2
1.2	SiO_4 tetrahedron, where silicon and aluminum atoms that are coordinated with each other through shared oxygen atoms, are assembled into a larger zeolite structure	3
1.3	MFI type structure with 10-member ring pore formation.....	5
1.4	Functionalization reaction of APDMMS molecules on the surface of NP is shown on this scheme	6
1.5	Energy splitting diagram for spin $I=1/2$ nuclei. When there is an applied magnetic field, the nuclei orient themselves with or against the larger applied field. These different states increase or decrease the effective magnetic field experienced by a nearby nucleus, allowing for two distinct signals.	10
1.6	Energy splitting diagram for spin $I=1$ nuclei. There are $(2I+1)$ possible orientations for each nucleus when external electromagnetic field is applied.	12
1.7	The discretized angular momentum values for a $I=1/2$. The magnitude is denoted by the arrow while the projection along the z-axis is denoted by the circle.	14
1.8	The diagram of a typical NMR spectrometer.	19
1.9	Magic-Angle-Spinning (MAS) nuclear magnetic resonance (NMR) experiment. The sample is spinning with high frequency (up to 70 kHz) inside the applied magnetic field (B_0). It is tilted by the magic angle ($\theta_M = 54.736^\circ$) with respect to the direction of B_0	21
1.10	Comparison of ^1H solid state NMR (a) and solution state NMR (b) spectra for the same sample.	23
2.1	Functionalization reaction of APDMMS molecules on the surface of silicalite-1-35 nm.	32

3.1	Representation of Bragg's law. The incident X-ray beam reflects from the upper plane and another X-ray beam reflects from the plane immediately below.	37
3.2	Powder X-ray diffraction pattern of silicalite-1 (35 nm)	38
3.3	Powder X-ray diffraction pattern of mesoporous silica (52 nm).	39
3.4	SEM image of silicalite-1 functionalized with APDMMS. Particle size is approximately 35 nm.	43
3.5	TEM image of mesoporous silica nanoparticles. Particle size is approximately 52 nm.	44
3.6	Histogram for mesoporous silica particle size distribution with average particle size 52 ± 7 nm, derived by counting over multiple images.	45
3.7	Histogram for silicalite-1 particle size distribution with average particle size 35 ± 7 nm, derived by counting over multiple images.	46
3.8	ζ -Potential Measurements of APDMMS functionalized silicalite-1 as a function of pH.	48
3.9	TGA graph for APDMMS functionalized silicalite-1	50
3.10	TGA graph for APDMMS functionalized MSN.....	51
3.11	FTIR spectrum of APDMMS functionalized silicalite-1	52
3.12	Solid state NMR ^{13}C - ^1H CPMAS spectrum of APDMMS functionalized silicalite-1.....	56
3.13	Solid state ^1H MAS spectrum of APDMMS functionalized silicalite-1.....	57
3.14	Solid state ^{29}Si MAS spectrum of APDMMS functionalized silicalite-1.....	58
4.1	Proton solution state NMR spectra (at pH=7) of: A) silicalite-1 in D_2O , B) APDMMS-functionalized silicalite-1, C) APDMMS in D_2O	65
4.2	Proton solution state NMR spectra for APDMMS-functionalized silicalite-1 in D_2O at varying pH's: a) 10.2, b) 10.4, c) 10.7, d) 10.9, e) 11.1, e) 11.5, g) 12.4, j) 12.6.....	71

4.3	Proton solution state NMR spectra for APDMMS-functionalized MSN in D ₂ O at varying pH's: a) 8.0, b) 10.4, c) 10.6, d) 11.1, e) 11.4, e) 11.6, g) 12.6, j) 12.9.....	72
4.4	Proton solution state NMR spectra for APTES-functionalized silicalite-1 in D ₂ O at varying pH's: a) 8.0, b) 10.2, c) 10.6, d) 10.8, e) 11.0, e) 11.1, g) 11.2, j) 11.6.....	73
4.5	Proton solution state NMR spectra for APTES-functionalized MSN in D ₂ O at varying pH's: a) 9.0, b) 9.8, c) 10.2, d) 10.5, e) 10.8, e) 10.9, g) 11.2, j) 11.5.....	74
4.6	Proton solution state NMR spectra for APTES-functionalized MSN in D ₂ O at varying pH's: a) 9.0, b) 9.8, c) 10.2, d) 10.5, e) 10.8, e) 10.9, g) 11.2, j) 11.5.....	75
4.7	Proton solution state NMR spectra for MPTMS-functionalized MSN in D ₂ O at varying pH's: a) 2.6, b) 3.2, c) 6.7, d) 8.2, e) 9.2, e) 9.7, g) 10.5, j) 12.0.....	76
4.8	Proton NMR titration curve for protons on C3 of APDMMS in D ₂ O (solid circles) and APDMMS-functionalized silicalite-1 (open triangles), APDMMS-functionalized mesoporous silica (crosses). The solid lines represent nonlinear least-squares fits to the experimental data using a monoprotic titration model.	80
4.9	Proton NMR titration curve for protons on C3 of APTES in D ₂ O (solid circles) and APTES-functionalized silicalite-1 (open triangles), APTES-functionalized mesoporous silica (crosses). The solid lines represent nonlinear least-squares fits to the experimental data using a monoprotic titration model.	81
4.10	Proton NMR titration curve for protons on C3 of MPTMS in D ₂ O (solid circles) and MPTMS-functionalized silicalite-1 (open triangles), MPTMS-functionalized mesoporous silica (crosses). The solid lines represent nonlinear least-squares fits to the experimental data using a monoprotic titration model.	82
5.1	Proton solution state NMR spectra (at pH=7) of: A) silicalite-1 in D ₂ O, B) APDMMS-functionalized silicalite-1, C) APDMMS in D ₂ O	92
5.2	The NOESY spectra for pure APDMMS molecules in D ₂ O	95
5.3	The NOESY spectra for MSN-APDMMS in D ₂ O	95

5.4	The NOESY spectra for Silicalite-APDMMS in D ₂ O.....	96
5.5	The diffusion coefficients measured by DOSY for the free APDMMS in D ₂ O (red) and silicalite-1-APDMMS in D ₂ O (blue)	97
5.6	Fast exchange between free APDMMS molecules in D ₂ O and nanoparticle surface bound APDMMS species in the presence of a large excess of free ligands.	103
6.1	Schematic representation of the toxic contaminants (chromate anions) adsorption process on the surface of APDMMS functionalized MSN.	108
6.2	² Proton solution state NMR spectra for chromate / free APDMMS in D ₂ O at varying pH's: a) 2.3, b) 8.6, c) 10.4, d) 10.8, e) 11.2, e) 11.4, g) 11.5, j) 12.7, k) 12.7	116
6.3	Proton solution state NMR spectra for chromate/APDMMS-functionalized MSN in D ₂ O at varying pH's: a) 7.8, b) 8.5, c) 10.8, d) 11.0, e) 11.2, f) 11.8.	117
6.4	Proton solution state NMR spectra for arsenate / free APDMMS in D ₂ O at varying pH's: a) 9.9, b) 10.64, c) 10.8, d) 11.1, e) 11.6, e) 11.5, g) 12.0.	118
6.5	Proton solution state NMR spectra for arsenate/APDMMS-functionalized MSN in D ₂ O at varying pH's: a) 7.3, b) 10.8, c) 11.4.....	119
6.6	The NOESY spectra for chromate/APDMMS-functionalized MSN in D ₂ O	120

CHAPTER 1

INTRODUCTION

1.1 Zeolites and Mesoporous Silica.

Research in porous materials is in the limelight because of the development of an enormous number of exciting practical applications that benefit society. Among the different types of inorganic nanomaterials, nanocrystalline zeolites and mesoporous silica nanoparticles (MSN), shown in Figure 1.1, have emerged as promising multifunctional platforms for many different research areas, such as sensors, optical materials, photocatalysis, fuel cells, thermo electrics, and even in the healthcare research area. Ordered porous nanomaterials were initially developed for catalyst applications. Since their introduction in the drug delivery landscape around 2001, porous materials for drug delivery are receiving growing scientific interest for their potential applications in the biotechnology and nanomedicine fields [1]. Mesoporous silica nanoparticles are widely used as nanomedical multifunctional platforms.

Zeolites are three dimensional crystalline microporous aluminosilicate materials with a well-defined framework and uniform-sized pores throughout their crystal structure. Many zeolites occur naturally as minerals and others are synthesized by various methods. Natural zeolites occur in many regions of the world, and over 170 types of synthetic zeolites are known. Crystal structure and chemical composition account for the primary differences. Particle density, cation selectivity, and molecular pore size are only some of the properties that can differ depending on the zeolite type. Zeolites are formed by the silicon and aluminum atoms that are tetrahedrally coordinated with each other through shared oxygen atoms, as shown in Figure 1.2. The oxygen

atoms are at the corner of the tetrahedra, with the other atoms at the center. The overall framework consists of many tetrahedra connected through the oxygen atoms on the vertices. Silicon tetrahedra are electrically neutral, though aluminum tetrahedra have an overall negative charge which should be balanced by another ion. Zeolites have void spaces (cavities or channels) that can host cations, water, or other molecules. The channels that are formed by these tetrahedra lead to an overall crystalline pore structure. The channels can take different shapes in different zeolites. Two common characteristics of separate types of zeolites are silicon to aluminum ratio and pore size/shape.

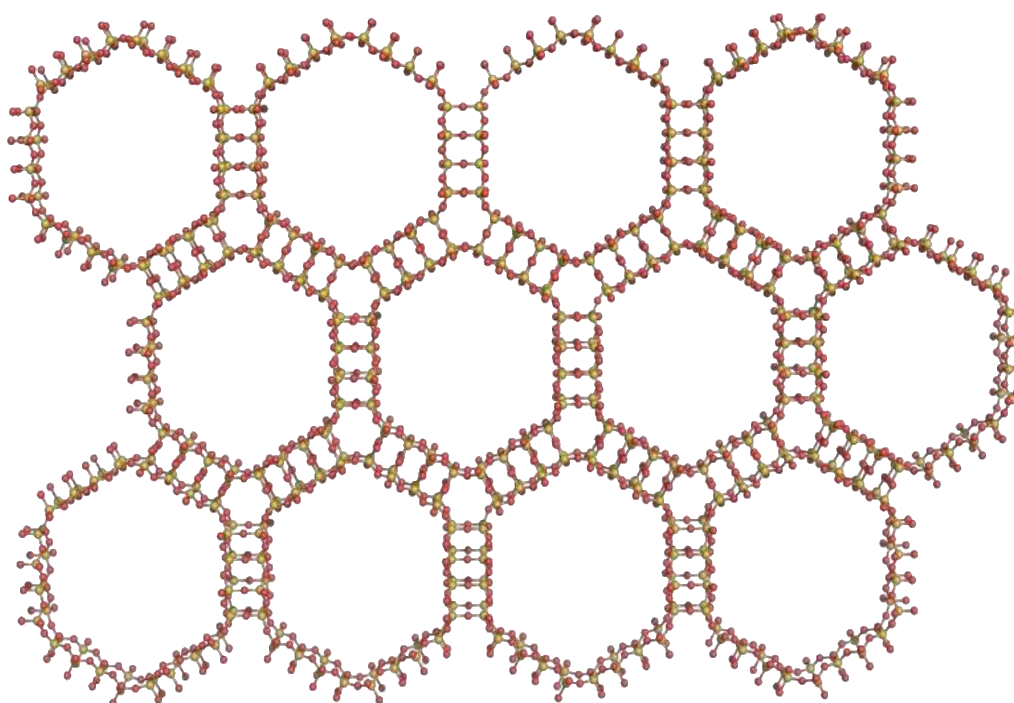


Figure 1.1 Silica-based mesoporous material MCM-41 showing the hexagonal pores.

The general formula for the composition of a zeolite is $M_{x/n}[(AlO_2)_x(SiO_2)_y]mH_2O$, where cations M of valence n neutralize the negative charges on the zeolite framework, m is the number of water molecules per unit cell, and x and y are the total number of tetrahedral atoms per unit cell. The x/y ratio (Si/Al ratio) ranges from 1 to 5 or 10 to 100 for high silica zeolites.

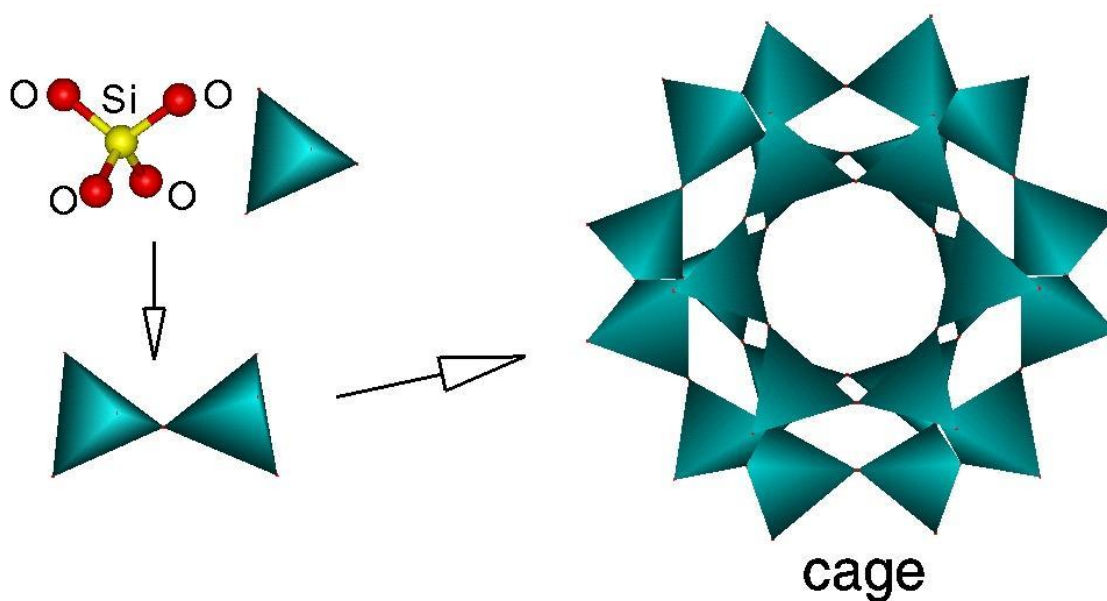


Figure 1.2 SiO_4 tetrahedron, where silicon and aluminum atoms that are coordinated with each other through shared oxygen atoms, are assembled into a larger zeolite structure.

In this study, silicalite-1, a purely siliceous form of zeolite with sinusoidal channels intersecting straight pores has been used. The MFI type structure [2], as seen in Figure 1.3, has two different 10-member ring pore types. One pore is straight and has an elliptical cross section, while the others are sinusoidal channels which intersect the straight pores at right angles and have a more circular cross section, with 5.6 Å pore diameters [3]. The absence of aluminum in silicalite zeolite is responsible for a high density of surface silanol groups $\sim 4/\text{nm}^2$ [4] and give them a small cation exchange capacity since no cations are necessary to compensate for aluminum tetrahedral charges in silicalite.

Zeolites are widely utilized in a variety of common commercial applications. They are catalytically active, and are frequently used for adsorption and separations applications [5]. Hydrogen exchanged zeolites or acid zeolites are widely used as petroleum catalysts for cracking, isomerization and fuel synthesis [6-10]. While zeolites have several properties that make them highly useful materials, they can be chemically modified to make them even more effective. The defined pore structures of zeolites are ideal for obtaining organized arrangements of a large variety of guest species on the surface of a nanosubstrate.

Physical and chemical properties of nanosized zeolites can be tailored for various applications such as separation, chemical sensing, environmental remediation, and catalysis, by the incorporation of specific organofunctional groups onto the surface of the inorganic silica framework. Functionalization of the surface of a zeolite changes the material in ways determined by the functional group. Adding an organic functional group on the zeolite allows fine tuning of the desired properties. Methods used for

functionalization of silanol groups in silica based materials, such as mesoporous silica [11, 12] can be readily adapted for zeolites with the main difference being that the functionalization occurs exclusively on the external zeolite surface due to the zeolite pore sizes that restrict access to the internal zeolite surface for most organosilane reactants [13].

F

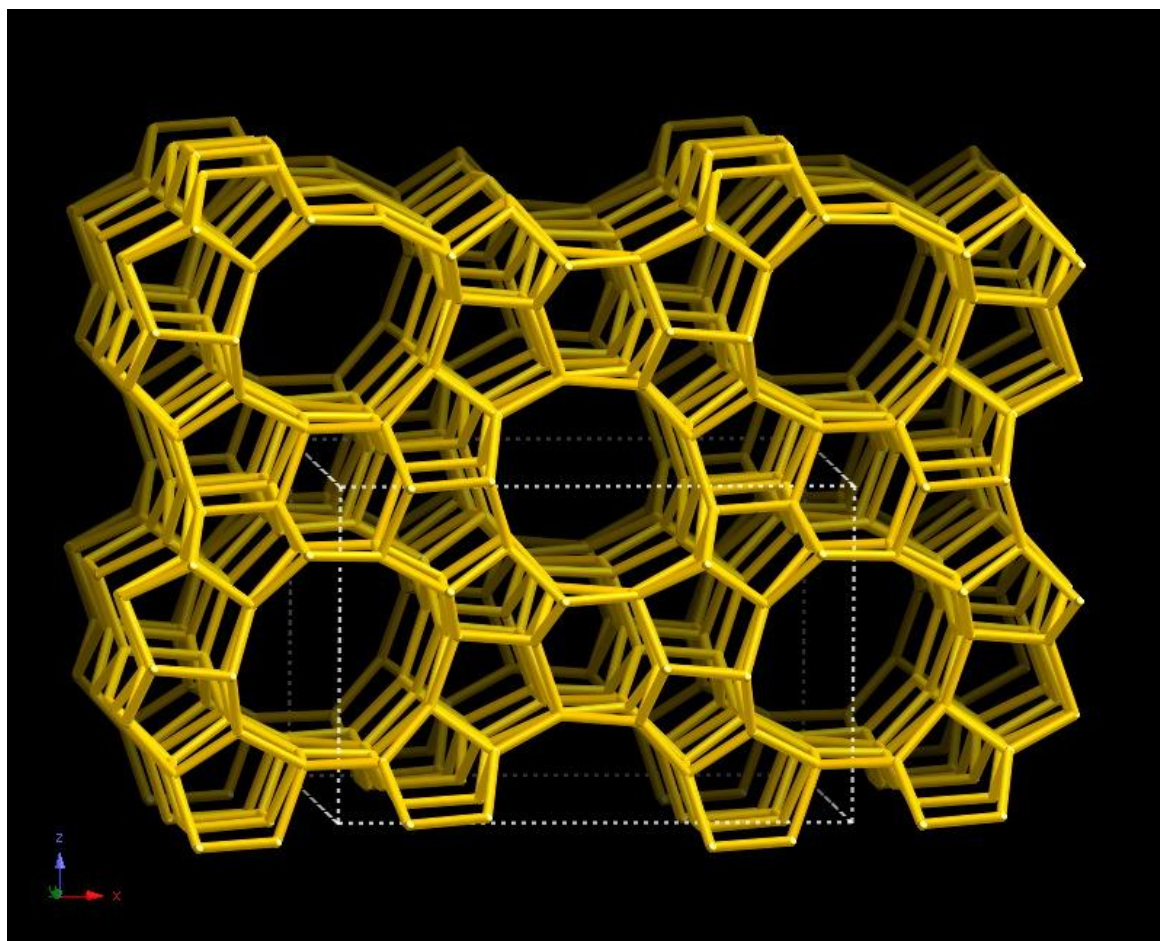


Figure 1.3 MFI type structure with 10-member ring pore formation [14].

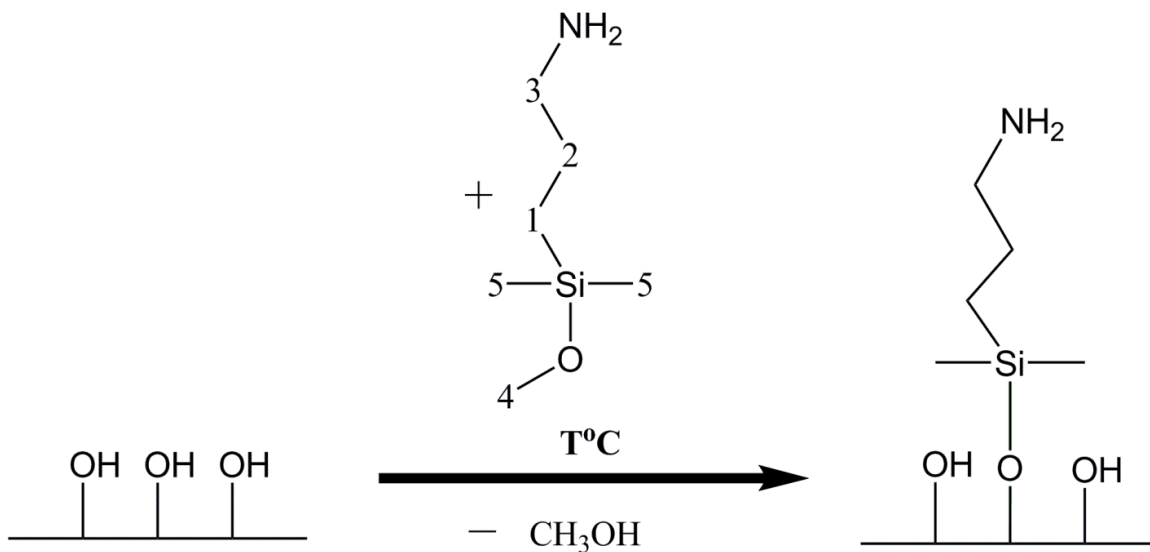


Figure 1.4 Functionalization reaction of APDMS molecules on the surface of NP is shown on this scheme.

The functionalization reaction of 3-aminopropyltrimethoxysilane (APDMS) molecules on the surface of nanoparticles is shown on this scheme in Figure 1.4. The advantage of nanocrystalline zeolites in this regard is the extremely high external surface area relative to micron-sized zeolites, which provides a lot of silanol sites available for this surface modification procedure.

For many industrial applications it is crucial to find porous materials with larger pores than zeolites can offer. The first silica-based mesoporous material MCM-41 shown in Figure 1.1 was produced almost simultaneously in the early 1990's by Mobil Corporation at USA and Kuroda research team at Japan [1]. Ordered mesoporous materials are structurally unique solids with order on the mesoscopic scale and disorder on the atomic scale. The materials consist of channels, cages, or pores

supported/separated by amorphous silica walls. Those cavities are arranged periodically on a lattice as artificial atoms or molecules in ordinary crystals, and this is why those materials are also known as “cavity crystal”. Since 1992 when first mesoporous silica material was synthesized, silica-based ordered mesoporous materials have experienced growing interest from biotechnology researchers due to their potential to host very different guest molecules. The host-guest interaction takes place between the silanol sites on the surface of the host matrices and the functional groups of the guest molecules. When targeting molecules with a size of few nanometers, mesoporous silica nanomaterials seem to be the correct choice since they are stable, with pores of 2-3 nm, have large surface areas and are very easy to functionalize to modulate their properties including hydrophobicity, hydrophilicity, molecular binding, and reactivity.

Surface functionalization of a mesoporous material may dramatically change their chemical properties and the nature of the change depends upon the kind of functional groups deposited on the surface. Therefore, the surface functionalization of mesoporous silicates has been intensively investigated. There are two major ways to functionalize the surface of mesoporous silicates by organic functional groups, named as post-synthesis grafting and co-condensation. Each of these two functionalization methods has certain advantages, which will be described in Chapter 2.

Surface modifications of porous nanomaterials need to be carried out very accurately and quantitatively. Since nanomaterials are solid-phase samples and they are coated with only a small amount of functional groups, identification and quantification of small organic molecules deposited on the surface are very challenging tasks. A variety of different techniques such as thermogravimetric analysis (TGA), photoelectron

spectroscopy (XPS), Fourier Transform Infrared Spectroscopy (FTIR), or Raman spectroscopy can be used to characterize the surface chemistry and structure of organic moieties after surface functionalization. Some useful information can be provided by each technique, and each of these methods has strengths and limitations. None of these methods can give full structure characterization of nanoparticle-bound molecules. The lack of such analytical methodologies has become an obstacle preventing us from successful chemical modifications of nanoparticle surfaces. For example, the accurate identity/concentration information about the surface composition and structure is absolutely necessary for biological or human health studies. Nuclear magnetic resonance (NMR) spectroscopy is one of the techniques that is currently used to investigate porous materials and their surfaces. In the next section the basic principles of NMR spectroscopy are described.

1.2 Nuclear Magnetic Resonance (NMR) Spectroscopy.

1.2.1 NMR Basics

Since its discovery by Felix Bloch and Edward Mills Purcell, Nuclear Magnetic Resonance, (NMR), has grown to be one of the major tools for scientists to obtain information about the structure and dynamics of molecules with atomic resolution. NMR spectroscopy has been widely used for many applications ranging from mineralogy, physics, materials science, and inorganic chemistry through organic chemistry and polymer research to analysis of proteins and nucleic acids in relation to molecular biology and medicine. By using NMR spectroscopy one can obtain qualitative and quantitative information about chemical species. After its discovery, there have been a significant number of enabling developments that have expanded applications for

nuclear magnetic resonance and greatly improved the efficiency of the technique. Relatively recent advances such as cross-polarization, magic-angle spinning, new probe design, signal receiver hardware configuration and pulse sequence design, multi-dimensional NMR experiments and many others allow us to solve more complicated structural problems or even obtain other important information, such as molecular dynamics, chemical exchange, molecular binding, screening, etc. Many of these new methods involve the parallel acquisition of spectra via multiple receivers for both small molecules and macromolecules. As compared to a number of other analytical techniques, NMR is definitely 'sensitivity challenged'. The question of sensitivity boils down to whether it is possible to detect the desired signal above the noise level. Though, it remains a unique and powerful tool for the structural elucidation of chemical compounds and determination of molecular dynamics.

Spectroscopy, the study of the interaction between matter and electromagnetic radiation, uses adsorption, scattering, or emission of electromagnetic radiation to analyze atoms and molecules qualitatively and quantitatively. Resulting spectra are obtained by the measurement of radiation intensity as a function of wavelength. Nuclear magnetic resonance, NMR, is a physical phenomenon in which atomic nuclei absorb and re-emit electromagnetic radiation. The resonance transition between magnetic energy levels happens when atomic nuclei are placed in an external magnetic field and then an electromagnetic radiation with specific frequency is applied. An NMR spectrum can be acquired by detecting the absorption signals. Positions, intensities and fine structure of resonance peaks in the resulting spectra are used to determine the structures of molecules and to analyze them quantitatively.

The adsorption process in NMR involves atomic nuclei that absorb electromagnetic radiation in the radio-frequency region when placed in an intense external magnetic field.

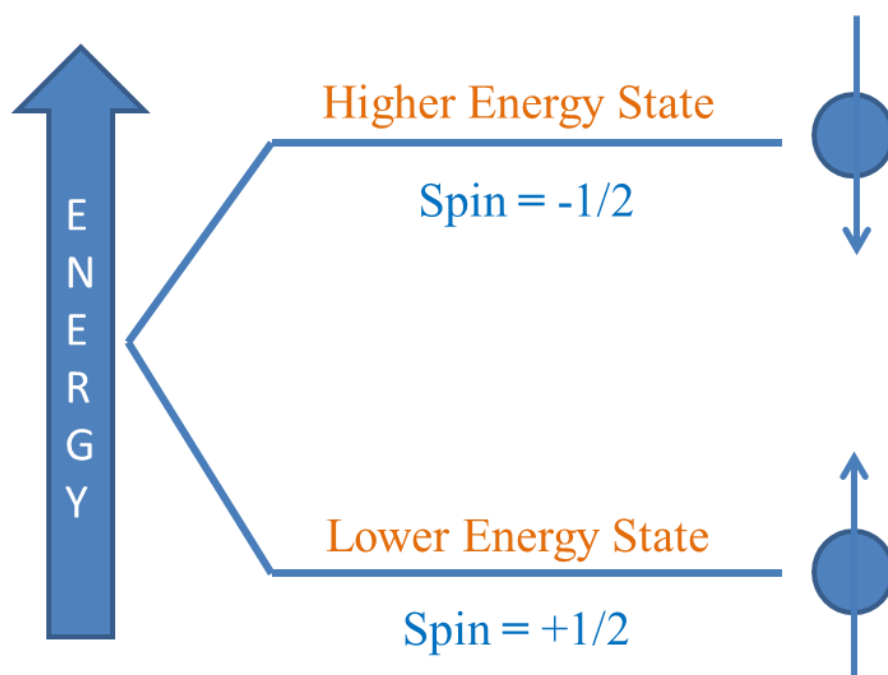


Figure 1.5 Energy splitting diagram for spin $I=1/2$ nuclei. When there is an applied magnetic field, the nuclei orient themselves with or against the larger applied field. These different states increase or decrease the effective magnetic field experienced by a nearby nucleus, allowing for two distinct signals.

The nuclei of many elemental isotopes have a characteristic spin which can be denoted using specific quantum numbers (I). Spin is a fundamental property of nature like electrical charge or mass. Because nucleons have spin, just like electrons do, their spin can pair up when the orbitals are being filled and cancel out. Some nuclei have integral spins (e.g. $I = 1, 2, 3 \dots$), some have fractional spins (e.g. $I = 1/2, 3/2, 5/2 \dots$), and a few have no spin, $I = 0$ (e.g. ^{12}C , ^{16}O , $^{32}\text{S} \dots$). NMR can only be performed on isotopes whose spin nuclear value is non-zero. Those nuclei that have spin of $1/2$ are NMR active and can be readily observed. Some of the nuclei routinely used in NMR are listed in Table 1.1. When placed in a magnetic field of strength B_0 , a particle with a net spin can absorb a photon, of frequency ν that depends on the gyromagnetic ratio, γ of the particle.

A spinning charge generates a magnetic field, as shown in Figure 1.7. The resulting spin-magnet has a magnetic moment (μ) proportional to the spin. The magnetic moment μ is related to the angular momentum of the nucleus by:

$$\mu = \gamma I \quad [1]$$

where γ is the gyromagnetic ratio, a proportionality constant unique to each nucleus. Table 1.1 below shows some of the gyromagnetic ratios for some commonly studied nuclei.

The application of a magnetic field splits the degenerate $2I+1$ nuclear energy levels. Energy splitting diagram for spin $I=1/2$ nuclei can be seen from Figure 1.5. The energy of a particular level is:

$$E = -\mu B_0 \quad [2]$$

where B_0 is the external magnetic field. Along the z-direction, which we assume the magnetic field is applied. The magnitude of the splitting therefore depends on the size of the magnetic field. When there is no external or applied magnetic field (B_0), the nuclear spins orient randomly; however, when there is an applied magnetic field, the nuclei orient themselves with or against the larger applied field. There are $2I+1$ possible orientations for each nucleus when external electromagnetic field is applied. Spin $\frac{1}{2}$ nuclei can be thought as tiny bar magnets that can have two possible orientations with respect to a larger external magnetic field. Thus, in the presence of an external magnetic field (B_0), for those nuclei, the angular momentum can have two possible values: $+1/2$ and $-1/2$. The magnetic moment of the lower energy $+1/2$ state is aligned with the external field, but that of the higher energy $-1/2$ spin state is opposed to the external field. Note that the arrow representing the external field points north.

The splitting of nucleic energy levels with a spin $I=1$ is shown in Figure 1.6.

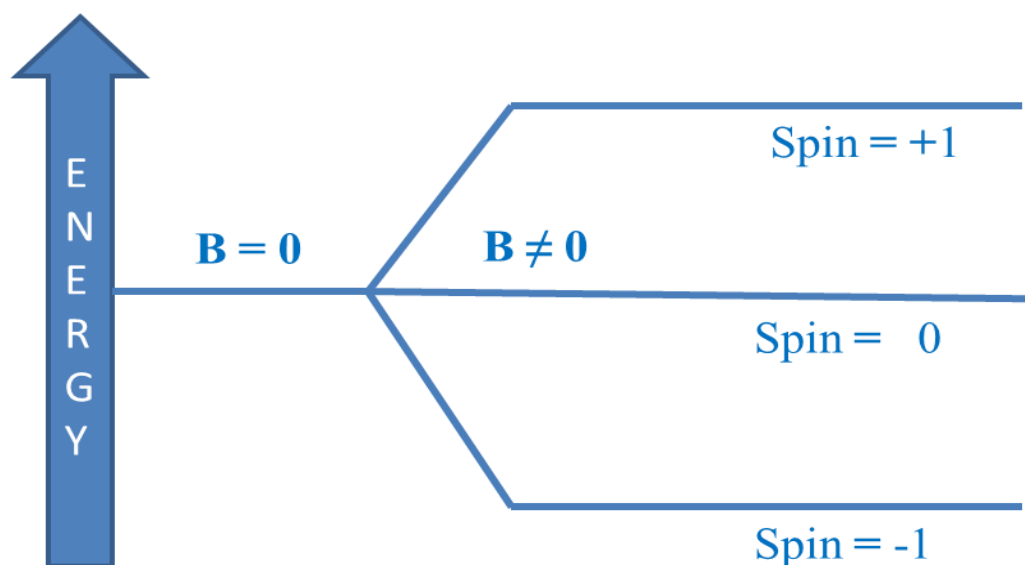


Figure 1.6 Energy splitting diagram for spin $I=1$ nuclei. There are $(2I+1)$ possible orientations for each nucleus when external electromagnetic field is applied.

According to this equation $2I+1$, observable magnetic quantum states m can be -1 , 0 , or $+1$. The difference in energy between the states, E , depends on the strength of the applied magnetic field, B_0 , according to the following equation:

$$\Delta E = E_{1/2} - E_{-1/2} = h\nu = \omega h / 2\pi \quad [3]$$

corresponds to the energy that can be absorbed or emitted by the system, described by the Larmor frequency ω .

$$\Delta E = \gamma B_0 h / 2\pi \quad [4]$$

In this equation γ is the gyromagnetic ratio, a fundamental property of each type of nucleus and h is Planck's constant.

$$\omega_0 = \gamma B_0 \quad [5]$$

The Larmor frequency can be understood as the precession frequency of the spins about the axis of the magnetic field B_0 , caused by the magnetic force acting on them and trying (I_z is quantized) to turn them completely into the field's direction (like a gyroscope "feeling" the pull of gravity). See Figure 1.7. This frequency depends only on the magnetic field strength B_0 and the spin's gyromagnetic ratio γ . For the field strength of 11.7 T the following resonance frequencies for the most important isotopes are listed in Table 1.2.

The signal in NMR is produced by absorption of electromagnetic radiation of a certain frequency. In the presence of external magnetic field, a nucleus can absorb electromagnetic radiation of the appropriate frequency and undergo a transition between the two energy states.

Table 1.1 Nuclear spins and the gyromagnetic ratios of the nuclei routinely used in NMR spectroscopy.

Nuclei	Unpaired Protons	Unpaired Neutrons	Net Spin	γ (MHz/T)
^1H	1	0	1/2	42.58
^2H	1	1	1	6.54
^{31}P	1	0	1/2	17.25
^{23}Na	1	2	3/2	11.27

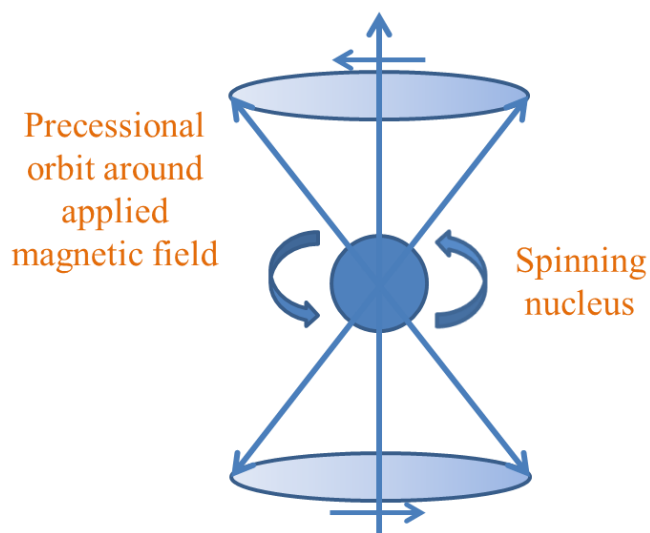


Figure 1.7 The discretized angular momentum values for a $I=1/2$ nucleus. The magnitude is denoted by the arrow while the projection along the z-axis is denoted by the circle.

The transitions occur from the lower energy (α) to the higher energy (β) spin states. If the number of nuclei in the lower energy state is equal to the number of nuclei in the higher state, the rate of absorption approaches the rate of relaxation. This process is called saturation. If the relaxation rate is fast, then saturation is reduced. In NMR, the difference in energy in the two spin states is very small therefore the population difference is also small (about 1 in 10,000 for ^1H in an 11.74 T magnetic field). The NMR signal is thus proportional to the population difference between the states. NMR is a very sensitive method allowing detection of very small population differences between the energy states. At room temperature, the number of spins in the lower energy level, N^α , slightly outnumbers the number in the upper level, N^β . According to Boltzmann statistics

$$N^\alpha/N^\beta = \exp(\Delta E/kT) = \exp(\gamma h B_0)/(2\pi kT) \quad [6]$$

ΔE is the energy difference between the spin states; k is Boltzmann's constant, 1.3805×10^{-23} J/Kelvin; and T is the temperature in Kelvin. From this equation one can see that the ratio of the number of spins in the lower energy level and the number in the upper level is temperature dependent. As the temperature decreases, so does the ratio N^α/N^β . As the temperature increases, the ratio approaches one, so

$$N^\alpha = N^\beta \quad [7]$$

Electrons in a molecule circulating around the nucleus produce a magnetic field which opposes the applied external magnetic field or shields it. The electron density around each nucleus in a molecule varies according to the types of nuclei and bonds in the molecule. The opposing field and therefore the effective field at each nucleus will vary. This is called the chemical shift phenomenon which is reported in ppm and given the

symbol delta, δ . By definition, the chemical shift of a nucleus is the difference between the resonance frequency of the nucleus (ν) and a standard (ν_0):

$$\delta = (\nu - \nu_0) \cdot 10^6 / \nu_0 \quad [8]$$

Tetramethylsilane, $\text{Si}(\text{CH}_3)_4$, abbreviated TMS, is used a standard in NMR spectroscopy.

Nuclei in various chemical environments will possess different electronic surroundings and thus will be shielded to a slightly different extent. Therefore, the chemical shift is a very precise metric of the chemical environment around a nucleus. Those nuclei experiencing different environment or having different chemical shifts are nonequivalent, while nuclei with the same chemical shift are called equivalent.

Table 1.2 The following resonance frequencies for the most important isotopes for the field strength of 11.7 T.

Nuclei	Natural abundance (%)	Resonance frequency at 11.7 T (MHz)
^1H	99.98	500
^{13}C	1.1	125
^{31}P	100	203
^{15}N	0.37	50
^{29}Si	4.7	99
^{19}F	100	455

1.2.2 NMR Instrumentation

There are two NMR spectrometer designs, continuous-wave (CW), and pulsed or Fourier-transform (FT-NMR). In earlier days, primarily continuous wave (CW) experiments were used. This NMR technique can be performed with a constant magnetic field where the frequency is varied. Even though this approach is a valuable tool to look at very sensitive and highly abundant nuclei such ^1H and ^{31}P , it becomes a very challenging task to observe nuclei with low natural abundance such as ^{13}C or ^{15}N . Continuous-wave NMR spectrometers have largely been replaced with pulsed FT-NMR instruments because the observed FT-NMR spectra have much higher signal-to-noise ratio and so Fourier-transform is a much more sensitive NMR method compared with CW. Fourier-transform NMR spectrometers use a pulse of radiofrequency (RF) radiation to cause nuclei in a magnetic field to flip into the higher-energy alignment. According to the Heisenberg uncertainty principle, the frequency width of the RF pulse (typically 1-10 μs) is wide enough to simultaneously excite nuclei in all local environments when more than one frequency is radiated simultaneously. The nuclei will re-emit RF radiation at their respective resonance frequencies and create an interference pattern in the resulting RF emission as a function of time, defined as a free-induction decay (FID). Because the FID results from the emission of nuclei in all environments, each pulse contains an interference pattern from which the complete spectrum can be obtained. Repetitive signals can be summed and averaged that allow to improve the signal-to-noise ratio of the resulting FID significantly.

The diagram for a typical FT NMR spectrometer can be seen from Figure 1.8. When a sample is placed in the probe of NMR spectrometer, a radiofrequency (RF)

pulse is transmitted by a coil that is surrounds the sample holder. Absorption takes place when the frequency of the applied magnetic field (B_0) resonates with a radiation frequency required for the transition between two energy levels to occur. FID of the resonated frequency can be detected by a RF receiver and Fourier transformed. A resulting NMR spectrum will be obtain and appear on the screen of the computer.

1.2.3 Solid State NMR

For rare spin NMR, analysis at natural abundance, sensitivity is always a problem. It is even more of a problem in the solid state where spin-lattice relaxation times can be exceptionally long. Indeed, there are numerous reasons to conduct NMR experiments on solids. Some examples would include the cases where chemical compounds are insoluble or unstable in solution. For instance, the process of cross linking to produce an insoluble polymer should be followed as a solid state reaction. The usual approach to this problem is to use solid state NMR technique.

In solution state, fast molecular tumbling and reorientational motion are responsible for all positive values of θ (eq. 9), where θ is an angle between the tensor principal axes system direction and the external magnetic field B_0 . The average value of $\cos^2\theta$ is $1/3$, so the dipolar coupling averages to 0. In solids, due to all different orientations of molecules this term $\cos^2\theta$ is non zero and causes line broadening. Furthermore, fast molecular motion in solutions results in the averaging of the chemical shifts for all molecules, while rigid architecture and various orientations of molecules in solid materials yield complex line shapes as a result of all possible chemical shifts being detected for differently oriented nuclei. Direct magnetic dipolar interactions between nuclear spins, and chemical shift anisotropy are two major contributors to NMR line

widths for solids. Homonuclear or heteronuclear dipolar couplings result from the interaction between one nuclear spin with the magnetic field created by another nuclear spin in close vicinity. Since the static magnetic field lies along the z axis, the dipolar interaction has an orientational dependence with respect to B_0 given by the expression $1-3\cos^2\theta$, where θ is an angle between the tensor principal axes system direction and the external magnetic field B_0 .

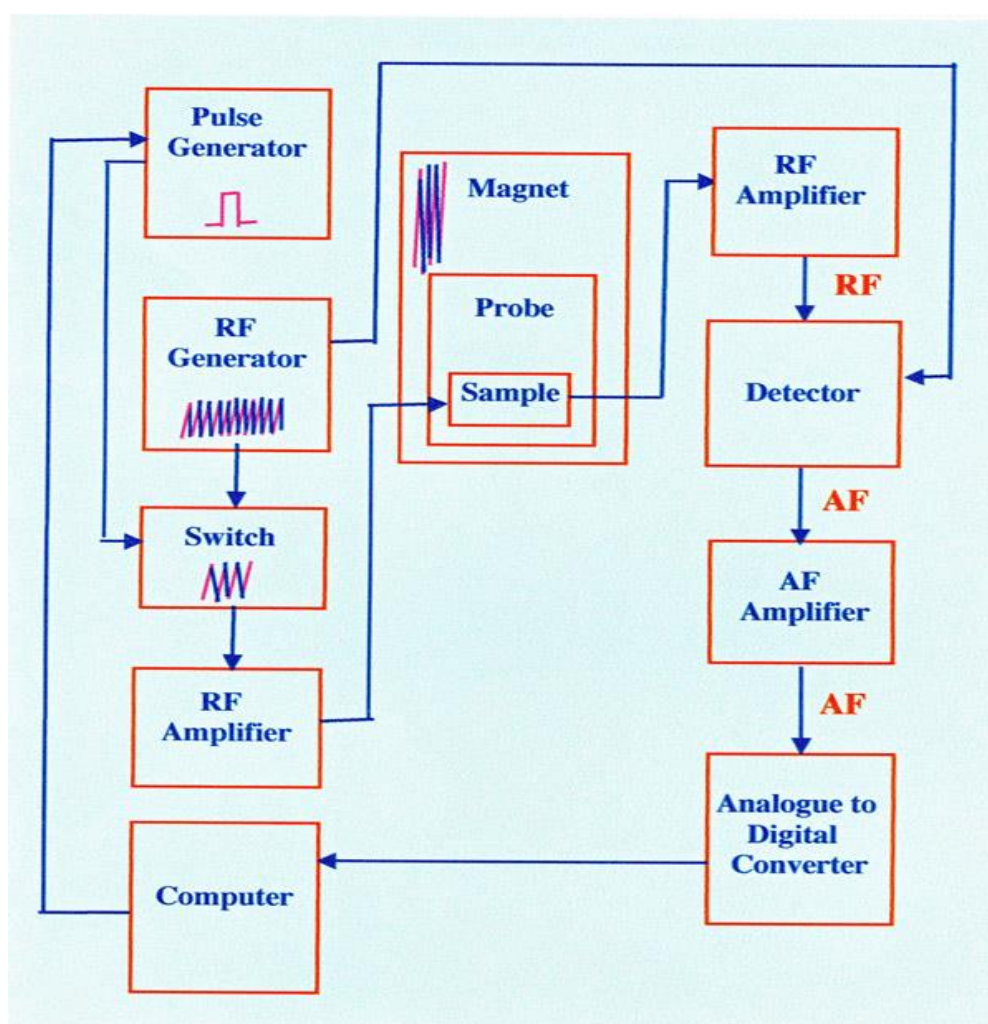


Figure 1.8 The diagram of a typical NMR spectrometer [15].

If the sample is spun at the magic angle θ_M , the orientation dependence of the interaction can be written as:

$$3\cos^2\theta - 1 = (1/2)(3\cos^2\theta_M - 1)(3\cos^2\beta - 1) + (3/2)\sin^2\theta_M \sin 2\beta \cos 2\Omega t + (3/2)\sin^2\theta_M \sin^2\beta \cos 2\Omega t \quad [9]$$

If the spinning is fast, we obtain a time average:

$$(3\cos^2\theta - 1) = (1/2)(3\cos^2\theta_M - 1)(3\cos^2\beta - 1) \quad [10]$$

We can choose the angle θ_M in a way that $(3\cos^2\theta_M - 1)$ becomes zero, then the anisotropic part of the interaction vanishes and only the isotropic contribution remains. This technique is called the “magic angle spinning” ($\theta_M = 54.736^\circ$ to the vertical B_0) or MAS. Thus, the anisotropic broadening for all crystallite orientations can be averaged to zero by rotating the sample under MAS. When the sample is spun with a rotation rate ω_r , all spin interactions become time dependent sidebands with a separation of ω_r appear in the spectrum. If the spinning rate ω_r is much faster than the anisotropic interaction, the sidebands are well separated and negligibly small. Hence, direct magnetic dipolar interactions between nuclear spins and the chemical shift anisotropy can be nullified for spin- $1/2$ nuclei (^1H , ^{13}C , etc.) by very fast spinning of the sample about the “magic angle” (Figure 1.9). However, to remove homonuclear dipolar coupling effects in solid ^1H -NMR spectra, extremely high spinning speeds on the order of 70 kHz and high-power pulses are required during the acquisition. Indeed, NMR spectroscopists have found ways of suppressing and controlling anisotropic interactions. A number of methods including magic-angle spinning, multiple-pulse sequences cross polarization and others have been developed to minimize large anisotropic NMR interactions between nuclei and increase S/N in NMR spectra. Even though recent studies in fast magic-angle

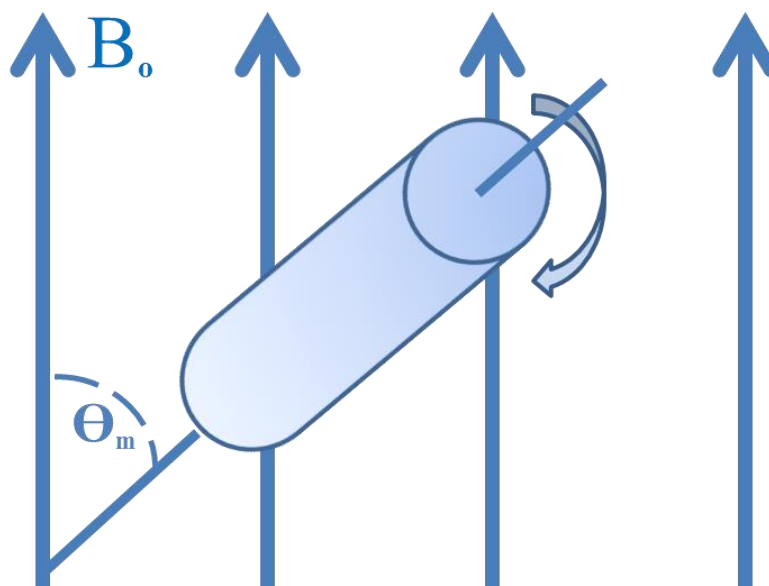


Figure 1.9 Magic-Angle-Spinning (MAS) nuclear magnetic resonance (NMR) experiment. The sample is spinning with high frequency (up to 70 kHz) inside the applied magnetic field (B_0). It is tilted by the magic angle ($\theta_m = 54.736^\circ$) with respect to the direction of B_0 .

spinning (MAS) methods has drastically improved the resolution and sensitivity of NMR spectroscopy of large biomolecules and materials in solids, the resolution of resulted spectra is usually not as good in the solid state as that achieved in solution, even in crystalline systems. This is because there are still other sources of line broadening and limits to polarization lifetimes not seen in low viscosity liquids. For instance, due to the very long relaxation times of most non-proton (e.g., ^{13}C) signals in the solid-state, relaxation delays of typically several minutes are required between pulses. Even though, the basic NMR techniques responsible for higher resolution spectra obtained for solids like decoupling, magic angle sample spinning, and cross polarization were early

developments in the science of NMR, new approaches to amplify and expand these methods and make them more useful are still being developed every day.

1.2.4 Solution State NMR of Nanomaterials

^1H solid-state NMR techniques are shown to provide unique structural insight for a diverse range of systems including pharmaceuticals, self-assembled supramolecular structures and silica-based inorganic/organic materials, such as microporous and mesoporous materials. It is considered the gold standard for characterization of solid samples or small organic molecules bound to the surface of solid nanoparticles. However, the restricted motional freedom of studied species often leads to significant line-broadening and results in reduced resolution relative to solution phase NMR spectroscopy. Both solution and solid state ^1H NMR spectra of a sample of functionalized silicalite (functionalization depicted in Figure) are shown in Figure 1.10. Solid-state NMR spectra are very broad due to anisotropic or orientation-dependent interactions. By contrast, as a result of averaging of anisotropic NMR interactions in solution by rapid random tumbling, solution NMR spectra consist of a series of very sharp lines. Recently, the potential of solution state NMR spectroscopy for the characterization of colloidal functionalized nanoparticles has been demonstrated in literature [16]. In this research work, we demonstrate that conventional solution phase NMR can be used for full structural elucidation of small organic molecules covalently bound to the surface of porous nanomaterials.

The fast rotational motion of the organic functional groups on the surface of the nanoparticles in solution reduces the line-broadening to the extent that NMR spectra of

the surface functional groups can be observed using solution NMR techniques. For example, solution NMR studies of functionalized gold nanoparticles have been used to

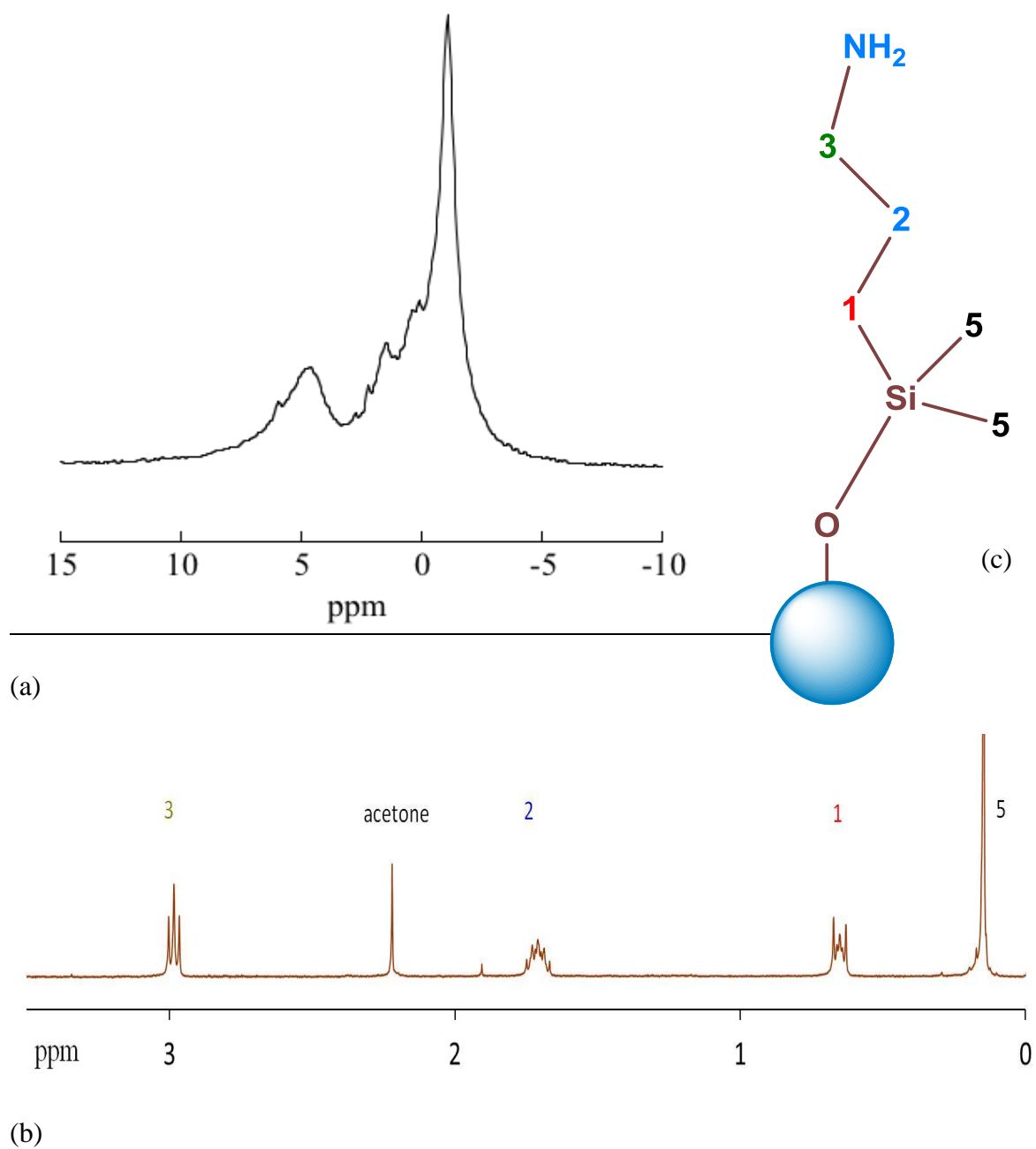


Figure 1.10 Comparison of ^1H solid state NMR (a) and solution state NMR (b) spectra for the same sample: APDMMS functionalized silicalite-1.

elucidate the organic substituents and ligand exchange reactions on gold surfaces [17-22]. Not only does solution NMR provide excellent spectral resolution, but it is also selective for surface protons because bulk protons are not motionally averaged and therefore not observed in solution NMR spectroscopy. Solution NMR techniques have been used to study functionalized gold nanoparticles and metal oxide nanoparticles but there are no reports of using these methods to study functionalized porous nanomaterials, such as zeolites or mesoporous silica. In porous aluminosilicate and silicate materials, it is particularly advantageous to be able to differentiate surface and bulk proton signals. These solution NMR methods applied to nanomaterial systems also have great potential for studies of environmental or biological interfaces involving nanoparticle surface processes. Porous nanomaterials [2, 23-26], such as zeolites and mesoporous silica, have emerged as nanomaterials with new properties and many potential applications, in areas such as environmental catalysis [27], drug delivery [28, 29], imaging [30-34] and other biomedical applications [35, 36]. While the large internal surface area of these materials has traditionally been exploited for applications in catalysis and ion-exchange, porous nanoparticles also have large external surfaces that can be tailored for specific applications in biomedicine or adsorption [37-42]. Characterization of the surface structure of the functionalized zeolite nanoparticles is critical in developing an understanding of the surface chemistry and the environmental and biological interfaces that result from applications of these materials. Information about surface structure and composition can also be used to design functionalized nanomaterials with specific applications.

1.3 Adsorption of Environmental Contaminants.

NMR spectroscopy can be a useful analytical method to obtain essential information about the characteristics of functionalized materials and chemical species that interact with their surfaces. This information is especially warranted for toxic chemicals that persist for an extended period of time in the environment. The concerns for the presence of a wide variety of contaminants in the environment call for development of analytical tools that provide valuable information about the surface chemistry of nanoparticles that can be used to prevent or minimize the adverse effect of contaminants on human welfare. As described previously, the properties of nanomaterials, such as zeolites and mesoporous silica, can be tailored by localization of the different functionalities needed to perform a desired task. In order to take advantage of some known interactions, certain functional groups can be synthesized on the surface of a substrate. For instance, the fact that sulfur interacts with lead suggests that nanoparticles functionalized with those chemical species can be successfully used in environmental remediation. Each contaminant has a unique set of characteristics and issues that must be evaluated to proceed with more detailed remediation efforts. In this thesis, contaminant/particle interactions will be characterized by using solution NMR spectroscopy as a specific surface probe.

1.3.1. Chromium (VI)

Chromium (Cr) is one of the most strategic materials widely used in the metals and chemical industries. Cr alloys enhance metal resistance to impact, corrosion, and oxidation. Owing to the many industrial uses of Cr(VI), there are numerous sites throughout the world with Cr(VI) contaminant problems [43]. Cr occurs in various

oxidation states, of which chromium (VI) [Cr(VI)] is a suspected carcinogen and a potential soil, surface water, and groundwater contaminant. Therefore, removal is important for health and safety. Adsorption of Cr(VI) by functionalized nanomaterials from aqueous solution is one of the available techniques [44]. Specific functionalities such as amine groups ($-NH_3$) bound to the surface of porous substrates can be utilized to remove the toxic metal through electrostatic interaction occurring between negatively charged chromate species and positively charged protonated amine functionalities.

1.3.2. Arsenic (V)

Arsenic is a naturally-occurring and widely dispersed element in the Earth's crust that can be found in water, air, rocks, soil, plants, and animals. Pure arsenic is a gray metal-like material which can be found in the environment combined with other elements such as oxygen, chlorine, and sulfur. When combined with these elements, arsenic is known as inorganic, while when combined with carbon and hydrogen, it is called organic arsenic. Arsenic is used in wood preservatives, paints, dyes, metals, drugs, soaps, and semiconductors, agricultural applications, mining, and smelting. About 90 % of industrial arsenic in the U.S. is currently used as a wood preservative. The wide industrial use of arsenic contributes to arsenic releases in the environment. Coal burning in Slovakia, Turkey, and China; use of arsenic as pesticides in Australia, New Zealand, and the US; exposure to wood preserving arsenicals in Europe and North America, and, most significantly, mining activities in India and China are sources of environmental contamination by arsenic. Endemic contamination by arsenic has serious consequences to human welfare [45]. Like many contaminants, at high levels arsenic is potentially hazardous for human health. Thus long term exposure to this toxic metal has been linked

to cancer of the bladder, lungs, skin, kidneys, nasal passages, liver and prostate. The legal requirements in US and currently recommended exposure level by the World Health Organization (WHO) is 10 ppb.

Arsenic exists in many oxidation states, with arsenic (III) and (V) being the most common forms. Soluble inorganic arsenate (V) predominates under normal conditions since it is thermodynamically more stable in water than arsenite (III). Trivalent arsenicals (arsenic-containing compounds) are more toxic than arsenic (V) and, unlike pentavalent, react with sulfhydryl ($-C-SH$ or $R-SH$) protein groups. Though due to the fact that these species interconvert, techniques for remediation have to be effective for both species and separation is difficult. Sorbents and filters are known techniques for removing arsenic from various environments. The most commonly used method for removing both As(V) and As(III) compounds from aqueous solution involves chemical precipitation using iron and aluminum salts. Ferric salts are more effective than aluminum salts for removing As(III), where the process of removal occurs through chemical adsorption and co-precipitation during the formation of ferric hydroxides [45]. Other methods for toxic metal removal involve reverse osmosis, activated charcoal, and coagulation etc. Among other techniques, the functionalized porous nanoparticles such as zeolites and mesoporous silica have been recently exploited to adsorb environmental pollutants including As containing chemical species from aqueous solutions.

1.4 Thesis Overview

The overall goal of this research work is to use 1H solution state NMR spectroscopy as an analytical tool for characterization of the surface chemistry of porous nanoparticles functionalized with small organic molecules. Although some

functionalization processes are already well studied and available even at industrial scale, the development of new functionalities requires detailed knowledge of fundamental aspects, related to the mechanisms occurring on the surface of nanomaterials. Deeper understanding of fundamental interfacial reaction phenomena is essential to the realization of innovative applications and can significantly contribute to the design and development of novel methodologies in nanotechnology. A real breakthrough is that the use of this technique results in high-resolution spectra even for molecules bound to the surface of solid nanoparticles and offers exclusive surface selectivity. Indeed, due to the increased motional narrowing of the surface functional groups when the porous nanomaterials are dispersed in solvent, highly resolved solution proton NMR signals from the surface functional groups are detected. In this investigation, ^1H solution NMR techniques have been used to selectively probe the surface structure and composition of functionalized nanoparticles in colloidal aqueous solutions.

In this thesis, advanced characterization of the surface bound chemical moieties, their structural analysis, and chemical reactivity by using NMR methods will be also discussed. The proton solution state NMR technique can provide valuable information about the surface composition of host materials and chemical properties of guest molecules. The study demonstrates that solution NMR titration can be used to determine the pKa of the surface bound functional group on covalently modified silicalite-1 nanoparticles as well as provide a number of important material properties including qualitative identification of surface bound functionalities.

Chapter 3 will focus on a wide range of methods that have been utilized to obtain a profound understanding of studied material properties that could be essential for their future applications. In this work, nanosized zeolites crystals and mesoporous silica nanoparticles have been altered through a functionalization process with aminopropyltriethoxysilane (APTES), aminopropyldimethylmethoxysilane (APDMMS), or aminopropyltrimercaptosilane (APTMS), and given interface amine and thiol functionalities. 2D NMR spectroscopy, namely Diffusion Ordered Spectroscopy (DOSY) and Nuclear Overhauser Effect Spectroscopy (NOESY) experiments, were conducted to provide further evidence that the organic functional groups observed in the NMR experiments are interacting with the surface of the host materials.

These porous nanomaterials were used to adsorb two heavy metal environmental contaminants, aqueous chromium and arsenic. The surface of functionalized silicalite-1 and mesoporous silica nanoparticles with toxic contaminants (chromate and arsenate anions) has also been explored by ^1H solution NMR. Obtained results revealed the sensitivity of solution NMR spectroscopy to the electronic environment of the surface functional groups on porous nanomaterials.

CHAPTER 2

SYNTHESIS AND FUNCTIONALIZATION OF SILICALITE-1 & MESOPOROUS SILICA

2.1 Introduction

Mesoporous silica nanoparticles (MSNs) and zeolites are materials that have porous structures with tunable pores, large surface areas, high pore volumes, and, in some cases, well-ordered structures. Good control of the morphology, particle size, uniformity and dispersity of porous nanomaterials has attracted more and more attention for their potential applications as catalyst, adsorbents, polymer fillers, optical devices, bio-imaging agents, drug delivery systems, and biomedical materials. There are different synthesis strategies to prepare well-dispersed MSNs with tunable dimensions ranging from a few to hundreds of nanometers. The methods include fast self-assembly, a Stöber method, soft and hard templating, dissolving–reconstruction and modified aerogel approaches.

The cooperative self-assembly of silica species and cationic surfactant cetyltrimethylammonium chloride (CTACl) and the formation of mesoporous silica nanoparticles occur following the hydrolysis and condensation of the silica precursor tetraethylorthosilicate (TEOS). Suitable additive agents, such as inorganic bases or alcohols, can be used to control the particle size because they affect the hydrolysis and condensation of silica species. Discovered as “boiling stones” more than 250 years ago, zeolites have received considerable attention since the twentieth century and the number of discovered zeolite structures has been growing. Currently, more than 200 different topologies have been found. Mostly, four zeolite frameworks (LTA, FAU, MOR and MFI topologies) are involved in industrial applications ranging from heterogeneous

catalysts to adsorbents and ion exchangers. Macroscopic properties such as crystal shape, size, polydispersity and framework composition can be achieved using the right synthesis procedures. One of the most commonly used methods for synthesis of zeolites is hydrothermal treatment where a mixture of silicon and aluminum sources, structure directing agents, and sources of other elements in water is treated in an aqueous solution at an elevated temperature and pressure. Zeolites are commonly synthesized in a highly basic medium in order to facilitate the dissolution of silicon precursors. The shape of structure directing agents controls the type of zeolite framework formed during the synthesis.

Reducing the particle size from tens of microns to around 100 nm or less, means a tremendous increase in the surface area (per gram of particles) and also enhances the kinetics of adsorption/desorption processes occurring on the surface of particles. The external surface area of nanoscale zeolites is up to several orders of magnitude larger than the external surface area for micrometer sized zeolites and provides an additional surface for reaction or functionalization. For instance, a 50 nm crystalline zeolite has an external surface area of $> 100 \text{ m}^2/\text{g}$, while a 500 nm zeolite crystal has less than $10 \text{ m}^2/\text{g}$ of external surface area [2, 46, 47]. Porous nanomaterials can be employed as hosts for functional molecules attached to their surfaces. Functionalization of nanocrystal surfaces can control their physical and chemical properties including hydrophobicity, hydrophilicity, binding to specific molecules and ions [12, 13, 48-50]. The utilization of the external surface will lead to the development of novel bifunctional, nanocrystalline materials with tunable properties. Those organic-inorganic hybrid materials with desired

functionalities can be useful for various applications such as catalysis, drug delivery, environmental remediation, and sensors.

Surface functionalization can be achieved through reaction of silanol sites with organosilane molecules. A typical functionalization reaction is schematically shown in Figure 2.1. Strategies for chemical modification of the interior and exterior surfaces of nanoparticles that can be used for functionalization of silanol groups in silica based materials, such as mesoporous silica, have been adapted for zeolites nanomaterials. Nanoparticle surface has been functionalized by post-synthetic grafting [11, 51-53]. This procedure can be done using silane functionalization, where surface silanol groups are reacted with organosilane reagents such as 3-aminopropyltrimethoxysilane (APTMS), 3-aminopropyltriethoxysilane (APTES), or 3-aminopropyltriethylmercaptopysilane (MPTMS). This functionalization reaction results in an amine or thiol functionalized materials as can be seen from Figure 2.1. Those organosilane molecules are usually too big to penetrate the zeolite pores, so only external functionalization can be possible for silicalite-1 particles, while mesoporous silica nanoparticles (MSN) functionalization takes place in the pores as well.

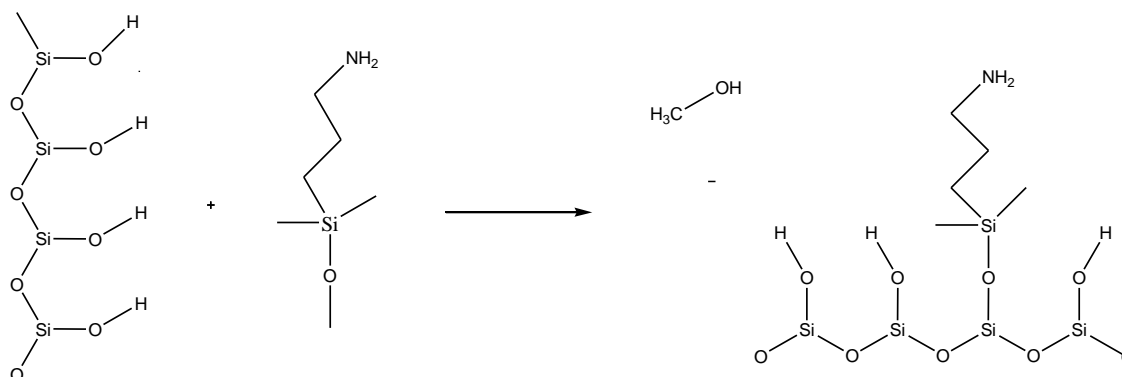


Figure 2.1 Functionalization reaction of APTMS molecules on the surface of silicalite-1-35 nm.

2.2 Synthesis of Silicalite-1

All silicalite-1 samples with a crystal size of 35 nm were synthesized from clear gel solutions according to the general procedure reported in the literature [17, 54]. The synthesis gel composition with the molar ratio of components tetraethyl orthosilicate (TEOS): tetrapropyl ammonium hydroxide (TPAOH):NaOH:H₂O as 25:9:0.16:495 were prepared. To start a synthesis, measured amounts of chemicals (H₂O, TEOS, NaOH, TPAOH solution) were mixed and stirred at room temperature overnight to ensure complete TEOS hydrolysis. Next, the clear solution was transferred into a 25 mL glass flask equipped with a water-cooled condenser and placed in an oil bath, where the clear solution was heated at 60°C for 9 days. Silicalite-1 crystals were recovered after three cycles of centrifuging at 14000 rpm (20817 x g) for 30 min to separate the particles from the supernatant, and washing once with ethanol and twice with deionized water, followed by drying at 120 °C overnight. The silicalite-1 crystals were calcined at 600 °C under air flow to remove the TPAOH template. The silicalite-1 average particle size was determined by BET method from the external surface area and was confirmed by using Scanning and transmission electron microscopies (SEM and TEM). The external surface of calcined silicalite was covalently modified by aminopropyltrimethoxysilane (APDMMS), 3-aminopropyltriethoxysilane (APTES) or mercaptopropyltriethoxysilane (MPTMS).

2.2.1 APDMMS (APTES) Functionalization of Silicalite-1

Functionalization of silicalite nanoparticles with amine groups was obtained by refluxing a mixture of 2 g of silicalite-1 and 2 g of 3-aminopropyltrimethoxysilane (APDMMS) in 60 mL of toluene for 4 h followed

by three cycles of centrifuging at 14000 rpm ($20817 \times g$) for 30 min to separate the particles from the supernatant, and washing of the silicalite powder with dichloromethane. APTES-functionalized silicalite was dried at 80°C overnight.

2.2.2 MPTES Functionalization of Silicalite-1

Functionalization of silicalite nanoparticles with thiol groups was carried out by refluxing a mixture of 2 g of silicalite and 4 g of 3-mercaptopropyltriethoxysilane (MPTES) in 60 mL of toluene for 24 h followed by three cycles of centrifuging at 14000 rpm ($20817 \times g$) for 30 min to separate the particles from the supernatant, and washing of the silicalite powder with ethanol. MPTES-functionalized silicalite was dried at 80°C overnight.

2.3 Synthesis of Mesoporous Silica Nanoparticles

Mesoporous silica nanoparticles with a particle size of approximately 50 nm were synthesized according to the procedure described previously by Karin Möller, Johannes Kobler, and Thomas Bein in the literature [55]. In a synthesis, cetyltrimethylammonium chloride (CTACl), ethanol, and water were combined and stirred at room temperature for approximately 10 min. Triethylamine (TEA) was added and the solution was allowed to stir for about an hour before being heated to 60 °C. Tetraethylorthosilicate (TEOS) was then added to the rapidly stirring solution at a rate of about 2 ml/min and the solution was stirred at 60 °C for 2.5 hours. The product was centrifuged, and the solid was resuspended in water and washed 3-5 times until the pH of the water was approximately 7. The solid product was then dried and calcined at 550 °C in air for 6 hours. The silica was calcined at 600 °C for 12 hours. The surface of

MSN was covalently modified by aminopropyldimethylmethoxysilane (APDMMS), 3-aminopropyltriethoxysilane (APTES) or mercaptopropyltrimethoxysilane (MPTMS).

2.3.1 APDMMS (APTES) Functionalization of

Mesoporous Silica Nanoparticles

Functionalization of mesoporous silica nanoparticles with amine groups was obtained by refluxing a mixture of 6 g (2 g) of silicalite-1 and 2 g of APDMMS (APTES) in 60 mL of toluene for 48 h followed by three cycles of centrifuging at 14000 rpm ($20817 \times g$) for 30 min to separate the particles from the supernatant, and washing of the silicalite powder with dichloromethane. APTES-functionalized silicalite was dried at 80°C overnight.

2.3.2 MPTMS Functionalization of

Mesoporous Silica Nanoparticles

Functionalization of mesoporous silica nanoparticles with thiol groups was carried out by refluxing a mixture of 2 g of silicalite-1 and 12 g of 3-mercaptopropyltrimethoxy- silane (MPTMS) in 60 mL of toluene for 24 h followed by three cycles of centrifuging at 14000 rpm ($20817 \times g$) for 30 min to separate the particles from the supernatant, and washing of the silicalite-1 powder with ethanol. MPTMS-functionalized silicalite was dried at 80°C overnight.

After the synthesis all samples were characterized. Resulting characterization data are reported in the next chapter.

CHAPTER 3.
PHYSICOCHEMICAL CHARACTERIZATION OF SYNTHESIZED
NANOMATERIALS.

3.1 Nanoparticle Characterization

3.1.1 XRD

X-ray diffraction is a widely used technique for structural analysis of crystalline materials. The basis for X-ray diffraction utilizes electromagnetic radiation. There are three types of scattering resulted from an X-ray beam going through a substance: coherent scattering, incoherent scattering, and absorption of X-ray beams followed by electron emission. Coherent scattering is the primary source of X-ray beams scattered from periodic lattices in a crystal [56]. Crystalline planes of studied materials can be treated as semi-transparent mirrors, from which X-ray beams are reflected. An intensive beam of radiation results from constructive interference between the scattered X-ray beams. In Figure 3.1, one X-ray beam reflects from the upper plane and another X-ray beam reflects from the plane immediately below. Different path lengths of the reflected X-ray beams can be used to determine the distance between the two planes, and the net difference between the planes can be calculated as:

$$AB + BC = 2d \sin \theta \quad [11]$$

where θ is the glancing angle. Those X-ray beams reflecting from the planes that have their path length difference equal to the integer number of their wavelength will result in a constructive interference. Thus, the distance between the lattice planes can be found by using the wavelength of the X-ray beam and the glancing angle.

The X-ray diffraction reflections of each crystalline material result in a unique pattern with the lines of different intensity and position representing the distance between atomic planes in the crystals. An X-ray diffraction pattern can be used as a fingerprint for a given type of crystalline material. Therefore, comparing an X-ray diffraction pattern against the patterns collected for known crystalline compounds, the composition of the analyzed material can be determined. Both mesoporous silica and silicalite nanocrystals were characterized using the powder X-Ray Diffraction (XRD) method performed on Siemens D5000 X-ray diffractometer with Cu K α radiation, nickel filter, and step size of 0.05, and a counting time of 0.04 s per step. The diffraction pattern agrees with the diffraction patterns for the silicalite-1 framework and mesoporous silica structure. XRD powder patterns for mesoporous silica (52 nm) and silicalite-1 (35 nm) can be seen from Figure 3.2 and 3.3.

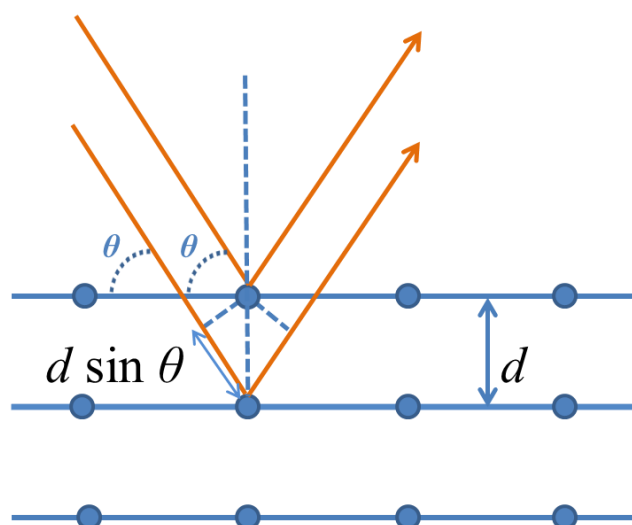


Figure 3.1 Representation of Bragg's law. The incident X-ray beam reflects from the upper plane and another X-ray beam reflects from the plane immediately below.

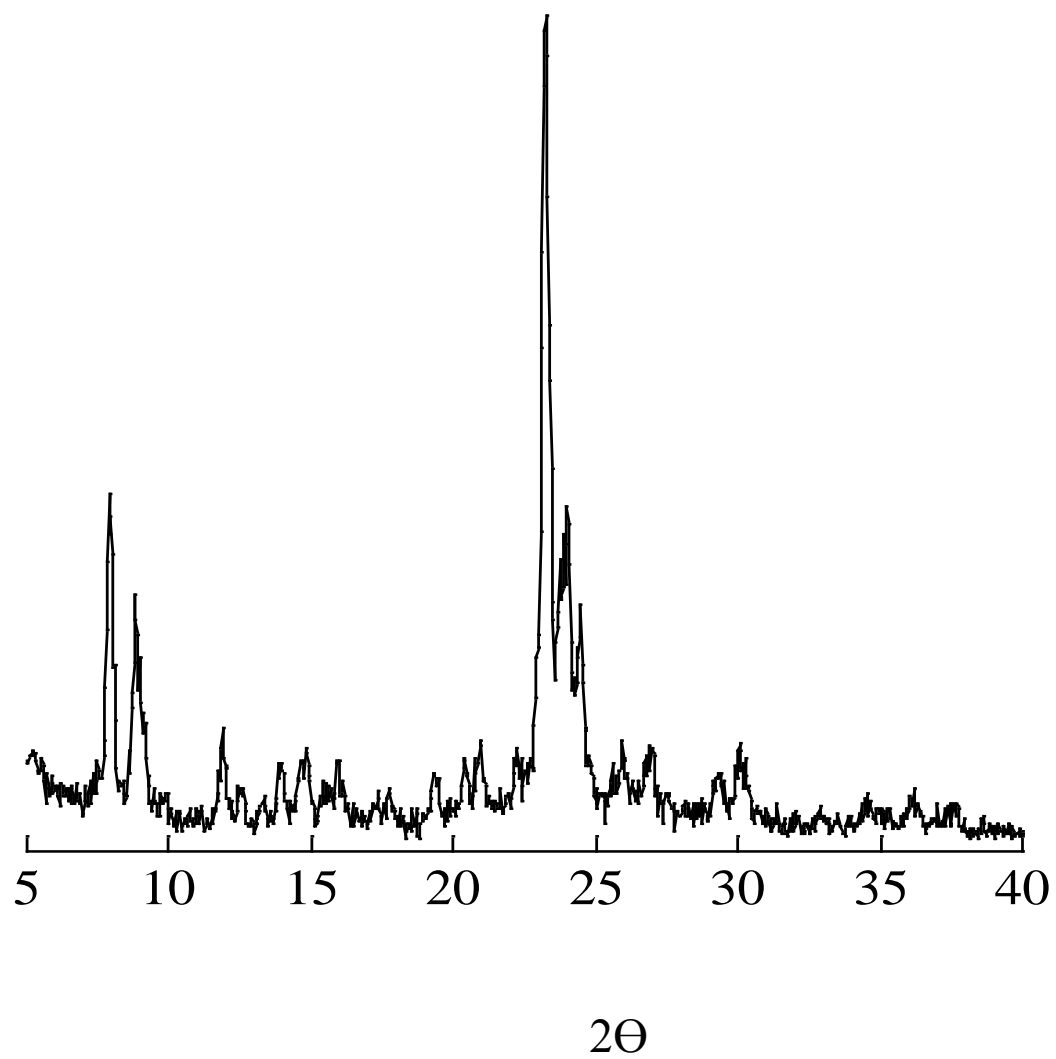


Figure 3.2 Powder X-ray diffraction pattern of silicalite-1 (35 nm).

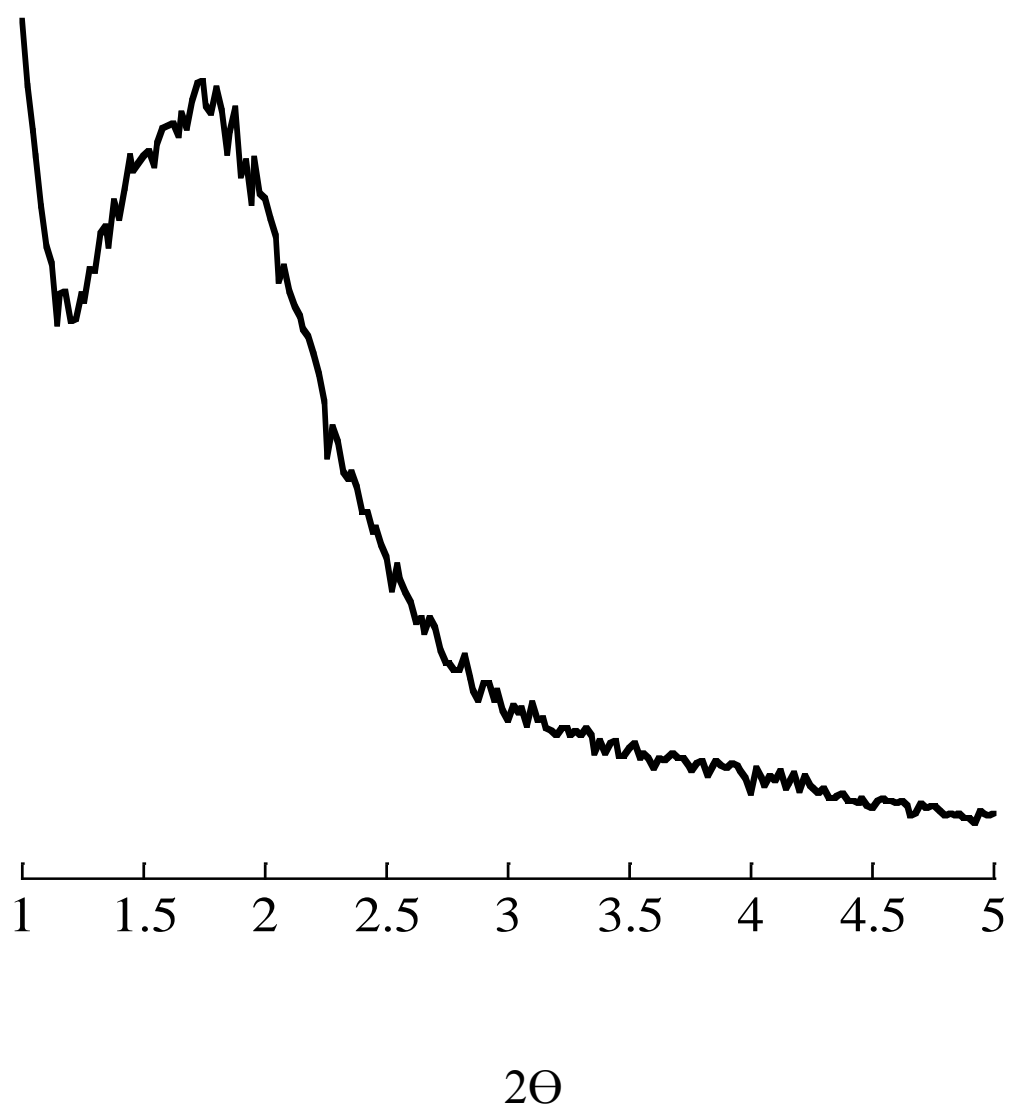


Figure 3.3 Low Angle powder X-ray diffraction pattern of mesoporous silica (52 nm).

3.1.2 BET

The surface area, pore volume and pore size distribution can be determined by BET methodology that is based on the physisorption processes of gas molecules on the surface of porous materials. Physisorption is a van der Waals weak interaction (on the order of $20 \text{ kJ}\cdot\text{mol}^{-1}$) between the adsorbate and the substrate. Nitrogen adsorption isotherms developed by Brunauer, Emmet and Teller, are used to determine material surface areas and can be obtained when the gas molecules are adsorbed and desorbed from the surface, and the surface coverage increases at lower temperatures. For the surface area calculation, the volume of a monolayer of adsorbed gas and the area that each gas molecule occupies can be used. Nitrogen and argon are typical gases that are adsorbed on the surface of studied materials. For zeolite, external and total surface areas are measured by collecting a BET isotherm for the sample before and after calcination.

In a typical nitrogen sorption isotherm, the first seven data points of the adsorption are used for BET surface area calculation. On this isotherm the highest adsorption point is indicative of the total pore volume. The adsorption, desorption or both curves can be used for pore size distribution calculations.

The nitrogen adsorption isotherm (Nova 1200, Quantachrome) was measured to calculate specific surface area and particle size (in the case of as-synthesized crystals) for silicalite samples. The external surface area, S_{ext} , of silicalite nanoparticles was obtained using the BET method on the as-synthesized samples, in which the template is still present in the pores. As described previously in the literature [46], the BET external surface area can be used to calculate the silicalite crystal size assuming uniform cubic crystals by using the following equation:

$$x = 3214/S_{\text{ext}} \quad [12]$$

where S_{ext} is the external surface area in m^2/g and x is the silicalite-1 crystal diameter in nm ($92 \text{ m}^2/\text{g}$). Using the BET method on the calcined silicalite and mesoporous silica samples, the total specific surface areas for each sample have been measured and reported in Table 3.1.

Table 3.1 Organic Loadings (mmol/g)^b Calculated from TGA Data, Particle Size Estimated from TEM Image (nm)^c and BET Specific Surface Area (m^2/g)^a.

Functional group	Silicalite-1	MSN
APDMMS (mmol/g) ^b	0.27	1.13
APTES (mmol/g) ^b	0.46	0.62
MPTMS (mmol/g) ^b	0.3	1.00
SEM, TEM based particle size (nm) ^c	35 (± 7)	52 (± 7)
BET Total Surface area (m^2/g) ^a	302	1088

3.1.3 SEM and TEM

Scanning and transmission electron microscopy (SEM and TEM) are used to analyze particle size and shape, surface morphology, degree of aggregation, and other important properties of crystalline nanomaterials. Electron microscopy utilizes the fact that the wavelength of electrons is much smaller than the wavelength of visible light and this offers increased resolutions of nanomaterials. The focused beam of electrons passing through a series of magnetic lenses and apertures “illuminates” the sample deposited on a thin metal grid typically coated with a thin layer of carbon and collected at the detector. The lattice fringes can be seen in the particles, and can be used to estimate the sample crystallinity.

By using scanning electron microscopy SEM, where secondary electrons are collected at the detector when the focused electron beam passes through the specimen surface, one can obtain some information about the surface morphology. Zeolite samples are often coated with a thin layer (several nanometers) of conductive material, to prevent artifacts in the image that are due to the charge gained from the electron beam. This happens because the zeolite surface is nonconductive and consists of atoms with low atomic numbers.

TEM images of the silicalite-1 crystals, shown in Figure 3.4, were obtained using a Hitachi S-4800 scanning electron microscope. To prepare the sample for SEM, a drop of dilute colloidal solution of the sample in methanol was dropped onto the SEM sample stud surface, and the sample stud was then dried for 15 min at room temperature. Shortly before acquiring an SEM image, the sample was coated with gold.

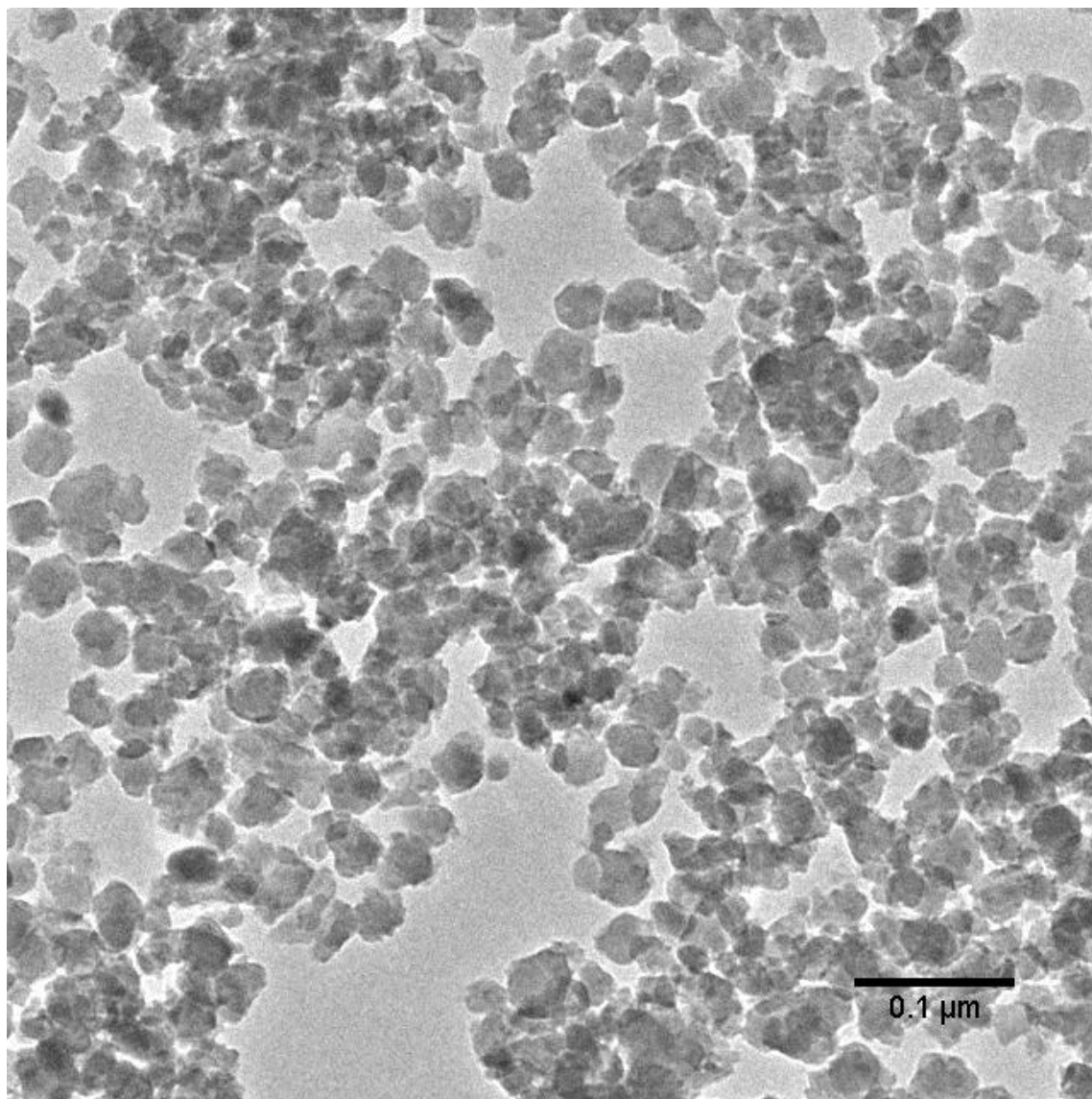


Figure 3.4 SEM image of silicalite-1 functionalized with APDMMS. Particle size is approximately 35 nm.

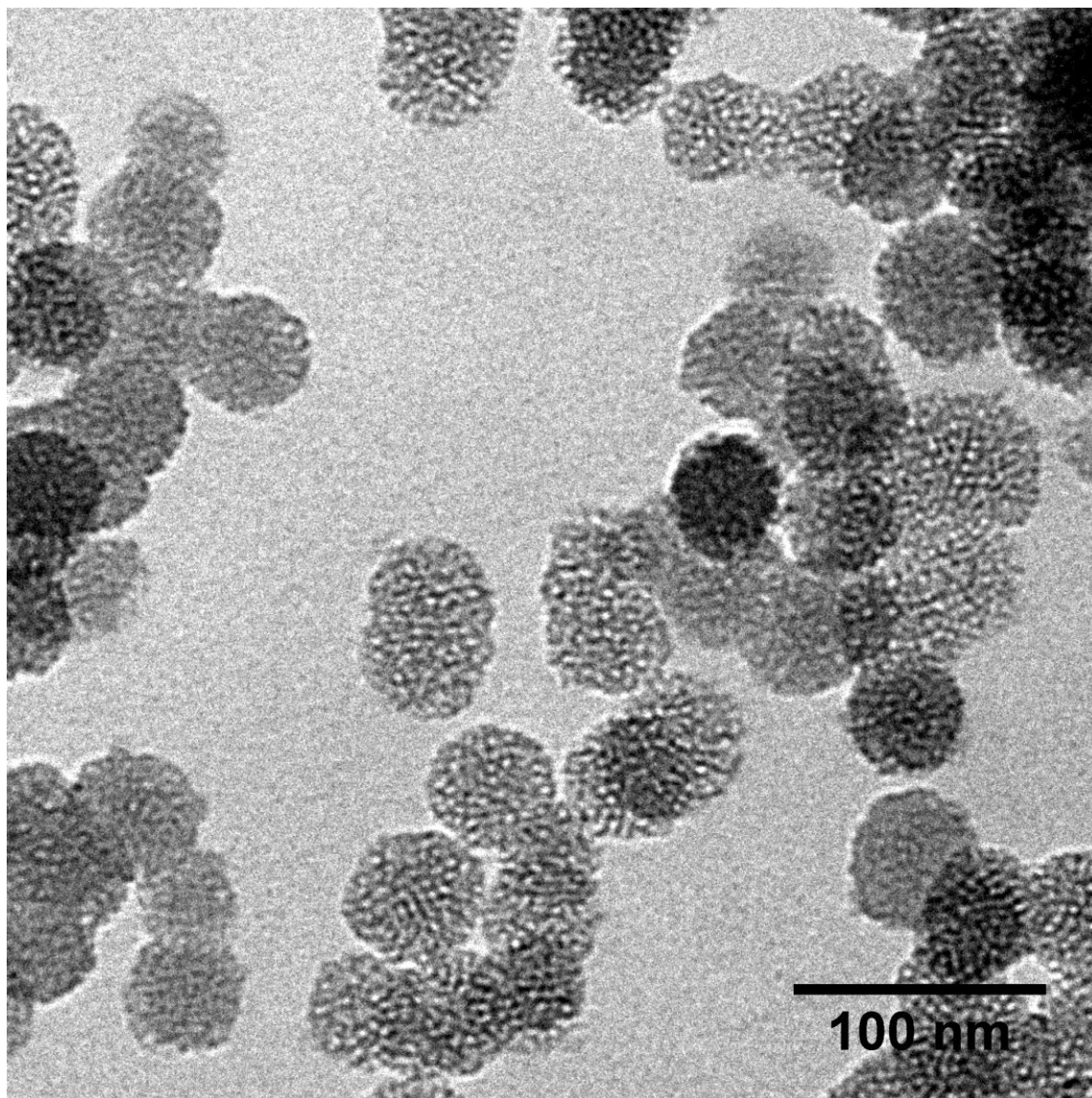


Figure 3.5 TEM image of mesoporous silica nanoparticles. Particle size is approximately 52 nm.

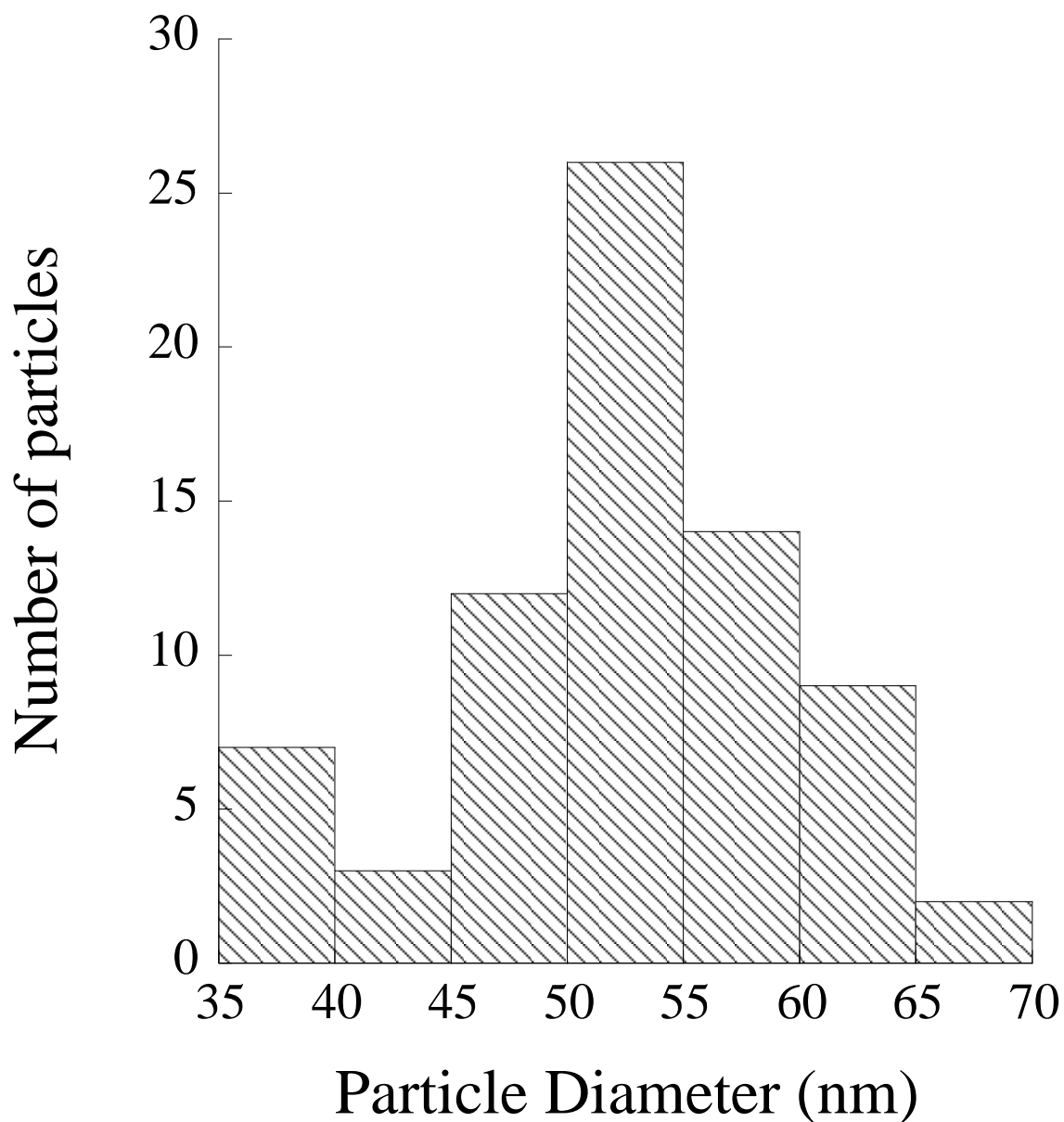


Figure 3.6 Histogram for mesoporous silica particle size distribution with average particle size 52 ± 7 nm, derived by counting over multiple TEM images. A total of 70 particles were analyzed.

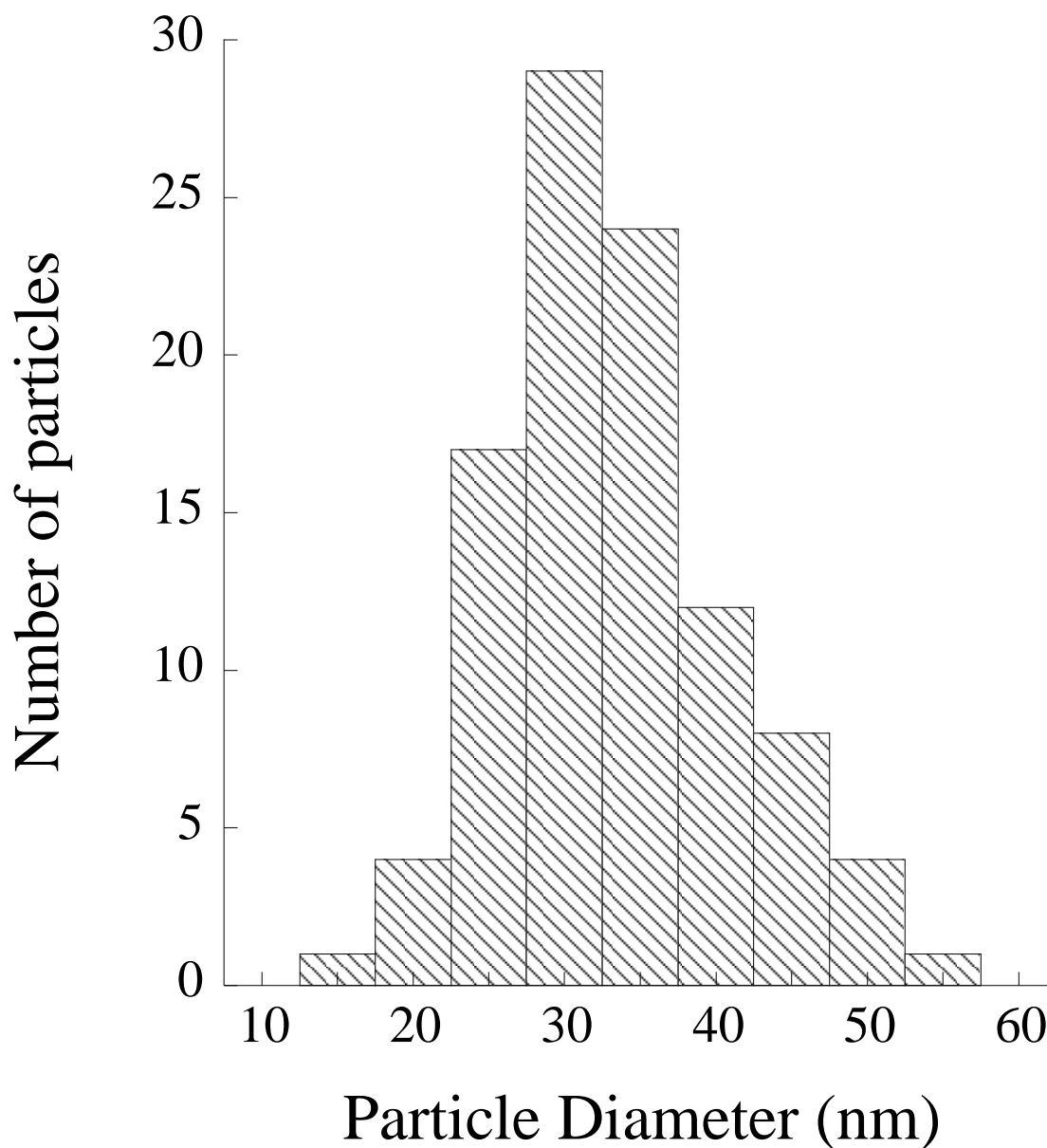


Figure 3.7 Histogram for silicalite-1 particle size distribution with average particle size 35 ± 7 nm, derived by counting over multiple TEM images. A total of 114 particles were analyzed.

For TEM imaging of MSN, a JEOL JEM-1230 Transmission Electron Microscope was used. For sample preparation the following method has been utilized. A drop of dilute sample suspension in methanol was placed on a holey carbon film (Ted Pella) and dried at room temperature prior to the measurement.

TEM and SEM images allowed us to assess the particle size and standard deviation of the zeolite nanocrystals and mesoporous silica nanosubstrates. The SEM and TEM images of both samples (Figure 3.4, 3.5) show typical morphological characteristic of silicalite-1 and MSN respectively. As shown in Table 3.1 the particles have an average size of 35 nm and 52 nm for silicalite and MSN respectively. The standard deviation from the average particle size was 7 nm in both cases.

3.1.4 ζ -Potential Measurements

The surface charge of functionalized and unfunctionalized silicalite and MSN nanomaterials has been investigated using the Zetasizer Nano-ZS (Malvern Instruments). The samples were prepared in the following way: 4 mg of sample was placed in disposable plastic tubes. Four milliliters of aqueous solutions (pH 2 - 12) with matching ionic strengths was added to the silicalite powder, and the resulting suspensions were sonicated for 1 h (1510 Sonicator, Branson). The suspensions were allowed to settle overnight, and their pH (Corning pH meter 320) was checked prior to and immediately after the ζ -potential measurements (Zetasizer Nano-ZS, Malvern Instruments).

The ζ -potential method measures the surface charge of the particles in solution as a function of pH. The variation of the ζ -potential with pH is shown in Figure 3.8 for APDMMS functionalized silicalite-1. The ζ -potential demonstrates identical behavior

of functional groups for both silicalite-1 and MSN with varying pH. The ζ -potential of functionalized silicalite (silica) ranged from -25 to +28 mV for the varying pH's (2-12), revealing that the functional groups were located on the surface and were deprotonated as pH of the overall solution increases.

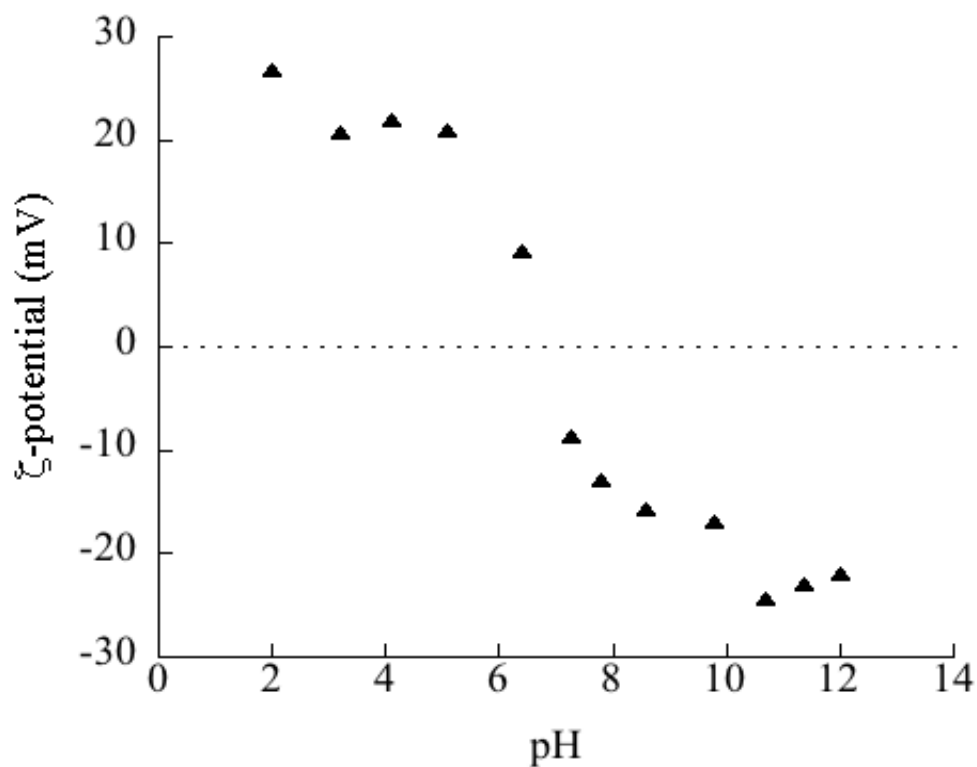


Figure 3.8 ζ -Potential measurements of APDMMMS functionalized silicalite-1 as a function of pH.

Functionalization of the silicalite surface results in surface charge changes depending on the organic groups deposited on the surface. Indeed, the ζ -potential for APDMMS-functionalized silicalite (MSN) is governed by the equilibrium involving the protonation of the surface amine groups. A positive shift of ζ -potential can be observed as a result of functionalization of silicalite with APDMMS in comparison with calcined silicalite samples. The fact that ζ -potential for APDMMS-silicalite-1 is more positive than the ζ -potential for the calcined silicalite (MSN) and ranged from approximately -25 to +28, indicates that the amine groups get protonated in this range of pH (around 10-11) and is in agreement with alkylamine behavior in aqueous solutions.

3.1.5 TGA

Thermogravimetric analysis analysis (TGA) can provide information about physical phenomena, such as second-order phase transitions, including vaporization, sublimation, absorption, adsorption, and desorption. This method detects the mass change of a substance measured as function of temperature during the heating process. While the temperature increases, various components of the sample are decomposed and mass change is measured. Resulting graphs with temperature on the X-axis and mass loss on the Y-axis can be analyzed and the percentage of surface deposited species can be determined.

After functionalization with different functional groups (amino and thiol), the silicalite-1 and MSN samples were further characterized by thermogravimetric analysis to estimate the functional group loading on the surface of host particles. TGA was employed for each sample by heating it from room temperature at 1.0 °C/min to 800 °C

under nitrogen. Resulting graphs were analyzed and the extent of functionalization has been estimated in mmol/g for each sample (Table 3.1). Surface functionalization percentage (the percentage of silanol reactive groups on the external surface that bound to organic guest molecules) has been calculated assuming 1 surface binding site (silanol group) to 1 APDMMS molecule ratio.

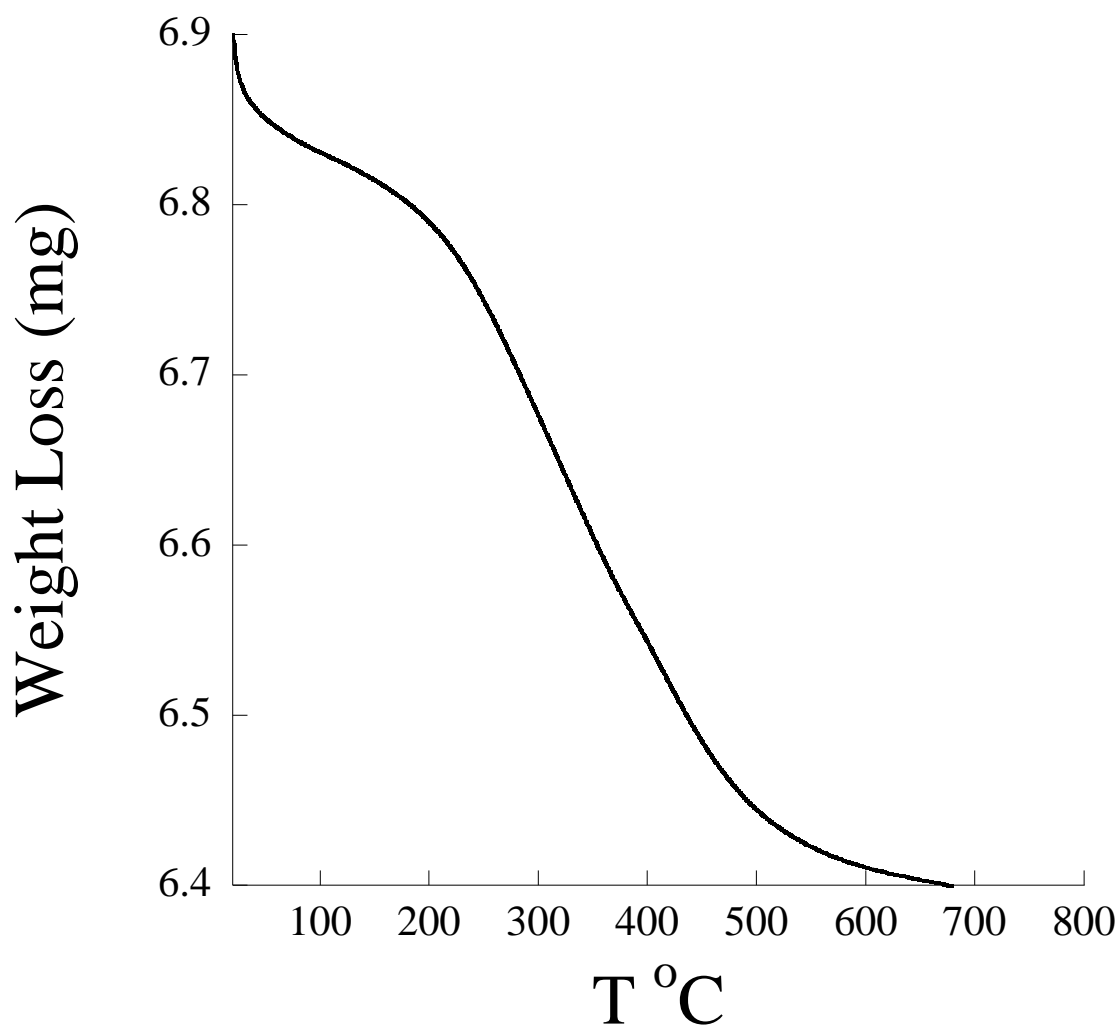


Figure 3.9 TGA graph for APDMMS functionalized silicalite-1.

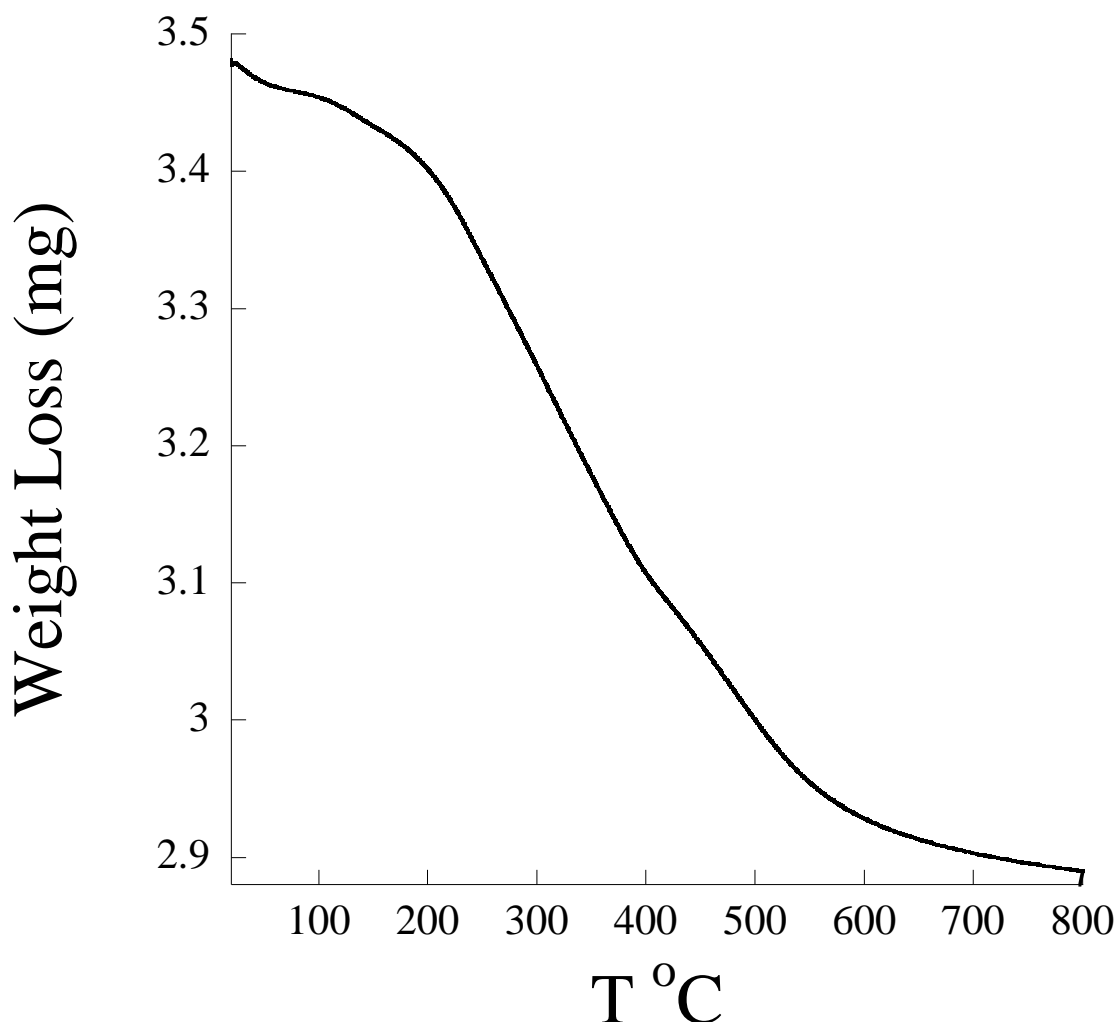


Figure 3.10 TGA graph for APDMMS functionalized MSN.

3.1.6 FTIR

Fourier Transform Infrared (FTIR) Spectroscopy was used to analyze APDMMS functionalized silicalite-1 samples in order to corroborate the presence of APDMMS functional groups on the surface of nanoparticles. Samples were analyzed using a KBr pellet and a Nicolet Nexus 670 FT-IR (Thermo Electron Company) instrument. The spectra were recorded in the range of 400-4000 cm^{-1} . The resulting spectrum can be seen in Figure 3.11. The position of vibrational stretching frequencies for particular

functional groups is governed by mass effect and the force constant effect. Hydrogen bonding, the neighboring functional groups and coupled vibrations also influence the position of the vibrational stretching frequencies.

Obtained FTIR spectrum of APDMMS functionalized silicalite-1 corroborates the presence of organic molecules attached to the surface of nanoparticles. Vibrational peaks are observed in the C–H stretching region around 2900 cm^{-1} . This spectrum shows peaks at 2962 , 2918 and 2852 cm^{-1} that are characteristic of the presence of –CH stretching vibrational bands mainly associated with the propyl group introduced by the functionalization of the nanoparticle surface with APDMMS.

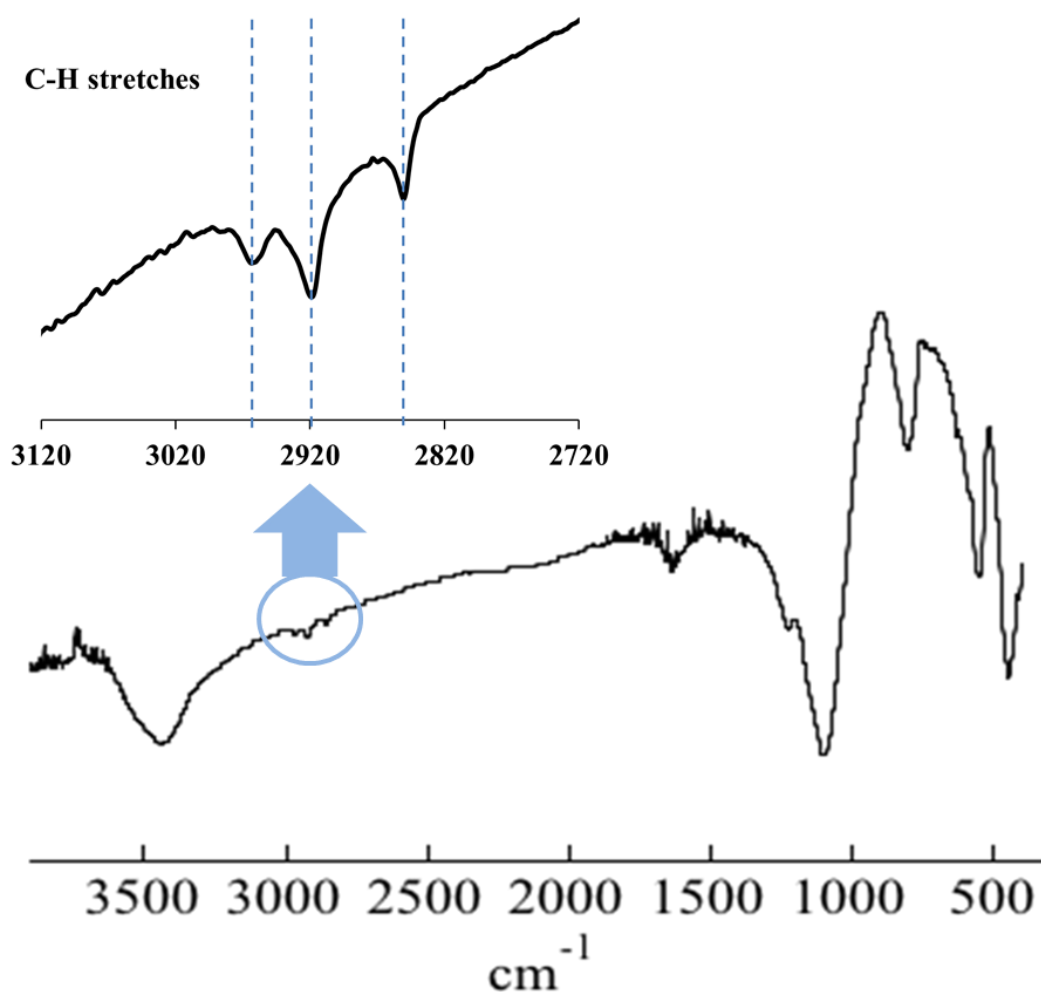


Figure 3.11 FTIR spectrum of APDMMS functionalized silicalite-1

3.1.7 Solid State NMR (^1H , ^{29}Si , ^{13}C)

Solid state NMR spectroscopy has been used to characterize functionalized nanoparticles and confirm the presence of functional groups on the surface of nanomaterials. A Bruker Avance 500 MHz spectrometer operating at 11.744 T (125.7 MHz for ^{13}C) was used to record ^{13}C and ^1H magic angle spinning nuclear magnetic resonance (MAS NMR). Samples were loaded in a 4 mm zirconia rotor and spun at 12 kHz to obtain ^{13}C MAS NMR. For ^1H MAS NMR, a 2.5 mm rotor was used and 30 kHz spinning applied. A 300 MHz (6.9 T) wide bore magnet spectrometer (Varian) with a TecMag Discovery Console was used to record ^{29}Si magic angle spinning nuclear magnetic resonance (MAS NMR). The ^{29}Si MAS NMR spectra were collected at a Larmor frequency of 59.621 MHz. About 250 mg of sample was loaded in a 7 mm zirconia rotor and spun in a Chemagnetics pencil probe at 7 kHz.

Solid state (^{13}C , ^1H , ^{29}Si) MAS NMR spectra of APDMMS functionalized silicalite-1 are shown in Figures 3.10, 3.11, and 3.12, respectively. ^{29}Si MAS NMR provides information about silicon atoms with different environments. Indeed, surface functionalization of zeolites with organosilanes such as APDMMS, APTES, and MPTMS results in the chemical shift of silicon atoms in a silane to be significantly different from those in the zeolite framework. For example, the chemical shift at approximately 10 ppm in Figure 3.14 comes from APDMMS molecules attached to the zeolite surface. The peaks arising from the presence of functional groups can be used to estimate the amount of organic molecules on the surface of studied materials by integrating the silane peak and dividing the area by the sum of integrated intensities of all silicon atoms in the sample.

A framework silicon peak is observed at -113 ppm and a second peak attributed to the silicon atom from the APDMMS is observed at ~ 10 ppm, which is indicative of the amine groups grafted on the nanomaterials surface. The intensity of the 10 ppm is proportional to the amount of functionalization of the zeolite surface and can be seen to increase with increasing APDMMS concentration. The solid state ^{29}Si MAS provides spectroscopic evidence that the functionalization occurs at the silanol groups on the nanosubstrate surface.

Silicon atoms located in the zeolite framework and connected to other silicon can environment, the respective peak located at -113 ppm is the most intense. Silicon atoms located on the surface, at defect sites, or in the pores of nanoparticles have one or more hydroxyl groups attached to them. Two resonances at -113 and -105 ppm could be attributed to ^{29}Si nuclei having four Si-O-Si linkages and ^{29}Si nuclei having three Si-O-Si linkages and one $-\text{OH}$, respectively.

Additionally, ^{13}C and ^1H solid-state NMR spectroscopy was employed to study the organic components of the synthetic hybrid materials. ^{13}C and ^1H MAS NMR spectra of the APDMMS-silicalite materials, presented in Figure 3.12 and 3.13, respectively, were obtained for functionalized materials and corroborated the presence of organic species on the surface of nanomaterials.

Examination of $^1\text{H}/^{13}\text{C}$ cross-polarization/magic angle spinning solid-state NMR spectrum (Figure 3.12) reveals that all samples exhibited peaks attributed to the different C atoms of the organic amino functional groups. As expected, the signals ranging within $10\text{--}60$ ppm attributed to the carbon atoms of the propyl groups were observed in the case of APDMMS-silicalite-1 materials [57-60]. The chemical shifts of the three carbons

in the APDMMS molecules ($\text{NH}_2\text{-CH}_2(3)\text{-CH}_2(2)\text{-CH}_2(1)\text{-Si-}$) were found at 43, 22, and 11 ppm, respectively. The chemical shift of the methyl carbons $\text{CH}_3\text{-Si-CH}_3$ was observed at ~0 ppm [61].

As can be seen from ^1H MAS spectra in (Figure 3.13), there are peaks at chemical shifts spanning the range from about 7 ppm to about 0 ppm. An identification of a major part of the ~ 6-5 ppm spectral contributions is hydrogens due to multi-layer or bulk water on the nanoparticle surface in regions below the hydrophobic organic surface or in the pores between the particles and silanol groups on the surface of nanomaterials [62]. This kind of hydrogen is essentially immobile, so the $^1\text{H}\text{-}^1\text{H}$ interactions between them are not averaged by atomic-level motion and are expected to give a characteristic broadening. Small peaks, that are responsible for protons from organic functionalities bound to the surface, are found between 0 and 4 ppm. They overlap with the adjacent broad “framework” signals and result in a reduced resolution spectrum.

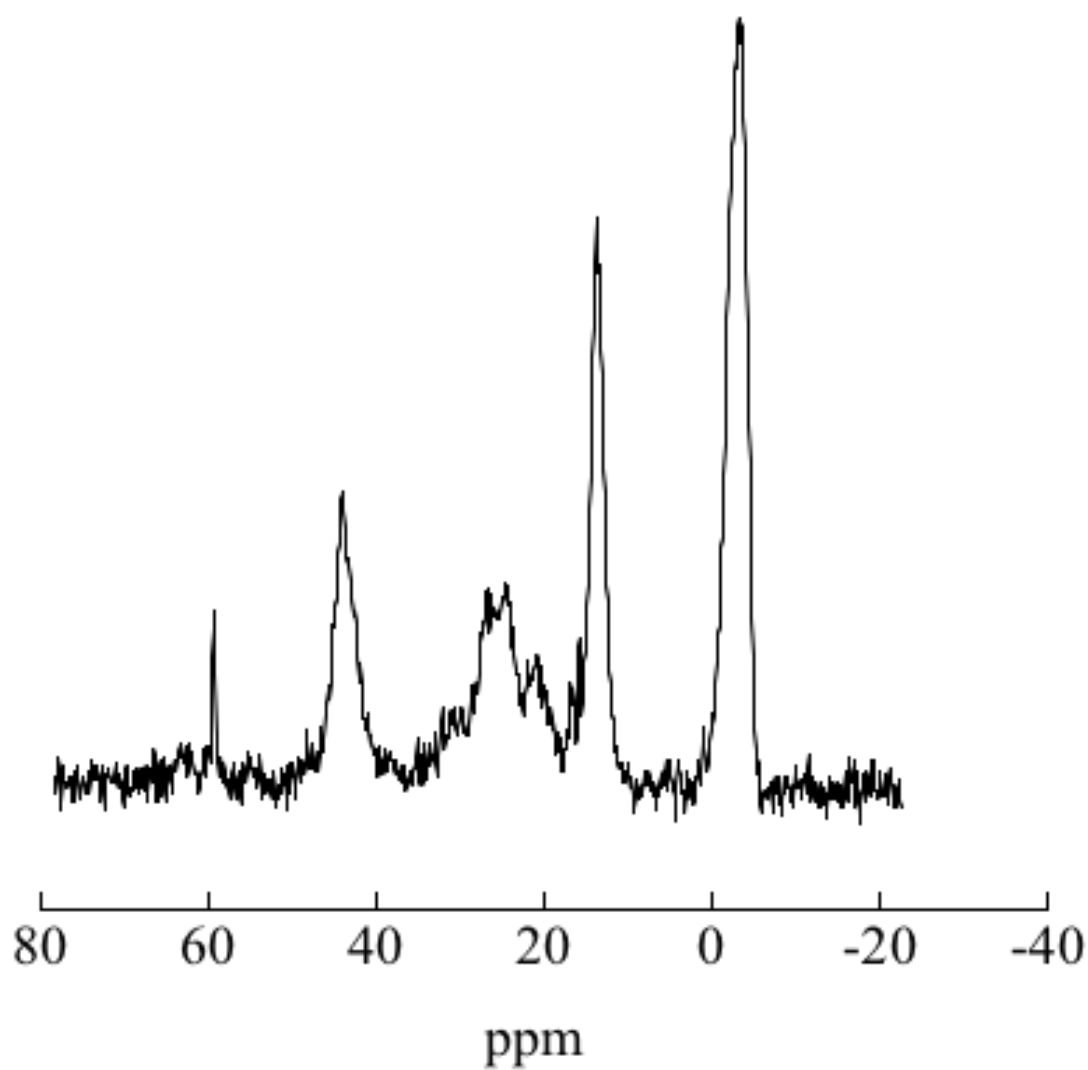


Figure 3.12 Solid state NMR ^{13}C - ^1H CPMAS spectrum of APDMMS functionalized silicalite-1.

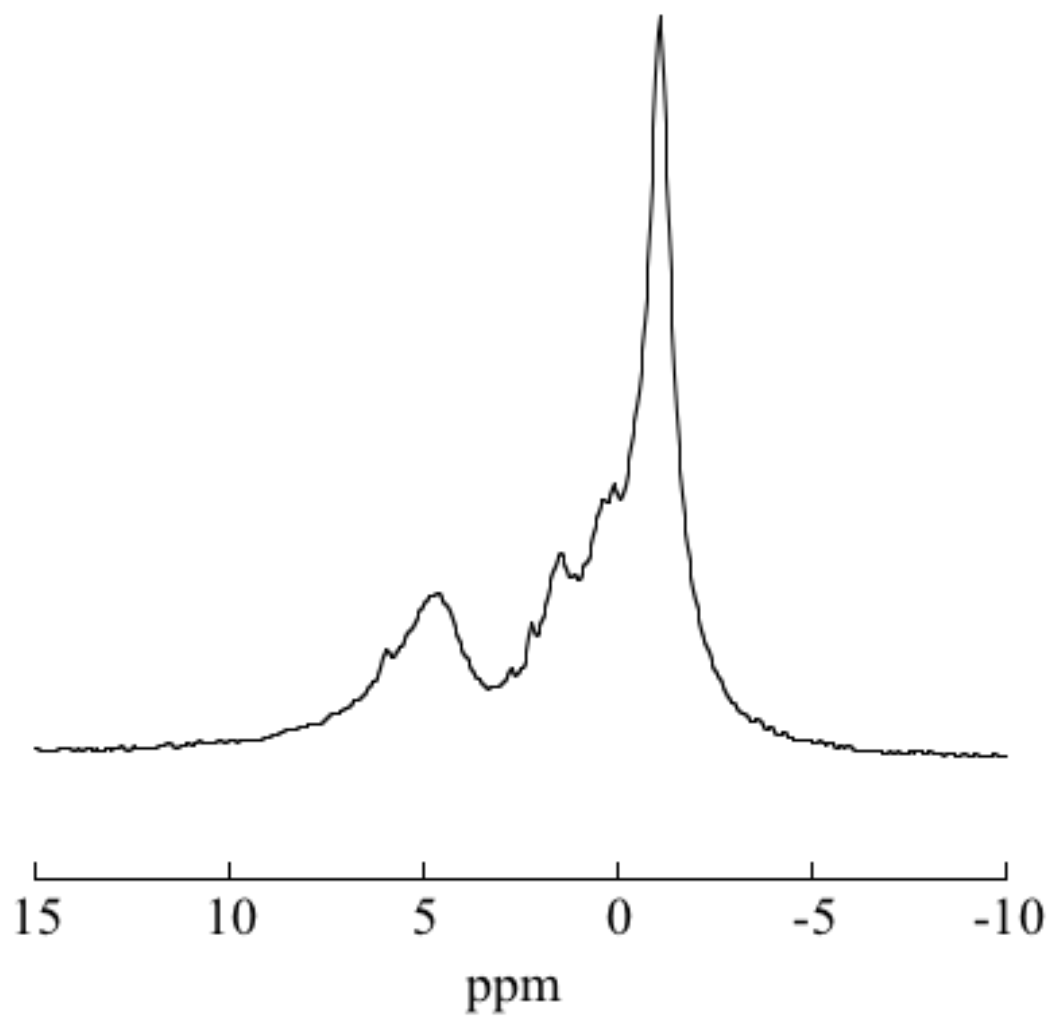


Figure 3.13 Solid state ^1H MAS spectrum of APDMMS functionalized silicalite-1.

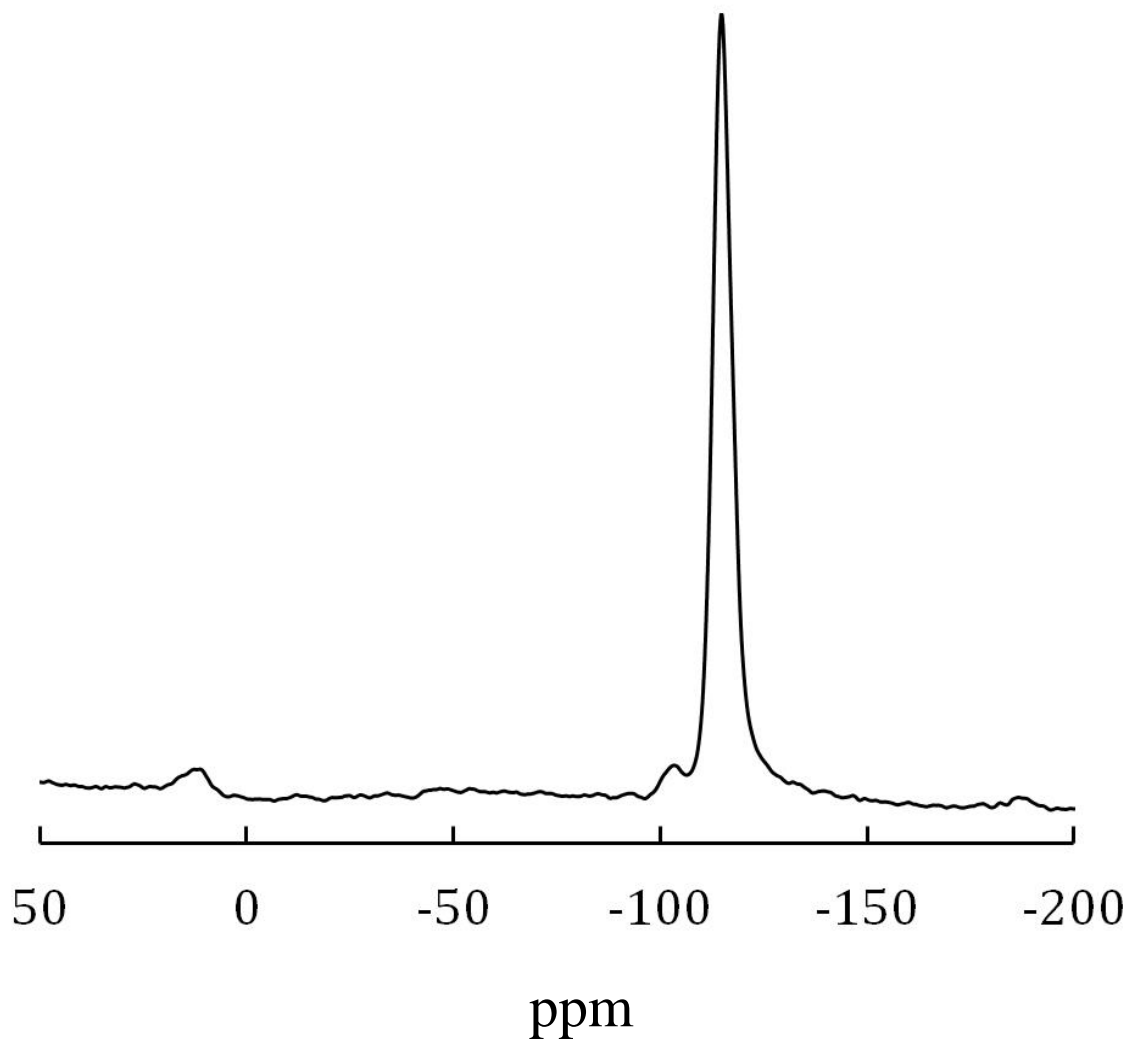


Figure 3.14 Solid state ^{29}Si MAS spectrum of APDMMS functionalized silicalite-1.

CHAPTER 4

pKa DETERMINATION FOR SURFACE BOUND FUNCTIONAL GROUPS AND FREE MOLECULES IN D₂O USING ¹H SOLUTION NMR TITRATIONS

4.1 Abstract

The surface chemistry of zeolite nanoparticles functionalized with the organosilanes: 3-aminopropyldimethylmethoxysilane (APDMMS), 3-aminopropyltriethylethoxysilane (APTES), and 3-mercaptopropyltrimethoxysilane (MPTMS), was selectively probed using solution ¹H NMR spectroscopy. The use of solution NMR spectroscopy results in high resolution NMR spectra and the technique is selective for protons on the surface organic functional groups due to their motional averaging in solution which causes significant line-narrowing. In this study, ¹H solution NMR spectroscopy was used to investigate the interface of the organic functional groups of APDMMS (APTES, MPTMS) functionalized silicalite (~35 nm) and mesoporous silica nanoparticles (MSN) (~52 nm) in D₂O. The pKa for the amine group of APDMMS (APTES) and the thiol group (-SH) of MPTMS functionalized silicalite nanoparticles and MSN in D₂O was determined using an NMR-pH titration method based on the variation in the proton chemical shift for the alkyl group protons closest to the amine (or thiol) group with pH. The resulting NMR spectra demonstrate the sensitivity of solution NMR spectroscopy to the electronic environment and structure of the surface functional groups.

4.2 Introduction

Nuclear Magnetic Resonance (NMR) spectroscopy is a widely used analytical technique for investigating a broad range of chemical systems. Solution NMR methods are routinely employed to identify organic products of synthetic reactions and to probe

structure in large biomolecules. When solution samples are not readily available, solid-state magic angle spinning (MAS) NMR spectroscopy provides structural insights for a range of solid systems but the resolution is generally reduced relative to solution phase NMR spectroscopy. Despite the decreased resolution, solid state MAS NMR spectroscopy is often the NMR technique of choice for studying solid phase nanomaterials.

A useful strategy in nanotechnology is the functionalization of nanomaterials to tailor the properties for specific applications. Many characterization methods for functionalized nanomaterials present challenges associated with differentiating surface and bulk chemical species. Solution NMR techniques have been used to selectively probe the surface structure and composition of functionalized nanoparticles in colloidal solutions [17, 18, 63-66]. The fast rotational motion of the organic functional groups on the surface of the nanoparticles in solution reduces the line-broadening to the extent that NMR spectra of the surface functional groups can be observed using solution NMR techniques. For example, solution NMR studies of functionalized gold nanoparticles have been used to elucidate the organic substituents and ligand exchange reactions on gold surfaces [17-22]. Not only does solution NMR provide excellent spectral resolution, but it is also selective for surface protons because bulk protons are not motionally averaged and therefore not observed in solution NMR spectroscopy. Solution NMR techniques have been used to study functionalized gold nanoparticles and metal oxide nanoparticles but there are no reports of using these methods to study functionalized porous nanomaterials, such as zeolites or mesoporous silica. In porous aluminosilicate and silicate materials, it is particularly advantageous to be able to

differentiate surface and bulk proton signals. These solution NMR methods applied to nanomaterial systems also have great potential for studies of environmental or biological interfaces involving nanoparticle surface processes.

Porous nanomaterials [2, 23-26], such as zeolites and mesoporous silica, have emerged as nanomaterials with new properties and many potential applications, in areas such as environmental catalysis [27], drug delivery [28, 29], imaging [30-34] and other biomedical applications [35, 36]. While the large internal surface area of these materials has traditionally been exploited for applications in catalysis and ion-exchange, porous nanoparticles also have large external surfaces that can be tailored for specific applications in biomedicine [37-39] or adsorption [40, 41]. Characterization of the surface structure of the functionalized zeolite nanoparticles is critical in developing an understanding of the surface chemistry and the environmental and biological interfaces that result from applications of these materials. Information about surface structure and composition can also be used to design functionalized nanomaterials with specific applications.

4.3 Experimental Methods

Nanocrystalline silicalite-1 (~35 nm crystal size), the purely siliceous form of the zeolite ZSM-5 with the MFI structure, and mesoporous silica nanoparticles (~52 nm) were synthesized [25, 26, 54]. Both samples were characterized by powder XRD (Siemens D5000 X-ray diffractometer with Cu K α and nickel filter) to determine crystallinity. The surface area of the as-synthesized MSN and silicalite-1 was measured using the BET method on a Nova 1200 Nitrogen Adsorption Instrument (Quantachrome). Approximately 100 mg of silicalite was dried overnight at 120 °C

under vacuum. A 7-point BET isotherm was obtained and the specific surface area was calculated for the sample. The samples were calcined at 600 °C for 12 hours.

Nanozeolites and MSN were functionalized [48] with 3-aminopropyldimethylmethoxysilane (APDMMS), 3-aminopropyltriethylethoxysilane (APTES), or 3-mercaptopropyltrimethoxysilane (MPTMS). Functionalized materials were characterized by powder X-ray diffraction (XRD), scanning electron microscopy (SEM), transmission electron microscopy (TEM), zeta-potential, thermal gravimetric analysis (TGA) and nitrogen adsorption isotherms. The external surface area of the as-synthesized silicalite-1 (with the organic template still in the pores) was 91 m²/g. The external surface area was used to estimate the size of the silicalite crystals as 35 nm according to a previously derived formula: $x = 3214/S_{\text{ext}}$, where x is the silicalite-1 crystal size in nm and S_{ext} is the measured external specific surface area in m²/g assuming cubic crystals [54]. The size was also confirmed by SEM and TEM images (shown in Figure 3.4 and 3.5). The characterization data and experimental details are provided in Chapter 2 and 3.

The surface of calcined silicalite and MSN was covalently modified with APDMMS (APTES, or MPTMS). The functionalization procedure was described previously in Chapter 2. The functionalization of nanomaterials with APDMMS is shown schematically in Figure 2.1 (Chapter 2). The functionalized MSN and silicalite-1 samples were characterized by ²⁹Si, ¹³C, ¹H solid NMR, (see Figures 3.10-3.12), and thermal gravimetric analysis (TGA) to assess the functional group loadings. Resulting TGA data were also presented previously in Chapter 3.

Samples were prepared for proton solution NMR experiments by dispersing approximately 10 mg of functionalized silicalite-1 (MSN) in 0.6 mL of D₂O. The pH was adjusted by adding NaOH or HNO₃ to the NMR sample tube. The pH was measured before and after the NMR experiment using a Corning 320 pH meter and the average of the two values was used in subsequent data analysis. The pH reading obtained before and after each NMR experiment differed by <0.1 pH units. The NMR samples were sonicated for approximately 0.5 hour immediately before the NMR experiments. The proton NMR experiments were conducted on a Bruker DRX-400 Instrument operating at 400 MHz. Single pulse ¹H and ¹H relaxation NMR experiments were performed. Single pulse experiments were performed with a pulse width of 7 μs and a recycle delay of 0.01 s with 128 scans. Inversion recovery (π - τ - $\pi/2$ -acquisition] experiments were conducted to measure the spin-lattice relaxation time (T₁).

4.4 Results and Discussion

4.4.1 Free Organic Molecules vs Surface Bound Functional Groups

¹H NMR spectroscopy was used to characterize APDMMS (APTES, or MPTMS)-functionalized silicalite-1 and MSN. For comparison, ¹H NMR spectra were obtained for APDMMS (APTES, or MPTMS) in D₂O. The solution proton NMR spectra of silicalite, APDMMS functionalized silicalite and APDMMS in solution, all in D₂O at pH~7, are shown in Figure 4.1 A-C, respectively. The proton NMR spectrum of unfunctionalized silicalite is shown in Figure 4.1A and only the solvent water peak is observed. No signals due to bulk or surface protons are observed for silicalite in D₂O presumably due to the lack of free rotation for surface hydroxyl groups.

The proton NMR spectrum of APDMMS-functionalized silicalite is shown in Figure 4.1B and peaks due to the protons in the functional group are observed as labeled on the inset molecule. The proton NMR spectrum for the surface groups of APDDMS-functionalized silicalite are observed due to the free rotation of the organic functional groups on the nanoparticle surface. Only the surface protons are observed in the solution spectrum because the protons located in the bulk nanoparticle are not free to rotate in solution and thus the resonances are too broad to be observed in solution NMR spectra. The amine protons are not observed due to hydrogen bonding with the solvent. The top spectrum (Figure 4.1C) is for APDMMS in D₂O and proton resonances due to the protons are observed in the NMR spectrum as labeled. The proton signal from the methoxy group (peak 4) is observed at 3.34 ppm in the spectrum of APDMMS in D₂O but is absent from the spectrum of APDMMS-functionalized silicalite because it is the leaving group in the surface functionalization reaction.

4.4.2 T₁/T₂ Measurements

The spin-lattice relaxation rate (T₁) was also measured for APDMMS and APDMMS-functionalized silicalite. T₁ values for each group of hydrogens and are listed in Table 4.1. The measured T₁ values for protons that are in close vicinity to the functional group were 1.9 s for APDMMS and 0.8 s for APDMMS-functionalized silicalite. The T₁ decreases for the surface bound functional group as expected due to the decrease in motion relative to the free APDMMS. Previously, Rivas-Cardon and Shantz measured T₁ values for alkyltripropylammonium silica mixtures and found that T₁ decreased with increasing silica concentrations in the mixtures of alkyltripropylammonium cations and silica [67-69].

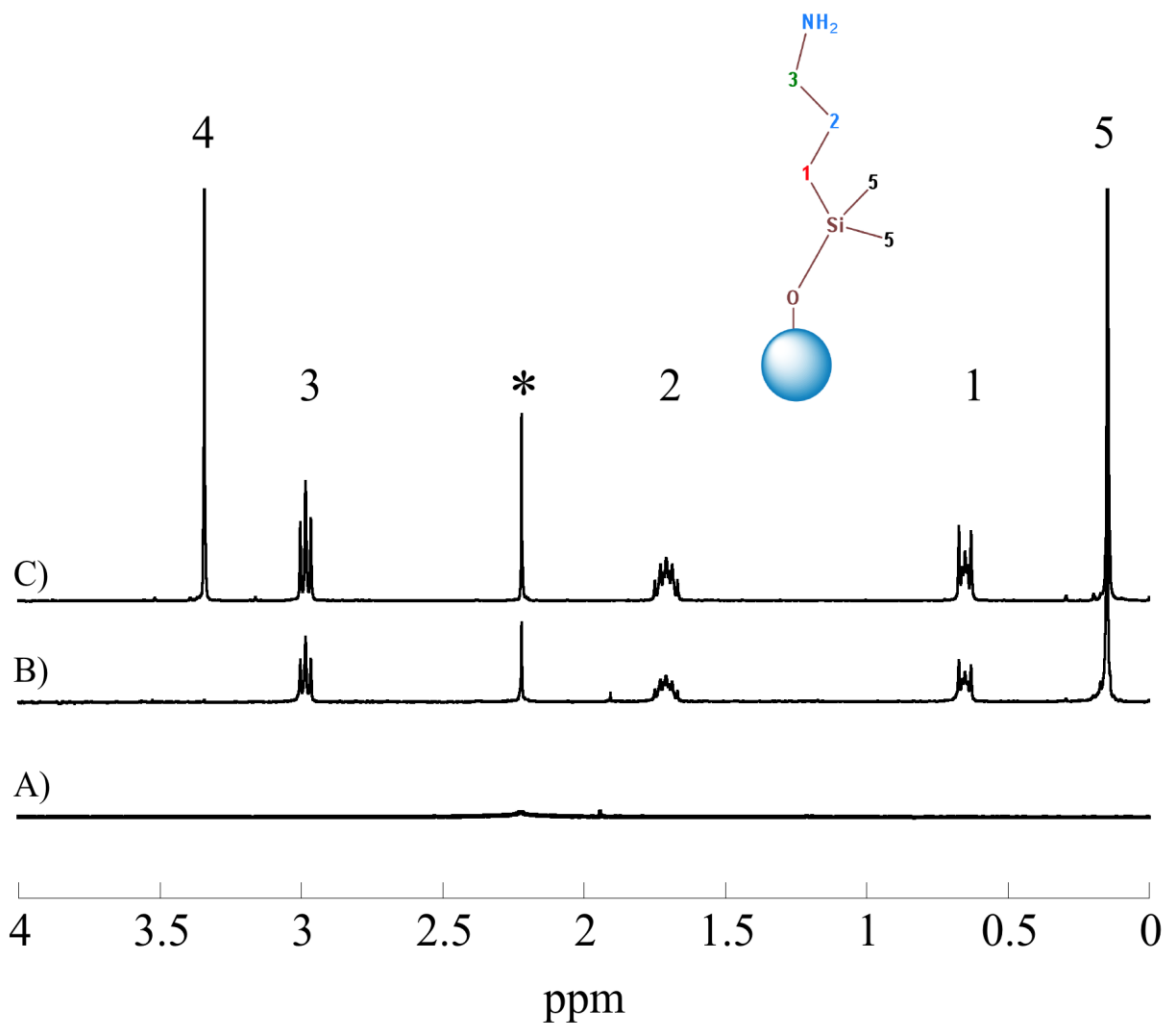


Figure 4.1 Proton solution state NMR spectra (at pH=7) of: A) silicalite-1 in D_2O , B) APDMMS-functionalized silicalite-1, C) APDMMS in D_2O . * is a peak assigned for acetone that was used as an internal standard for all ^1H solution state MNR experiments. 1, 2, 3, and 5 are peaks due to the protons in the functional group on the inset molecule.

Table 4.1 The longitudinal relaxation time (T_1) (in seconds) for APDMMS and APDMMS functionalized silicalite-1 sample.

	Protons 1 ^a	Protons 2 ^b	Protons 3 ^c	Protons 5 ^d
APDMMS in D ₂ O	1.8	1.9	1.9	2.5
APDMMS-silicalite-1 in D ₂ O	0.9	0.8	0.8	---

^a Protons that are closest to the surface (in position 1) according to the proton NMR spectral assignments as shown in the molecular scheme in Figure 4.1,

^b Protons in position 2 (Figure 4.1),

^c Protons (in position 3) that are closest to NH₂ (Figure 4.1),

^d Protons in position 5 (Figure 4.1).

Table 4.2: Proton Chemical Shift Assignments for APDMMS at pH=7 in D₂O.

Resonance	Chemical Shift (ppm)- APDMMS	Chemical Shift (ppm)- APDMMS- silicalite-1	Multiplicity	Assignment
1	0.65	0.65	triplet	Si-CH ₂ -CH ₂ - CH ₂ -NH ₂
2	1.71	1.71	quintet	Si-CH ₂ -CH ₂ - CH ₂ -NH ₂
3	2.98	2.98	triplet	Si-CH ₂ -CH ₂ - CH ₂ -NH ₂
4	3.34	--	singlet	-Si-OCH ₃
5	0.15	0.15	singlet	Si(CH ₃) ₂

Table 4.3: Proton Chemical Shift Assignments for APTES at pH=7 in D₂O.

Resonance	Chemical Shift (ppm)-APTES	Chemical Shift (ppm)-APTES- silicalite-1	Multiplicity	Assignment
1	0.71	0.71	triplet	Si- CH ₂ -CH ₂ -CH ₂ - NH ₂
2	1.77	1.77	quintet	Si-CH ₂ - CH ₂ -CH ₂ - NH ₂
3	3.00	3.00	triplet	Si-CH ₂ -CH ₂ - CH ₂ - NH ₂
4	1.72	--	triplet	--Si-OCH ₂ -O CH ₃
5	3.64	--	quartet	--Si-O CH ₂ -OCH ₃

Table 4.4: Proton Chemical Shift Assignments for MPTMS at pH=7 in D₂O.

Resonance	Chemical Shift (ppm)-MPTMS	Chemical Shift (ppm)- MPTMS- silicalite-1	Multiplicity	Assignment
1	0.89	0.89	triplet	Si-CH ₂ -CH ₂ -CH ₂ -S
2	1.70	1.70	quintet	Si-CH ₂ -CH ₂ -CH ₂ -S
3	2.56	2.56	triplet	Si-CH ₂ -CH ₂ -CH ₂ -S
4	3.59	--	triplet	-Si-OCH ₃

4.4.3 pKa Determination

The proton chemical shifts for APDMMS (as well as APTES) vary with pH with the protons closest to the functional group exhibiting the largest shifts as shown in Figures 4.2-4.5. Tables 4.2 and 4.3 list the proton NMR spectral assignments for APDMMS and APTES molecules respectively. This downfield chemical shift displacement reflects a change in amine group protonation. Protonation typically takes place on the time scale of diffusion; therefore in the NMR spectrum, the resonance

observed will be a weighted average of the chemical shifts for the protonated and nonprotonated forms. NMR-pH titrations have been reported in solution NMR studies such that the change in the chemical shift has been used to calculate the pKa value [70-72]. The protons closest to the amine functionality in APDMMS (APTES) experience different electronic environments depending on whether the amine is neutral or protonated. (Figure 4.2 – 4.5) The protons closest to the thiol group in MPTMS revealed similar behavior indicating that deprotonation of the functionality varies the electron environment of neighboring protons and results in its chemical shift displacement. The proton chemical shifts for MPTMS molecules vary with pH as can be seen from Figure 4.6 and 4.7, where the protons closest to the functional group also show the largest chemical shift displacements. Table 4.4 lists the proton NMR spectral assignments for MPTMS molecules.

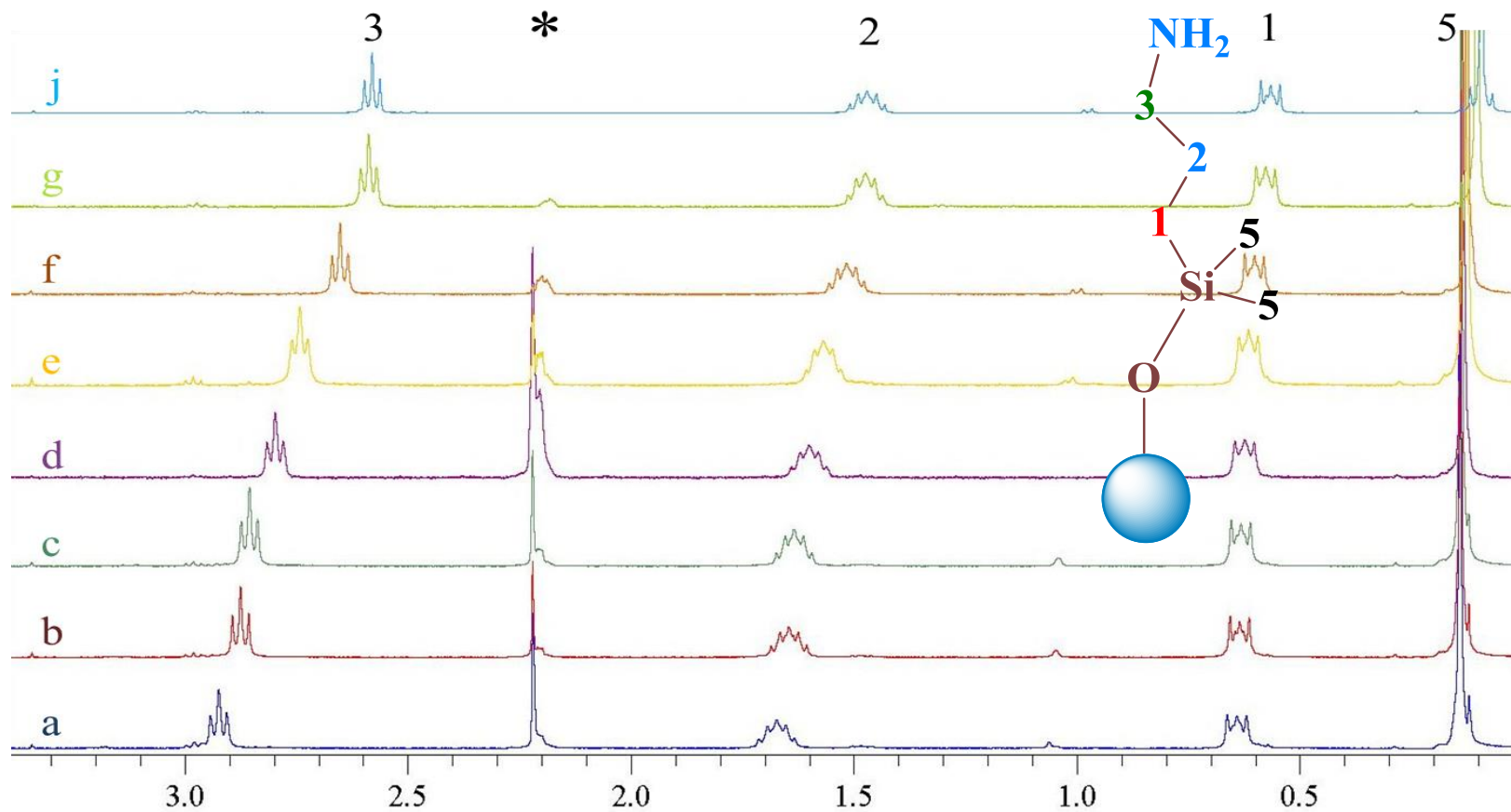


Figure 4.2 Proton solution state NMR spectra for APDMMS-functionalized silicalite-1 in D₂O at varying pH's: a) 10.2, b) 10.4, c) 10.7, d) 10.9, e) 11.1, e) 11.5, g) 12.4, j) 12.6. * is a peak for acetone (used as an internal standard), 1, 2, 3 and 5 are peaks due to the protons in the functional group on the inset molecule.

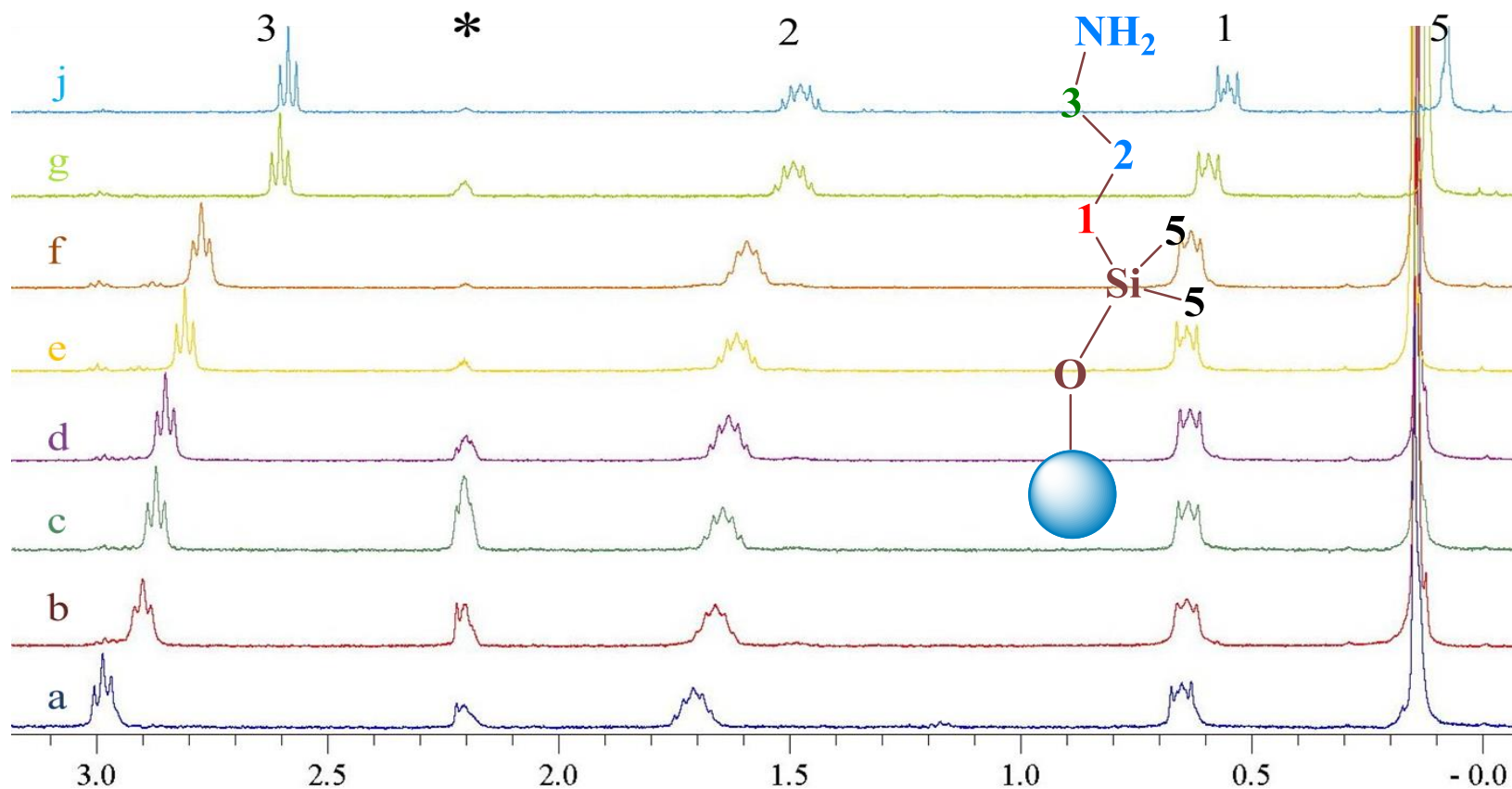


Figure 4.3 Proton solution state NMR spectra for APDMMS-functionalized MSN in D₂O at varying pH's: a) 8.0, b) 10.4, c) 10.6, d) 11.1, e) 11.4, e) 11.6, g) 12.6, j) 12.9. * is a peak for acetone (used as an internal standard), 1, 2, 3 and 5 are peaks due to the protons in the functional group on the inset molecule.

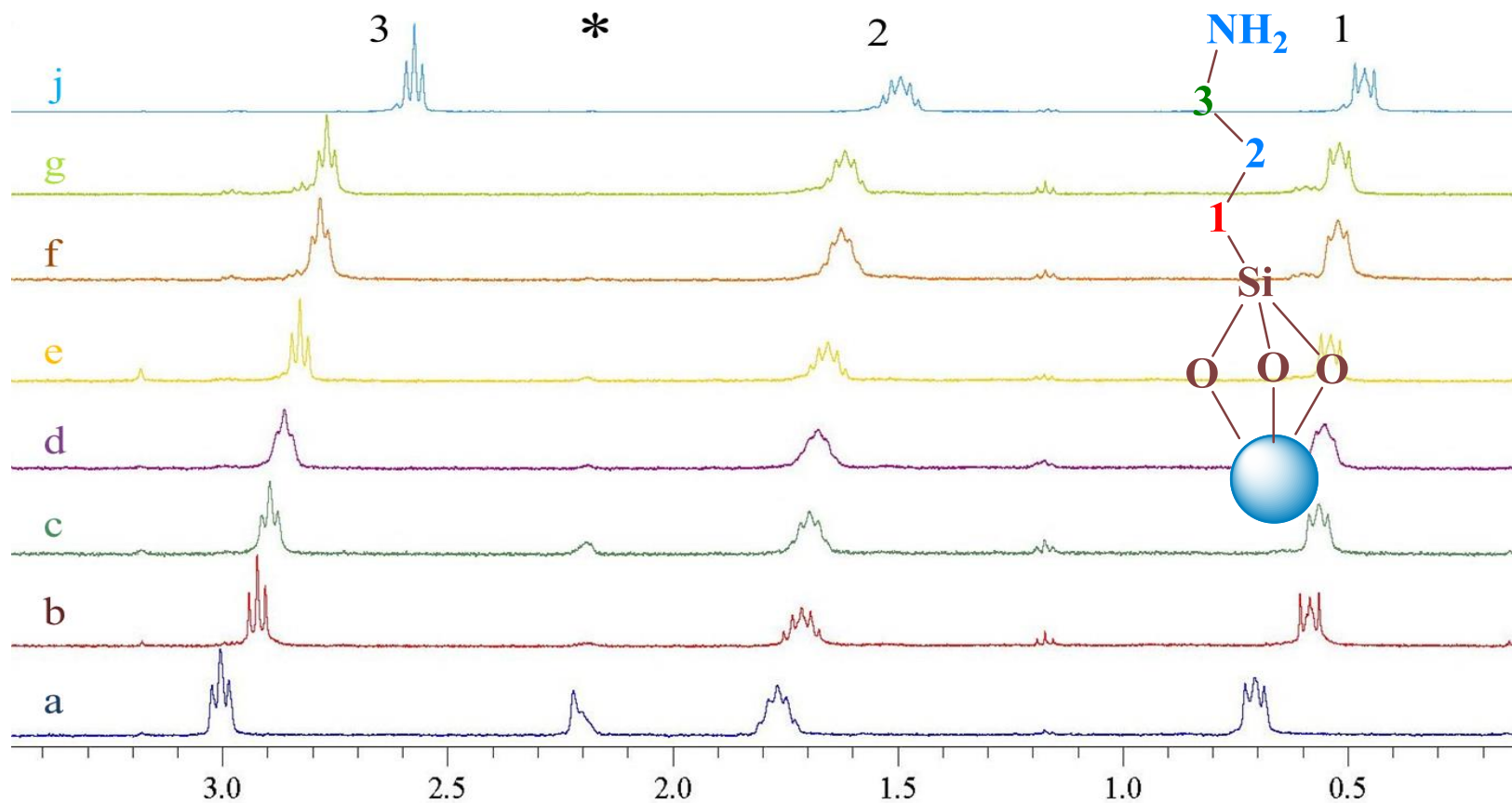


Figure 4.4 Proton solution state NMR spectra for APTES-functionalized silicalite-1 in D_2O at varying pH's: a) 8.0, b) 10.2, c) 10.6, d) 10.8, e) 11.0, e) 11.1, g) 11.2, j) 11.6. * is a peak for acetone (used as an internal standard), 1, 2, and 3 are peaks due to the protons in the functional group on the inset molecule.

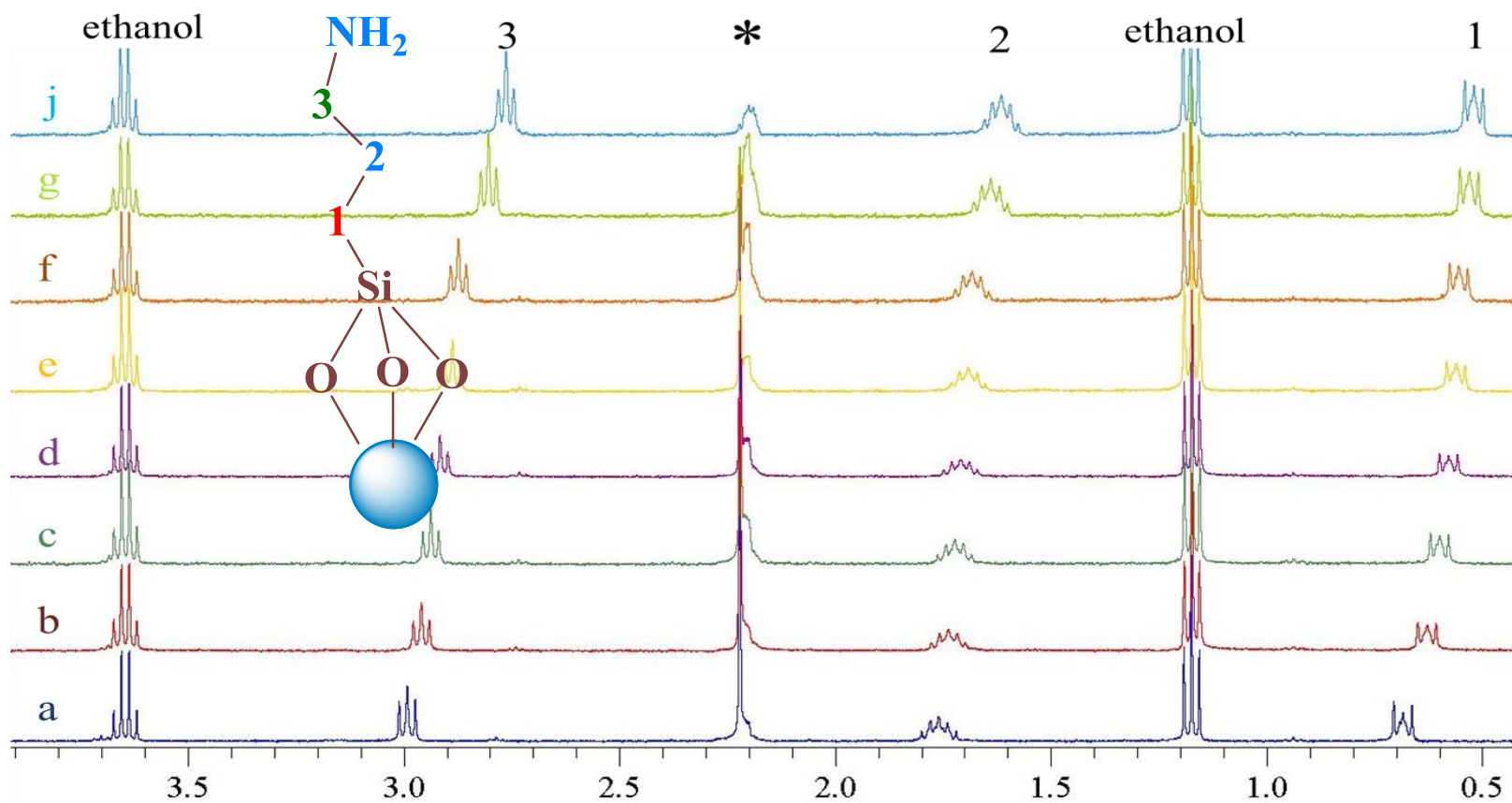


Figure 4.5 Proton solution state NMR spectra for APTES-functionalized MSN in D₂O at varying pH's: a) 9.0, b) 9.8, c) 10.2, d) 10.5, e) 10.8, e) 10.9, g) 11.2, j) 11.5. * is a peak for acetone (used as an internal standard), 1, 2, 3 and 4 are peaks due to the protons in the functional group on the inset molecule.

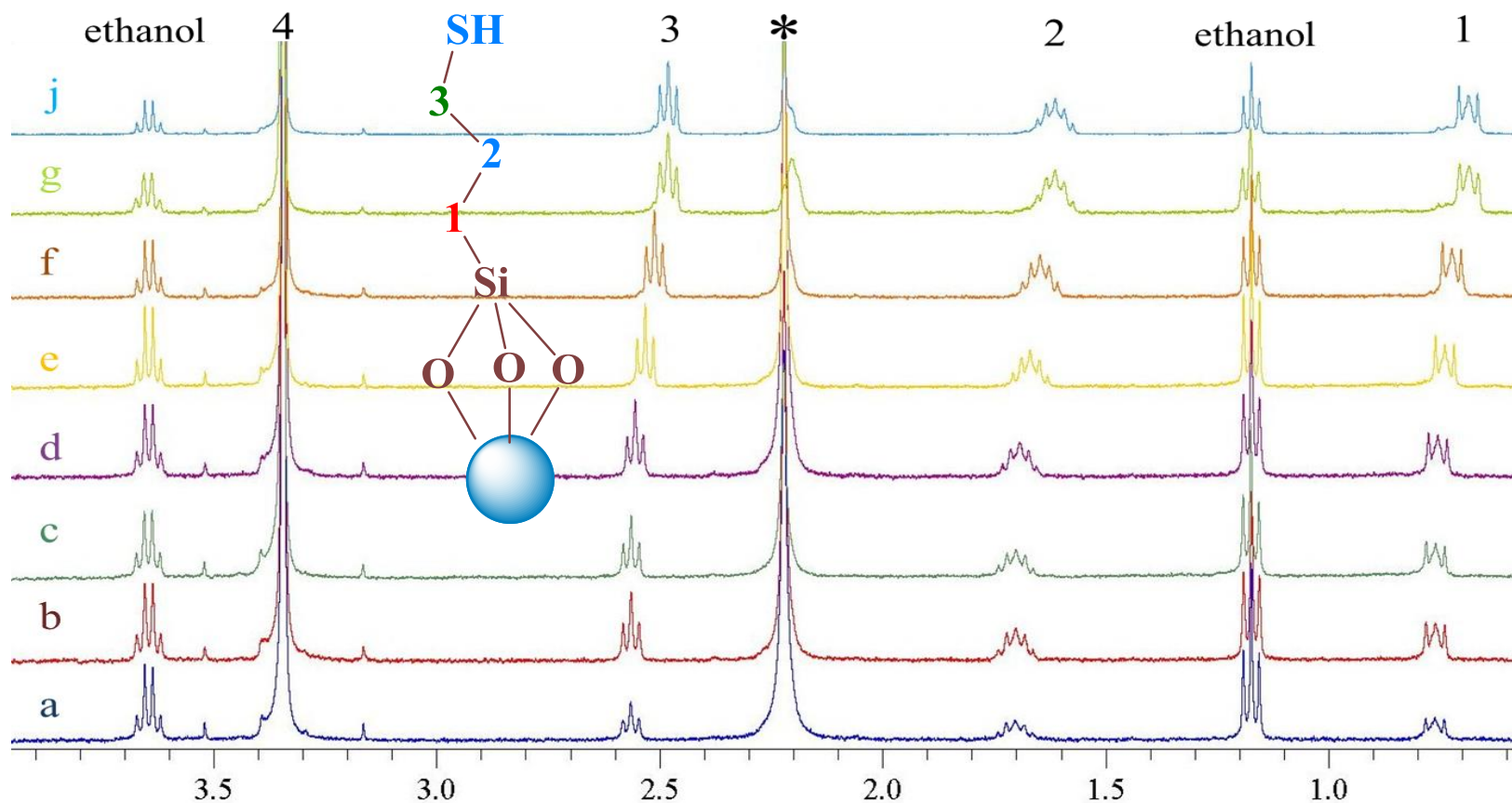


Figure 4.6 Proton solution state NMR spectra for MPTMS-functionalized silicalite-1 in D_2O at varying pH's: a) 6.6, b) 7.9, c) 8.5, d) 9.0, e) 10.2, e) 10.7, g) 10.8, j) 11.2. * is a peak for acetone (used as an internal standard), 1, 2, 3 and 4 are peaks due to the protons in the functional group on the inset molecule.

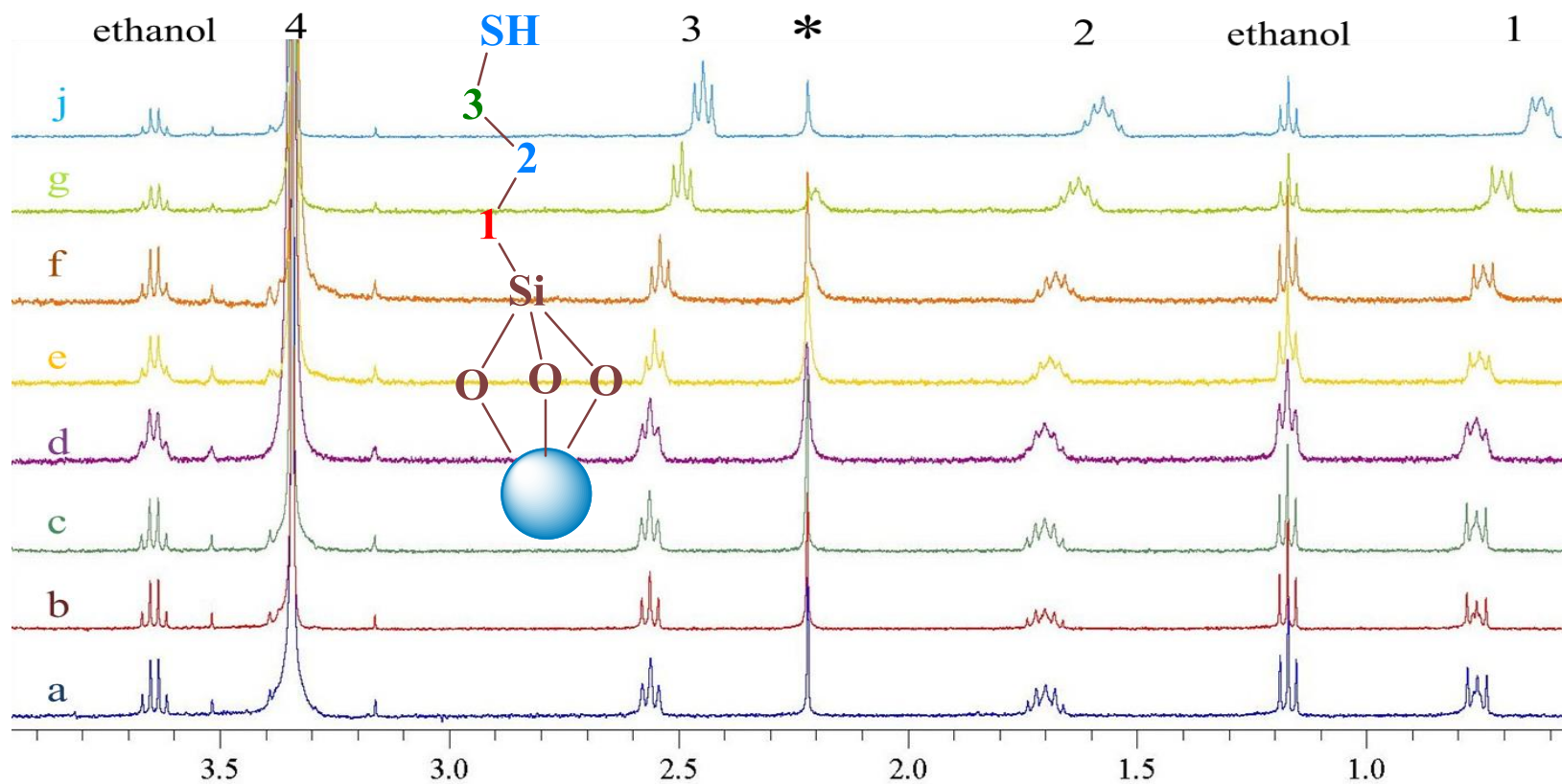


Figure 4.7 Proton solution state NMR spectra for MPTMS-functionalized MSN in D_2O at varying pH's: a) 2.6, b) 3.2, c) 6.7, d) 8.2, e) 9.2, e) 9.7, g) 10.5, j) 12.0. * is a peak for acetone (used as an internal standard), 1, 2, 3 and 4 are peaks due to the protons in the functional group on the inset molecule.

The variation in chemical shift with pH can be used to determine the pKa according to the following relationship:

$$\delta_{obs} = \frac{\delta_L + \delta_{LH^+} * 10^{pK_a - pH}}{1 + 10^{pK_a - pH}} \quad [13]$$

where δ_L is the chemical shift of the basic form and δ_{LH^+} is the chemical shift of the protonated form. δ_{obs} is the measured chemical shift [70]. The experimental chemical shift obtained as a function of pH can be fit to this functional form using a nonlinear least squares method to obtain the fitted value of the pKa. Using this method, the pKa's for the functional group of APDMMS (APTES, or MPTMS) in solution and those functionalities on the surface of MSN and silicalite in D₂O can be determined from the proton chemical shift.

For the determination of the pKa, the protons on C3 (see the molecular scheme in Figure 4.1) will be used. For APDMMS molecules the variation of the proton chemical shift of C3 versus pH is shown in Figure 4.8 along with the nonlinear least squares fits to equation 1 above with $\delta(\text{NH}_3^+) = 2.98$ ppm and $\delta(\text{NH}_2) = 2.59$ ppm. For APTES molecules the variation of the proton chemical shift of C3 versus pH is shown in Figure 4.9 where the nonlinear least squares are with $\delta(\text{NH}_3^+) = 3.00$ ppm and $\delta(\text{NH}_2) = 2.59$ ppm. For MPTMS molecules the variation of the proton chemical shift of C3 versus pH is shown in Figure 4.10 where the nonlinear least squares are with $\delta(\text{SH}) = 2.56$ ppm and $\delta(\text{S}^-) = 2.45$ ppm.

The fitted pKa values and corresponding errors for all functionalities are listed in Table 4.5. The pKa for APDMMS in D₂O is 10.51(±0.01) compared to 10.55 (±0.01) for APDMMS functionalized silicalite and 10.54 (±0.02) for APDMMS functionalized MSN.

The reported errors are the statistical fitting errors; however, a slightly larger error is expected due to uncertainty in the measured pH which is estimated to be ~0.1 pH units. Taking this into account, these results indicate that the pKa for the surface functional group and the free amine functional group are the same within experimental error.

The pKa's of functional groups at the interface have been measured using many different experimental techniques, including contact angle measurements, titration of the surface functional group [72] and sum frequency generation spectroscopy. In general, the pKa has been found to be lower at the interface relative to the solution and this has been attributed to increased electrostatic repulsion at the interface [72]. In a study by Kumar and Oliver, amines at the air/water interface were investigated by proton NMR spectroscopy [72]. The pKa for the hexadecyl amide at the air/water interface was found to be ~0.5 pKa units lower than the pKa for related amines in solution. The lowering of the pKa was attributed to an increase in electrostatic repulsion at the interface and therefore a favoring of the neutral form of the molecule at the interface according to the following equilibrium. In our study, the pKa does not change appreciably for the surface bound organic molecules relative to those that are free in solution. This is interpreted as an indication that the surface functional groups are oriented sufficiently far from the surface so that the electrostatic influence of the surface is negligible with respect to stabilizing the protonated or nonprotonated forms of the functional group. These results suggests that the properties of the covalently attached functional group on silicalite-1 (MSN) with respect to adsorption of an environmental contaminant or biological molecules will be predictable based on the solution phase reactivity of the functional group. Furthermore, these results indicate that future NMR studies of the functional

group interface with environmental contaminants or biological molecules will provide insight into the molecular structure of the interface.

Table 4.5: pKa values calculated from fits to proton NMR data collected as a function of pH. The variation in chemical shift with pH was used to determine the pKa according to equation 13. The reported errors are the fitting errors. A larger error is observed due to uncertainty in the measured pH which is estimated to be ~ 0.1 pH units.

Functional group	pKa Silicalite-1	pKa Mesoporous Silica	pKa Free in D ₂ O
APDMMS ^a	10.51 (± 0.01)	10.54(± 0.02)	10.50(± 0.01)
APTES ^b	10.64(± 0.03)	10.76(± 0.02)	10.68(± 0.02)
MPTMS ^c	9.73(± 0.03)	9.69(± 0.05)	9.68(± 0.03)

^a The pKa was calculated from equation [1] using δ (NH₃⁺ form) = 2.98 ppm and δ (NH₂ form) = 2.59 ppm and the experimental data,

^b The pKa was calculated from equation [1] using δ (NH₃⁺ form) = 3.00 ppm and δ (NH₂ form) = 2.59 ppm and the experimental data,

^c The pKa was calculated from equation [1] using δ (SH form) = 2.56 ppm and δ (S⁻ form) = 2.45 ppm and the experimental data.

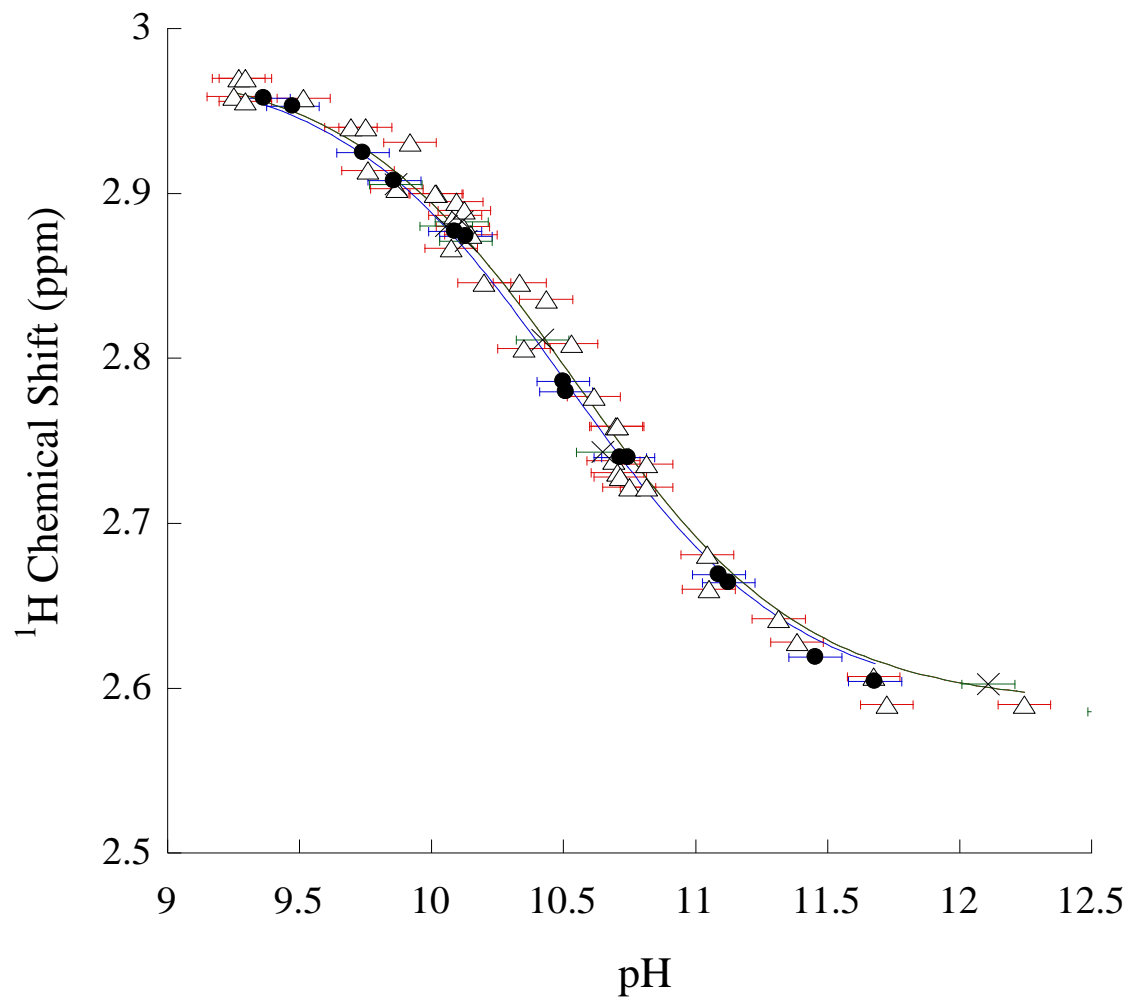


Figure 4.8 Proton NMR titration curve for protons on C3 of APDMMS in D_2O (solid circles) and APDMMS-functionalized silicalite-1 (open triangles), APDMMS-functionalized mesoporous silica (crosses). The solid lines represent nonlinear least-squares fits to the experimental data using a monoprotic titration model.

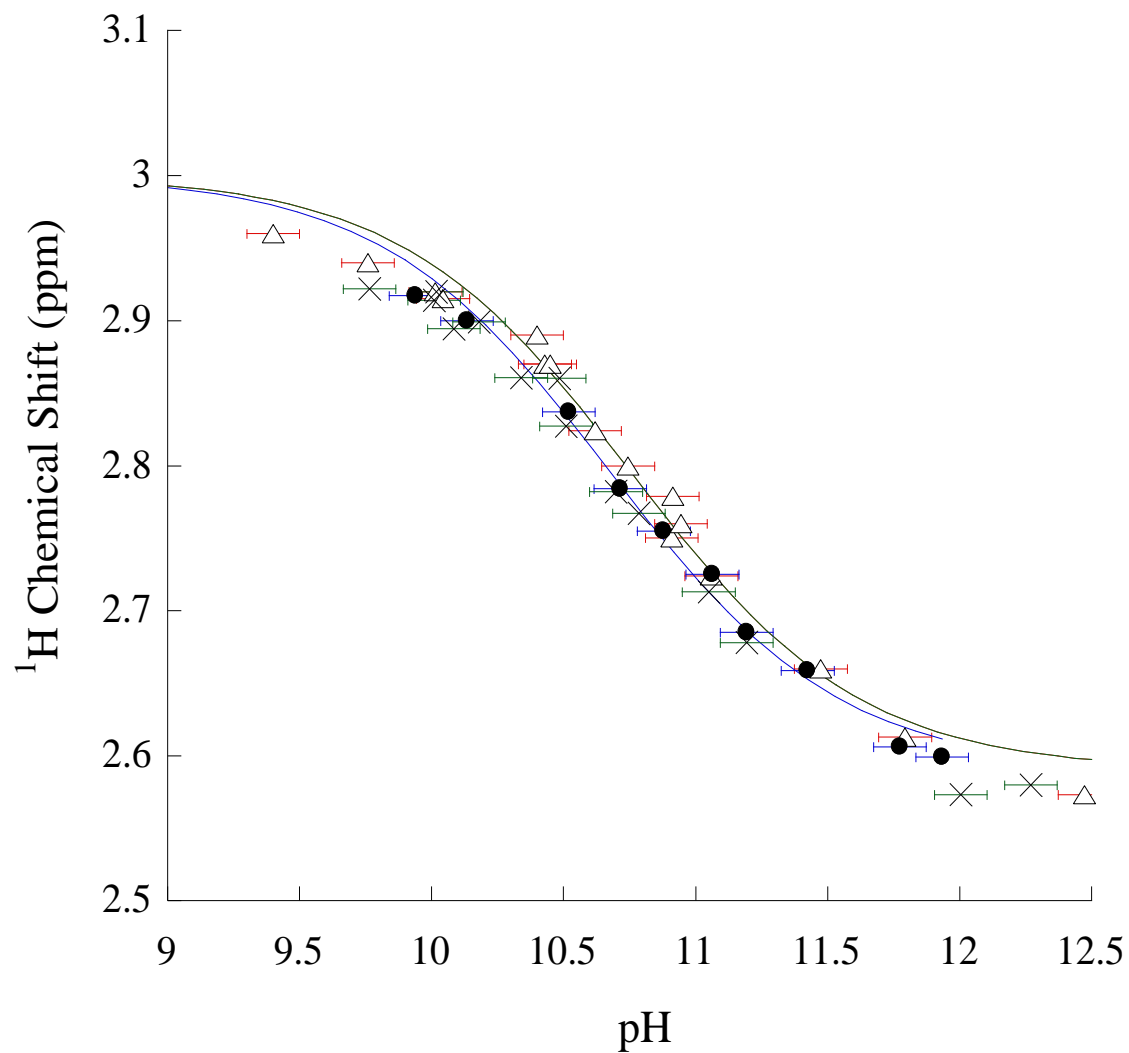


Figure 4.9 Proton NMR titration curve for protons on C3 of APTES in D_2O (solid circles) and APTES-functionalized silicalite-1 (open triangles), APTES-functionalized mesoporous silica (crosses).. The solid lines represent nonlinear least-squares fits to the experimental data using a monoprotic titration model.

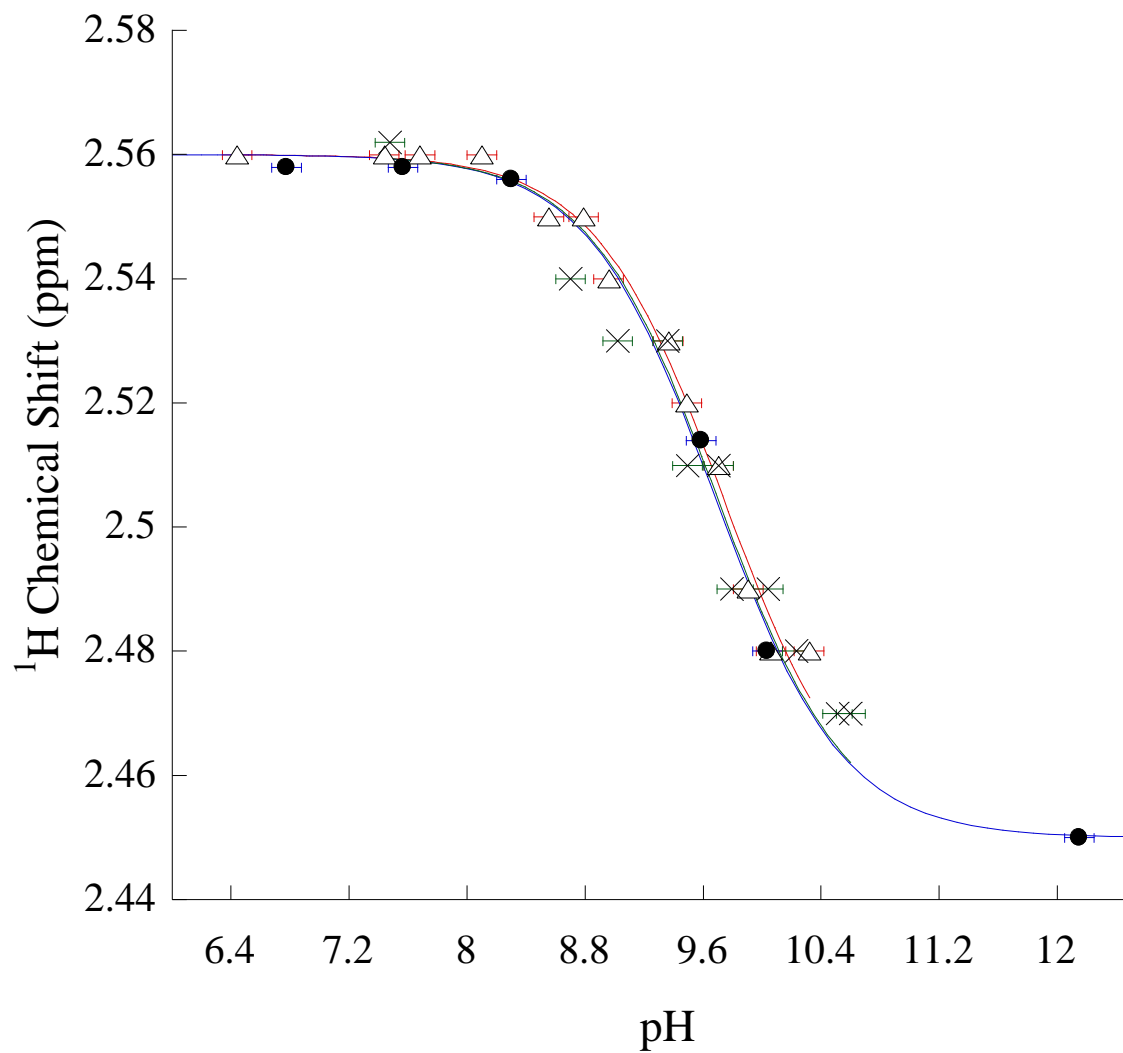


Figure 4.10 Proton NMR titration curve for protons on C3 of MPTMS in D_2O (solid circles) and MPTMS-functionalized silicalite-1 (open triangles), MPTMS-functionalized mesoporous silica (crosses). The solid lines represent nonlinear least-squares fits to the experimental data using a monoprotic titration model.

4.5 Conclusions

The characterization of the physical properties of nanocrystalline materials is critical to the realization of their innovative applications in a broad range of areas including catalysis, drug delivery, imaging, environmental protection, and sensing. The surface chemistry of silicalite-1 and mesoporous silica nanoparticles functionalized with organosilanes (APDMMS, APTES, or MPTMS) was selectively probed using solution ^1H NMR spectroscopy. The use of solution NMR spectroscopy results in high-resolution NMR spectra. This technique is selective for protons on the surface organic functional groups due to their motional averaging in solution. This study has demonstrated the feasibility of using ^1H solution NMR spectroscopy as a tool to investigate the interface of the organic functional groups in D_2O . The pK_a for these functional groups covalently bound to the surface of nanoparticles was determined using an NMR–pH titration method based on the variation in the proton chemical shift for the alkyl group protons closest to the amine group with pH. In our study, the pK_a does not change appreciably for the surface bound APDMMS relative to APDMMS that are free in the solution. This is interpreted as an indication that the surface functional groups are oriented sufficiently far from the surface so that the electrostatic influence of the surface is negligible with respect to stabilizing the protonated or nonprotonated forms of the functional group.

CHAPTER 5

SURFACE SELECTIVE ^1H SOLUTION NMR STUDIES OF FUNCTIONALIZED NANOPARTICLES5.1 Abstract

The characterization of the physical properties of nanocrystalline materials is critical to the realization of their innovative applications in a broad range of areas including catalysis, drug delivery, imaging, environmental protection, and sensing. The surface chemistry of silicalite-1 and mesoporous silica nanoparticles functionalized with 3-aminopropyldimethylmethoxysilane (APDMMS) was selectively probed using solution ^1H NMR spectroscopy. The use of solution NMR spectroscopy results in high-resolution NMR spectra. This technique is selective for protons on the surface organic functional groups due to their motional averaging in solution. In this study, ^1H solution NMR spectroscopy was used to investigate the interface of the organic functional groups in D_2O .

In this study, functionalized silicalite-1 and MSNs with a size of approximately 35 nm and 50 nm, respectively, were characterized using solution proton NMR spectroscopy. Silicalite-1 and MSNs were grafted with APDMMS. The functionalized nanoparticles were dispersed in D_2O and solution proton NMR spectra were obtained. Due to the increased motional narrowing of the surface functional groups when the MSNs are dispersed in solvent, highly resolved solution proton NMR signals from the surface functional groups are observed. Diffusion ordered spectroscopy (DOSY) and Nuclear Overhauser Effect Spectroscopy (NOESY) were used as NMR techniques that enable bound ligands to be distinguished from free ligands. For MSN-APDMMS and silicalite-APDMMS, the cross peaks and the diagonal peaks in the NOESY spectrum

exhibit the same sign indicating that APDMMS is bound to the surface. DOSY was used to measure the diffusion coefficients of the surface bound ligands. On the basis of 1D ^1H and DOSY and NOESY spectroscopy, it was found that APDMMS molecules interact with the nanomaterial surface, although the APDMMS ligands resonances and diffusion coefficient resemble those of free molecules. These observations suggest that these NMR observables are a weighted average of a free and a bound state of organic functional groups. These results demonstrate the sensitivity of solution NMR spectroscopy to the electronic environment and structure of the surface functional groups on porous nanomaterials.

5.2 Introduction

Mesoporous silica is a porous material that has pore dimensions of $>10 \text{ \AA}$ and amorphous silica walls [73-75], while zeolites are three dimensional crystalline microporous aluminosilicate materials with well-defined framework and uniform-sized pores ($<10 \text{ \AA}$) throughout their crystal structure. In this study, MSNs with a worm-like pore morphology and silicalite-1, a purely siliceous form of zeolite with sinusoidal channels intersecting straight pores and the MFI type structure have been used. There has been a burgeoning interest in zeolite and mesoporous silica nanoparticles (MSNs) with sub-100 nm particle sizes and their potential biomedical or environmental applications [19, 21, 76, 77]. Many applications for porous nanomaterials are being developed including the adsorption of environmental contaminants or biomedical applications [76, 78-80] such as imaging or drug delivery. Development of mesoporous silica and zeolite nanomaterials for environmental or biomedical applications typically involves organic functionalization to enhance drug loading, biocompatibility and/or electrostatic

interactions with an adsorbate. The standard methods of characterization of these solid materials include methods such as solid state NMR, FTIR, X-Ray techniques, CHN analysis, Inductively Coupled Plasma/Optical Emission Spectroscopy (ICP/OES) and electron microscopy. There are very few methods (dynamic light scattering, optical spectroscopy) that have been used for characterizing MSNs dispersed in solution despite the need to characterize MSNs in this highly relevant environment.

Solid state NMR methods have been widely and successfully implemented for studying MSN [81-86]. Magic Angle Spinning (MAS) and High Resolution MAS (HRMAS) NMR methods have been utilized to determine structural details of functionalized [87-89] or drug loaded MSNs [90-92]. Recently, solution NMR methods have been used for characterization of the surface chemistry of colloidal nanomaterials with emphasis on colloidal semiconductor nanocrystals or “quantum dots” [76]. Solution NMR methods, such as single pulse proton NMR, nuclear Overhauser effect spectroscopy (NOESY) and diffusion ordered spectroscopy (DOSY) have been used to study ligands bound to semiconductor or metal oxide nanoparticles. [20, 76]. Most of the NMR studies have focused on protons but there have been phosphorous NMR experiments reported as well [93]. However, despite the progress that has been made in this area, solution NMR spectroscopy has only recently been extended to a porous silicate nanomaterial, the nanocrystalline zeolite, silicalite in which the pKa of the propylamine surface group was determined [16].

Solution NMR methods, such as those applied to colloidal semiconductor and metal oxide nanocrystals, offer great potential to provide detailed chemical information about covalently modified MSNs dispersed in solution which is critical to the

development of these nanomaterials for solution-phase based applications. In chapter 4, we demonstrated that a solution NMR titration can be used to determine the pK_a of the surface bound functional group on covalently modified silicalite-1 nanoparticles [16]. In this chapter, we show that DOSY and NOESY experiments can be used to provide further insight into the surface organic functional groups. Pulsed field gradient spin-echo (PGSE) techniques, such as DOSY experiments can be used to sort species according to their size, because the diffusion coefficient is inversely proportional to the hydrodynamic radius, while NOESY enables nanoparticle-ligand interactions to be pinpointed, even with ligands in a fast adsorption/desorption equilibrium and in complex solvent mixtures. The solution NMR methods described here provide critically important molecular level details about surface bound ligands in highly relevant porous silicate systems.

5.3 Experimental Methods

5.3.1 Synthesis and Surface Modification of Nanoparticles

All silicalite-1 samples with a crystal size of 35 nm were synthesized from clear gel solutions according to the general procedure reported in literature [54]. Mesoporous silica nanoparticles with a particle size of approximately 50 nm were prepared according to the procedure described by Karin Möller, Johannes Kobler, and Thomas Bein previously [55]. (See more details in Chapter 2.)

The silicalite and MSNs were covalently modified in a post-synthesis grafting treatment by 3-aminopropyldimethylmethoxysilane (APDMMS). Functionalization procedure with amine groups was carried out as described in Chapter 2.

5.3.2 Sample Characterization

Silicalite-1 and MSNs were characterized by powder x-ray diffraction (pXRD), nitrogen adsorption isotherms and thermal gravimetric analysis (TGA). Powder X-ray diffraction (pXRD) was obtained using a Siemens D5000 X-ray diffractometer. A powder pattern was obtained from $2\theta = 1$ to 55° with a 0.04° step size, 1 s/step. Nitrogen adsorption experiments were conducted using a Nova 1200 Nitrogen Adsorption Instrument (Quantachrome). Approximately 100 mg of powder was dried at 120°C under vacuum overnight. A 7-point BET isotherm and a 50-point adsorption/desorption isotherm were obtained and used for calculation of the specific surface area and the pore volume. The samples were evaluated by thermogravimetric analysis (TGA) using a TA Q5000 TGA instrument with a heating rate of $5^\circ\text{C}/\text{min}$ under nitrogen flow. As samples were heated from room temperature to $\sim 800^\circ\text{C}$, the weight change was recorded and was used to approximate the loading of the organic functional group. (See greater details in Chapter 2)

5.3.3 Solution NMR Experiments

Samples were prepared for proton solution NMR experiments by dispersing approximately 5 mg of MSNs or silicalite samples in 0.6 mL of D_2O . NaOH or HCl was added to adjust the pH. The pH was measured before and after the NMR experiment using a Corning 320 pH meter and the average of the two values was taken as the pH for the experiment. Typically, the pH reading obtained before and after each NMR experiment differed by <0.1 pH units. The NMR samples were sonicated for approximately 30 minutes immediately before the NMR experiments. The NMR experiments were conducted on a Bruker DRX-400 Instrument operating at 400 MHz.

Single pulse ^1H NMR experiments were performed. Single pulse experiments were performed with a pulse width of 7 μs and a recycle delay of 0.01 s with 128 scans.

5.3.4 Experimental Parameters for Pulse Field Gradient

Spin-echo (PGSE) NMR Experiments.

The DOSY experiments were conducted on a Bruker DRX-400 Instrument operating at 400 MHz. All diffusion measurements were made using the stimulated echo pulse sequence with bipolar gradient pulses. The diffusion delay (Δ) and the gradient pulse duration (δ) were varied from 20 to 300 ms, and from 1.6 to 3 ms, respectively, and were optimized in order to obtain 1-5% residual signal with maximum gradient strength. The recycle delay was adjusted to 4s. Rectangular shapes were used for the gradients and a linear gradient ramp with 16 increments between 2% and 95% was applied for the diffusion relevant gradients. The strength of the gradient (56.0 Gauss/cm at a current of 10A) was calibrated by measuring the self-diffusion of the residual HDO signal in a 100% D_2O sample at 298K ($1.90 \times 10^{-9}\text{m}^2\text{s}^{-1}$). Diffusion coefficients were obtained by integrating the resonances of interest and fitting the data to the Stejskal–Tanner equation [94].

5.3.5 Experimental Parameters for

2D NOESY NMR Spectroscopy

2D NOESY experiments were recorded on a Bruker Avance 500 spectrometer that was equipped with a 5 mm triple resonance inverse Z-gradient probe. All of the samples were prepared in D_2O . 2D NOESY spectra were recorded using a ^1H spectral width of 7.00 ppm. Typically 150 t_1 increments, consisting of 16 scans of 2048 sampled data points each, were recorded with a 4 s relaxation delay. ^1H spectral widths and 90°

pulse widths are optimized for each sample. A recycle delay (D_1) of 4.0 s was used in all the 2D experiments. An optimal range of mixing times for NOESY experiments was determined using the one-dimensional version of spin-lattice relaxation measurements. 2D NOESY with mixing times of 200, 500, 1000, and 1500 ms were recorded. All NMR data were processed with TOPSPIN 1.3 or 2.1 suites of software programs. The 2D NMR data were processed with the zero-filling to 2,048 points and 1,024 points in acquisition and second dimension, respectively.

5.4 Results and Discussions

MSNs and silicalite-1 nanomaterials were synthesized, modified with the organosilane, APDMMS, in a post-synthesis treatment and characterized. A schematic diagram illustrating the organic functionalization is shown in Figure 2.1 (Chapter 2). The organic functional groups are located only on the external surface of silicalite, while both the external and internal surfaces of the MSNs are modified with the organosilanes. The MSNs used in this study had a worm-like pore morphology. The average particle size of the MSNs is $\sim 52(\pm 7)$ nm and $\sim 35(\pm 7)$ nm for silicalite samples as determined from the TEM images shown in Figure 3.5 and 3.4 (Chapter 3). The specific surface area of the MSNs prior to functionalization is $1088 \text{ m}^2/\text{g}$ and drops to $438 \text{ m}^2/\text{g}$ after functionalization indicating that the functionalization occurs on the internal surface. The specific surface area of the silicalite prior to functionalization is $302 \text{ m}^2/\text{g}$ and drops to $177 \text{ m}^2/\text{g}$ after functionalization. TGA measurements were used to estimate the organic functional group loading in mmol/g and the results are listed in Table 3.1 (Chapter 3). APDMMS functional groups loadings were calculated to be 1.1 mmol/g on MSN-APDMMS and 0.6 mmol/g on silicalite-APDMMS.

5.4.1 Proton Solution NMR Spectroscopy of Functionalized Silicalite and Mesoporous Silica

Proton solution NMR spectra were obtained for each of the functionalized samples in D₂O. The proton NMR spectra for pure APDMMS, unfunctionalized nanoparticles, and APDMMS functionalized silicalite, at pH=7 are shown in Figure 5.1. The proton NMR peaks are well-resolved and correspond to the protons of the organic functional groups, APDMMS. The bulk protons from the silanol groups and water adsorbed on the nanoparticle surface or in the pores are not observed in the solution proton NMR spectrum because these protons are not subject to motional averaging and thus are too broad to be observed in the solution NMR spectrum. The peak assignments for the proton NMR spectra in Figure 5.1 are listed in Table 4.2. At pH=7, the amine groups are present in the fully protonated form. The protons (1, 2 and 3) attached to the propyl group carbons are observed in the proton spectra in the chemical shift range of 0.5-3 ppm. Acetone was added as a pH independent chemical shift standard and appears at a chemical shift of approximately 2.2 in the proton NMR spectra and residual water from the D₂O appears at 4.7.

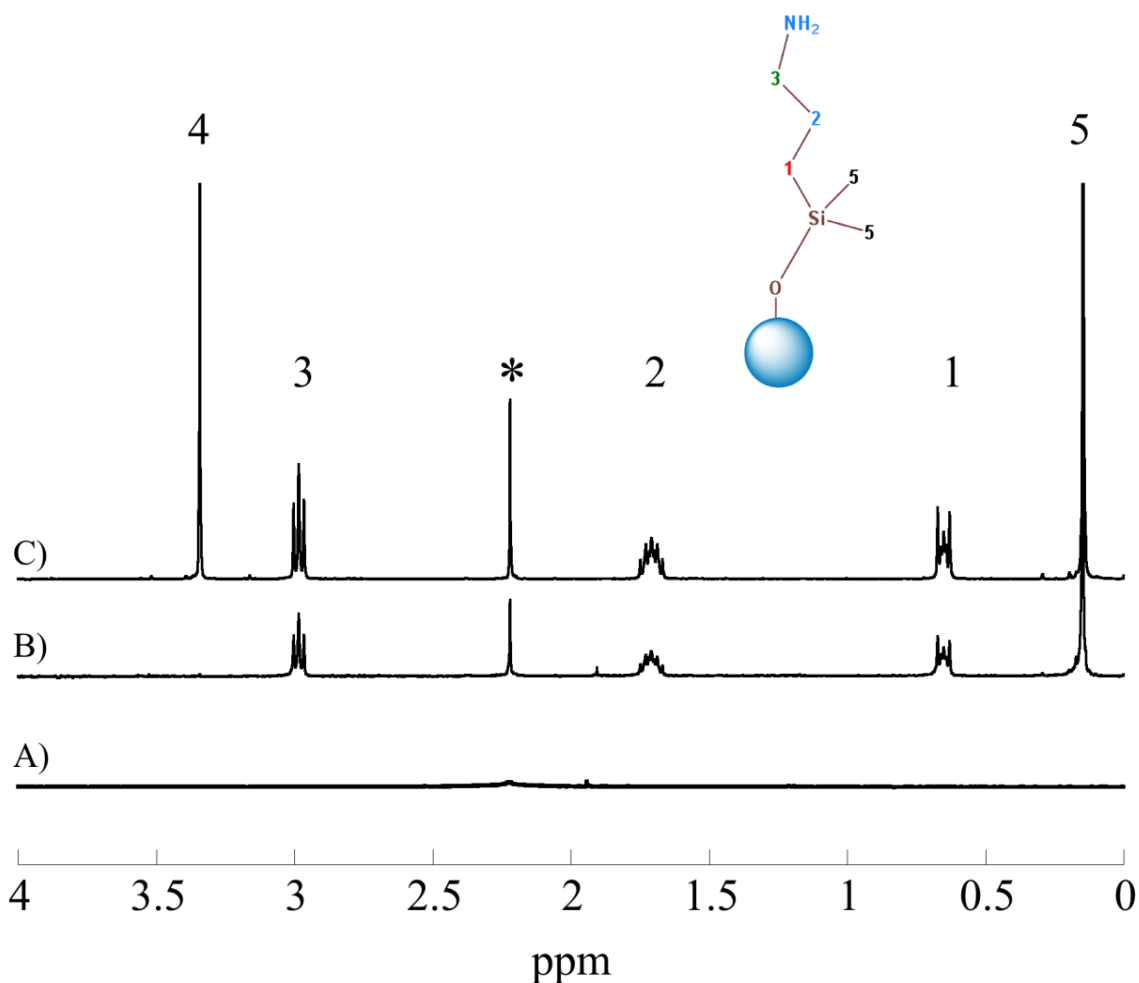


Figure 5.1 Proton solution state NMR spectra (at pH=7) of: A) silicalite-1 in D₂O, B) APDMMS-functionalized silicalite-1, C) APDMMS in D₂O. The functional group loading was quantified using proton NMR spectroscopy. An internal standard of acetone was used to calibrate the signal from the surface functional group. * is a peak assigned for acetone that was used as an internal standard for all ¹H solution state NMR experiments. 1, 2, 3, and 5 are peaks due to the protons in the functional group on the inset molecule. Peak 4 is for the protons of methoxy groups in the free APDMMS.

5.4.2 NMR/TGA Quantitative Analysis

After functionalization with functional groups (APDMMS), nanomaterials were further characterized by TGA to assess the functional group loadings. TGA was employed by heating each sample by heating each sample in flowing N₂ from room temperature at 3°C/min to 900°C. Characteristic thermogravimetric curves have been obtained for APDMMS modified materials and the amount of functional groups has been estimated in mmol/g and reported in Chapter 3 (Table 3.1). When used in combination with NMR, the TGA/NMR method is capable of detailed quantitative analysis of the investigated samples. NMR spectra can provide some quantitative information about the relative amount of chemical species in the solution based on the integrated areas of their resonance signals. So if the signal integrated area and actual amount of the chemical moieties in the solution are known, we can use this compound as an internal standard and estimate the unknown concentration for other species based on the integrated areas of their NMR signals.

Quantitative analysis of the NMR spectra for APDMMS functionalized MSN agrees well with the TGA results. Based on TGA results the amount of APDMMS species in the studied sample (2 mg of APDMMS functionalized MSN) has been found to be 0.0023 mmol. According to NMR spectral analysis of obtained for APDMMS-MSN in D₂O, the amount of functional groups (APDMMS) on the surface of nanomaterials has been found to be 0.0024 mmol in the sample (2 mg of APDMMS functionalized MSN in 0.6 mL of D₂O). TGA and NMR results are in very good agreement. Therefore, NMR spectroscopy is an analytical toolbox that can provide some useful quantitative information.

5.4.3 NOESY Experiments

As illustrated previously for semiconductor quantum dot nanomaterials, NOESY experiments can be used to differentiate between free and bound ligands on nanoparticles [19-21, 76]. The Nuclear Overhauser Effect (NOE) occurs between dipolar coupled protons and the NOE intensity is governed by the internuclear distance ($\sim 1/r^6$). The sign of the NOE depends on the rotational correlation time, τ_c which for a rigid spherical molecule is given by:

$$\tau_c = \frac{4\pi\eta r^3}{3k_B T} \quad [14]$$

where η = viscosity, k_B = Boltzmann constant, T = temperature in Kelvin and r = radius of the spherical particle. If τ_c is less than ω_0^{-1} , the NMR spectrometer frequency, the sample is in the extreme narrowing region and exhibits small molecule behavior and weak positive NOEs. If τ_c is greater than ω_0^{-1} , then the sample is in the spin diffusion limit and large negative NOEs are observed suggesting a surface bound ligand. When a negative NOE is present, cross peaks with the same sign relative to the diagonal peaks are observed and for a positive NOE, cross peaks have the opposite sign relative to the peaks along the diagonal. The NOESY spectra for APDMMS in D_2O , MSN-APDMMS in D_2O , and Silicalite-APDMMS in D_2O are shown in Figure 5.2, 5.3, and 5.4, respectively. For the NOESY spectrum of APDMMS in D_2O , cross peaks with signs opposite to the diagonal peaks are observed consistent with small molecule behavior. For MSN-APDMMS and silicalite-APDMMS, the cross peaks and the diagonal peaks in the NOESY spectrum (Figure 5.3, 5.4) exhibit the same sign indicating a bound APDMMS surface group.

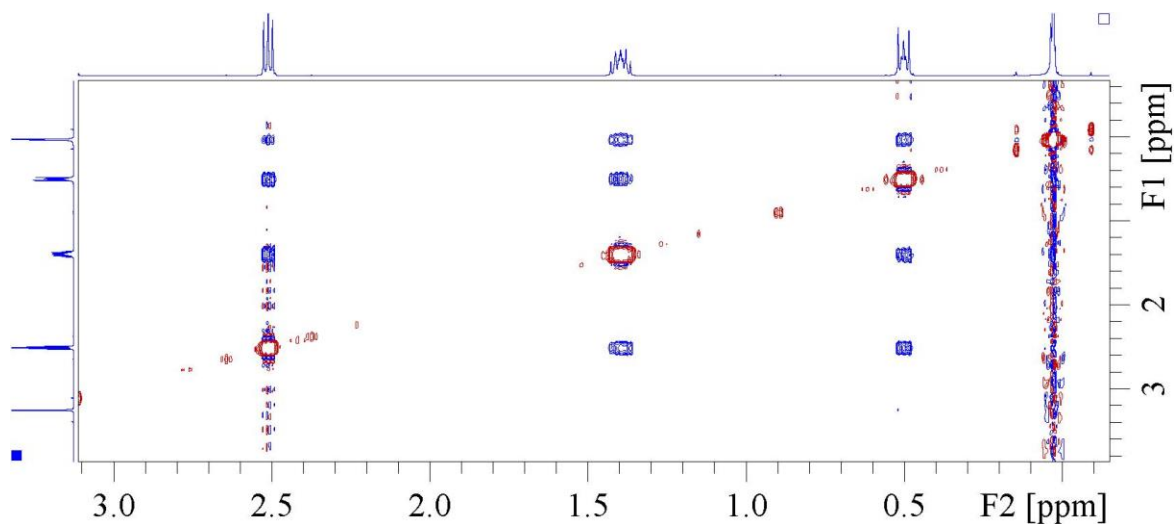


Figure 5.2 The NOESY spectra for pure APDMMS molecules in D₂O at pH=11.6 (with mixing time 200 ms).

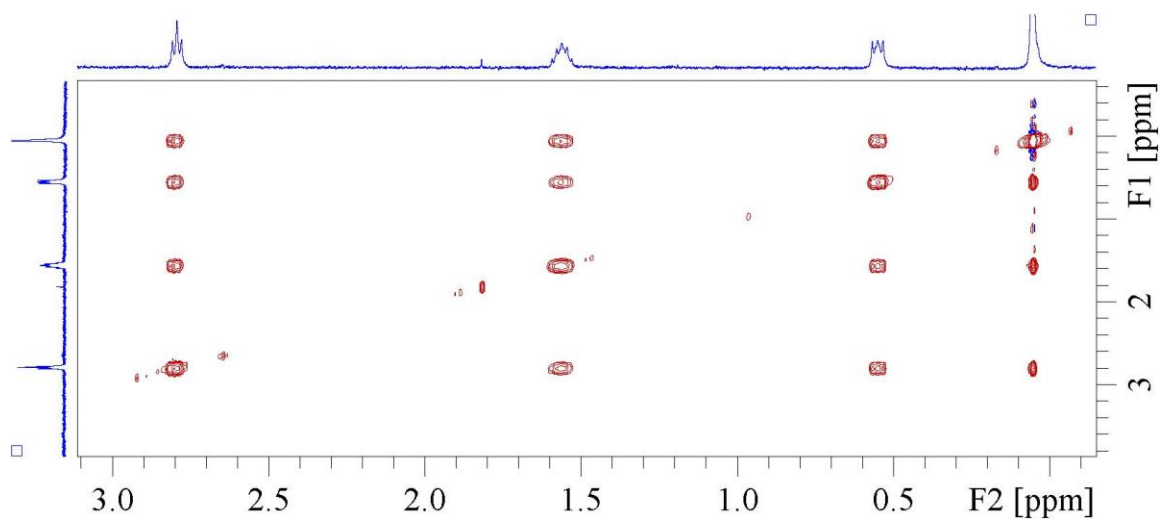


Figure 5.3 The NOESY spectra for MSN-APDMMS in D₂O at pH=11.6 (with mixing time 200 ms).

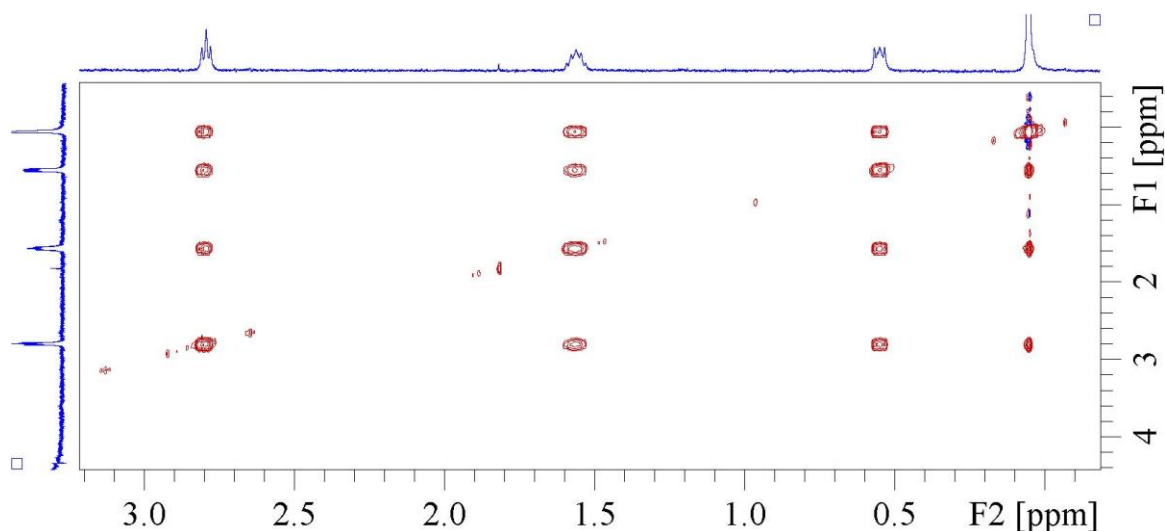


Figure 5.4 The NOESY spectra for Silicalite-APDMMS in D₂O at pH=11.6 (with mixing time 200 ms).

5.4.4 DOSY Experiments

DOSY is the two dimensional form of PFG NMR. DOSY has been used effectively to characterize ligands bound or in fast exchange between the surface and solution for colloidal nanocrystals [76]. DOSY has also been used to characterize alkylammonium-silica mixtures to provide insights into zeolite crystallization [95-100]. In the DOSY experiment, pulsed field gradients are applied and as the molecules in the sample undergo translational diffusion, the NMR signal is attenuated. Analysis of the DOSY data results in a determination of the diffusion coefficient. As expected, for ligands strongly bound to the nanoparticle surface, the observed diffusion coefficient is much smaller (often an order of magnitude) relative to the free ligand. Recently, there have been reports in which the diffusion coefficient of the “bound” ligand was only ~10% smaller than the “free” ligand [20, 21, 76]. In the case of octylamine and CdSe quantum dots, the diffusion coefficients of free octylamine and octylamine in the presence of CdSe were similar [19]. However, NOESY experiments clearly demonstrated that the octylamine

molecules interacted with the CdSe surface. The diffusion coefficients measured by DOSY for the free APDMMS and MSN-APDMMS (silicalite-APDMMS) are similar as listed in Table 5.2 and shown in Figure 5.4. The diffusion coefficients for free APDMMS in D₂O and MSN-APDMMS (silicalite-APDMMS) in D₂O are $\sim 6.1 \times 10^{-10} \text{ m}^2/\text{s}$. The magnitude of the diffusion coefficient for peak 4, which is due to hydrogens from methoxy groups, in the DOSY of APDMMS was found to be $1.37 \times 10^{-9} \text{ m}^2/\text{s}$. The larger magnitude of the diffusion coefficient can be attributed to the fact that when APDMMS molecules are hydrolyzed, the methoxy groups are leaving groups and so they are separated from APDMMS molecule in aqueous solution. The magnitude of the diffusion coefficient for APDMMS in D₂O is reasonable compared to the diffusion coefficient for MPTMS which was reported to be $5.02 \times 10^{-10} \text{ m}^2/\text{s}$ [94]. However, since the negative NOEs are observed in the NOESY data indicating surface bound APDMMS, the DOSY data is interpreted as being indicative of a fast exchange between APDMMS and surface bound APDMMS.

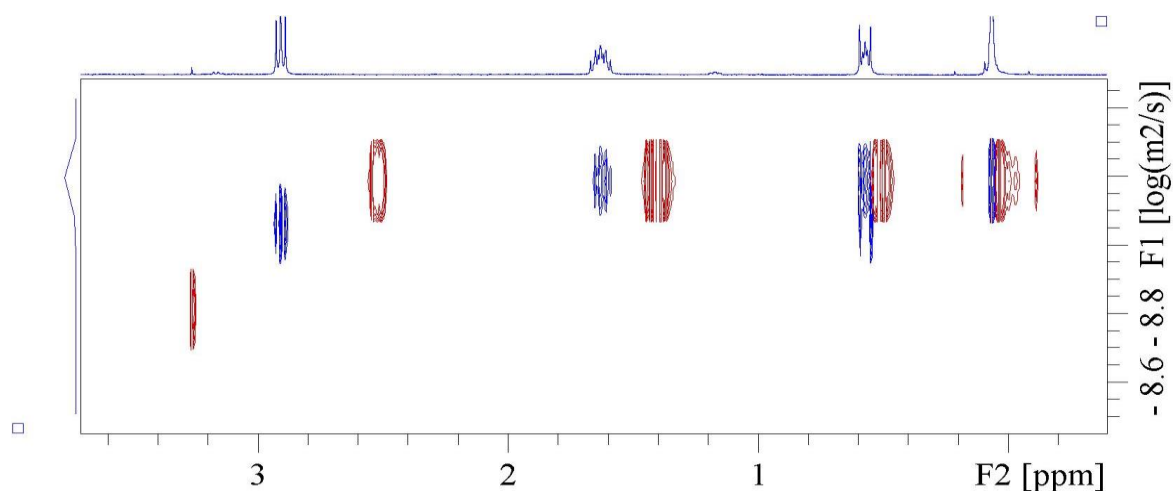


Figure 5.5 The diffusion coefficients measured by DOSY for the free APDMMS in D₂O (red) and silicalite-1-APDMMS in D₂O (blue) at pH=11.6.

Table 5.1: Proton Chemical Shift Assignments for APDMMS, APDMMS Functionalized silicalite-1 at pH=7 in D₂O.

	<u>Chemical Shift</u> (ppm)- <u>APDMMS</u>	<u>Chemical Shift</u> (ppm)- <u>APDMMS-</u> <u>silicalite-1</u>	<u>Multiplicity</u>	<u>Assignment</u>
1	0.65	0.65	triplet	Si-CH ₂ -CH ₂ - CH ₂ -NH ₂
2	1.71	1.71	quintet	Si-CH ₂ -CH ₂ - CH ₂ -NH ₂
3	2.98	2.98	triplet	Si-CH ₂ -CH ₂ - CH ₂ -NH ₂
4	3.34	--	singlet	-Si-OCH ₃
5	0.15	0.15	singlet	Si(CH ₃) ₂

Table 5.2: Diffusion Coefficients (m^2/s) obtained from DOSY Experiments. Proton NMR spectra (at pH=7) of silicalite-1 in D_2O , APDMMS-functionalized silicalite-1, and APDMMS in D_2O are shown in Figure 5.1 A, B, and C respectively.

	Peak 1 @0.55 ppm	Peak 2 @1.6 ppm	Peak 3 ~2.9 ppm	Peak 4 @3.25 ppm	Peak 5 @0.1 ppm
Pure APDMMS	6.11×10^{-10}	6.12×10^{-10}	6.11×10^{-10}	1.37×10^{-9}	6.11×10^{-10}
Silicalite- APDMMS	6.14×10^{-10}	5.69×10^{-10}	6.33×10^{-10}	--	6.14×10^{-10}
MSN- APDMMS	6.49×10^{-10}	6.26×10^{-10}	6.67×10^{-10}	--	6.46×10^{-10}

5.4.5 DOSY NMR Data Processed by DECRA method

DOSY NMR employs a pulse-field gradient spin-echo NMR experiment with different components diffusing in the solution. The signal of each component decays with different diffusion rates as the gradient strength increases, resulting into a bilinear NMR data set of a mixture. By calculating the diffusion coefficient for each component, a two-dimensional NMR spectrum can be obtained: one dimension is for the conventional chemical shift and the other for the diffusion coefficient.

Data processing is very essential DOSY NMR interpretation. It is not a trivial task to analyze complex samples, which components are with insignificant variation in diffusion coefficients, or severely overlapping in the chemical shift dimension. There are different methods, including single channel method (SPLMOD), continuous diffusion coefficient (CONTIN), and two multivariate methods: direct exponential curve resolution algorithm (DECRA) and multivariate curve resolution (MCR), that are used to process DOSY data sets. Even though all of them might be useful to determine the composition of complex mixtures, DECRA analysis was used in this study for DOSY NMR data set processing.

DECRA is based on the generalized rank annihilation method (GRAM) and can be applied to the DOSY NMR data to resolve each individual component in the complex mixture and obtain their respective diffusion coefficients. In the typical DECRA spectrum the resolved components are ranked from fast-moving at the top to slow-moving at the bottom. The spectra are normalized in such a way as to show accurate component composition of the studied sample. Though, there are significant drawbacks associated with DECRA methodology, namely, the severe spectral overlap of the signals

in the spectrum or close exponential decay rates of different components (normally less than 2 s).

We used DECRA analysis to attempt to differentiate between functionalities that are interacting with the surface and those that are free the solution. The spectra and contribution profiles obtained by DECRA methodology did not reveal the different components of interest based on the variations in the motional behavior of functional groups in the solution. DECRA might be helpful in the identification of some sample composition, for our systems DECRA simply was not able to resolve the primary components possibly due to their highly overlapped spectral features and small differences of the corresponding diffusion coefficients.

5.5 Conclusions

For the first time, the solution NMR toolbox has been applied to covalently modified zeolite and mesoporous silica nanoparticles. NMR signals from the bulk silica hydroxyl protons are not observed due to limited molecular motion. The NMR results suggest that the nanoparticle–ligand systems are in fast exchange in aqueous solution. Quantitative analysis of the NMR spectra for APDMMS functionalized MSN agrees well with the TGA results. 1D proton NMR, NOESY and DOSY experiments were conducted on MSN and silicalite-1 samples covalently modified with APDMMS. The solution NMR toolbox selectively provides a method for detailed, quantitative characterization of the surface modification. In this toolbox, techniques such as 1D ^1H , diffusion-ordered (DOSY), and nuclear Overhauser effect spectroscopy stand out because they enable

bound ligands to be distinguished from free ligands, and tightly bound ligands from dynamic ligands in a rapid adsorption/desorption equilibrium.

The NOESY spectra confirm that the organic functional groups are bound to the nanoparticles. Using APDMMS functionalized nanomaterials, where the ligands are covalently bound to the substrate, we demonstrate that bound and free functional groups have strongly different NOE spectra, where only bound ligands rapidly develop strong and negative NOEs that can be generated only while the ligand is bound to the nanoparticle surface. Consequently, the fact that the chemical shifts and the diffusion coefficients in surface bound APDMMS system are close to the free APDMMS values is interpreted in terms of fast exchange (Figure 5.6) between ligands in solution and on the surface.

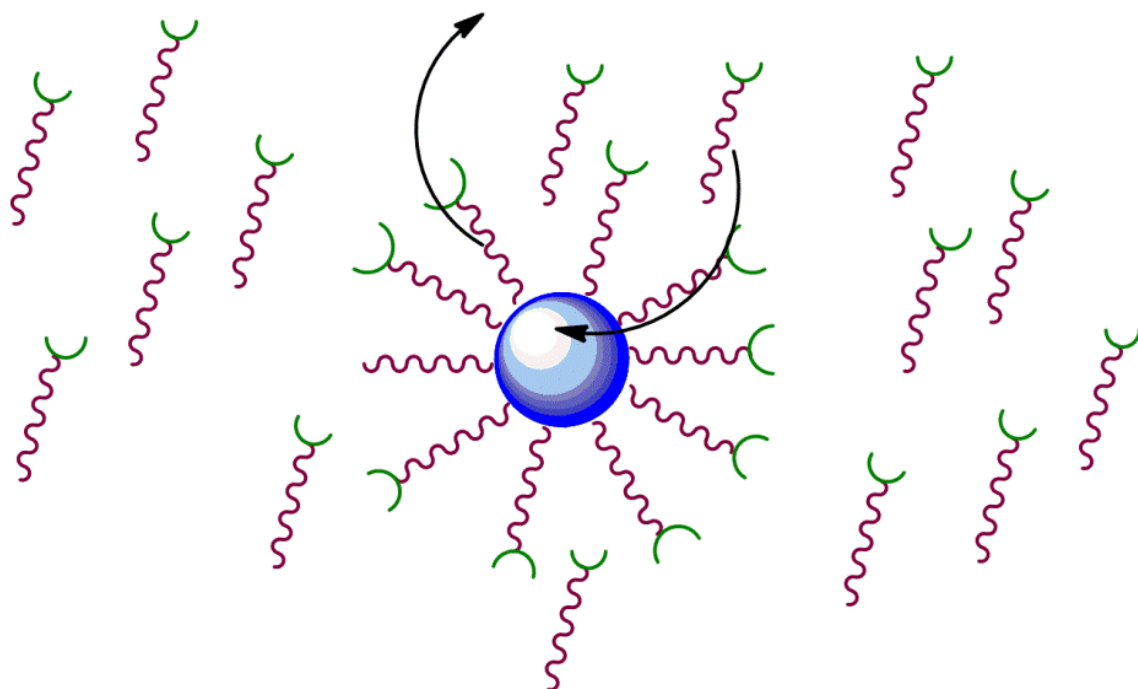



Figure 5.6 Fast exchange between free APDMMS molecules  in D_2O and

nanoparticle  surface bound APDMMS species.

CHAPTER 6

PROTON NMR STUDIES OF THE ADSORPTION OF HEAVY METAL ENVIRONMENTAL CONTAMINANTS

6.1 Abstract

The characterization of the physical properties of nanocrystalline materials is critical to the realization of their innovative applications in a broad range of areas including catalysis, drug delivery, imaging, environmental protection, and sensing. The surface chemistry of mesoporous silica nanoparticles functionalized with organosilanes (APDMMS) was selectively probed using solution ^1H NMR spectroscopy. The use of solution NMR spectroscopy results in high-resolution NMR spectra. This technique is selective for protons on the surface organic functional groups due to their motional averaging in solution. In this study, ^1H solution NMR spectroscopy was used to investigate the interface of the organic functional groups in D_2O with an environmental contaminant.

The adsorption of toxic contaminants (chromate or arsenate anions) on the surface of functionalized mesoporous silica nanoparticles has been studied by solution NMR spectroscopy. With this method, the surface bound contaminants are detected. These results demonstrate the sensitivity of solution NMR spectroscopy to the electronic environment and structure of the surface functional groups on porous nanomaterials.

6.2 Introduction

Environmental contamination and exposure to heavy metals such as arsenic and chromium is a serious growing problem throughout the world. Chromium is widely used in production of chrome-steel or chrome-nickel-steel and other alloys because of its great ability to increase resistance and durability of metals and chrome plating. It is also

applied to manufacturing of bricks in furnaces, dyes and pigments, leather tanning, and wood preserving. Manufacturing and disposal of chromium containing products as well as fossil fuel burning release the toxic metal into the air, soil, and water and lead to serious environmental contamination. As a result of an exponential increase in the use of heavy metals in industrial processes and products, human intoxication from heavy metals has risen significantly in the last few decades.

The heavy metal chromium is a carcinogenic, tasteless and odorless chemical that is linked to industrial waste from metal plating manufacturing. Severe acute chromium intoxication has been reported in literature [101-104]. The high doses are known to cause certain abnormalities and diseases [105-109]. Chromium has been associated with serious health problems through inhalation, ingestion and skin contact. This metal was discovered to be highly toxic to living organisms. For instance, chromium aerosols affect people in several ways from eyes and skin irritating to causing cancer. Indeed, it has been reported that dust of chromium species can lead to lung carcinoma. Health effects related to hexavalent chromium exposure include serious damage to liver and kidney, chromosome abnormalities [110], diarrhea, stomach and intestinal bleedings. When ingested, it was found to cause nausea and hemorrhage. Chromium can be also responsible for skin dermatitis, nasal membrane inflammation, ulceration, allergic and asthmatic reactions [111]. Its absorption by the body may severely irritate gastrointestinal tract, leading to circulatory shock and renal damage. Hexavalent chromium is mutagenic, and toxic effects may be passed on to children through the placenta. Chromium (VI) oxide is a strong oxidant, so in the body when chromic acid is formed, it corrodes the

organs and leads to paralysis. The lethal dose is approximately 1-2 g. Most countries apply a legal limit of 50 ppb chromium in drinking water.

Dangerous arsenic concentrations in natural waters are now a worldwide problem. Arsenic exists naturally in rocks and soil, water, and air. It can get into drinking water supplies drawn from groundwater that contains arsenic from natural deposits in the earth or from agricultural and industrial practices. Approximately 90 percent of industrial arsenic in the U.S. is currently used as a wood preservative, but high arsenic levels can also come from certain fertilizers, copper smelting, mining and coal burning.

Arsenic is a large problem in groundwater in Bangladesh and other places in the world. 10 ppb is the maximum exposure level by the World Health Organization (WHO) and the legal limit in the US. Arsenic has been linked to cancer of the bladder, lungs, skin, kidney, nasal passages, liver, prostate, variety of mental and physical symptoms, neurological problems and death.

Arsenic usually exists in two different forms, or valences, in a natural setting depending on the amount of oxygen available in groundwater: arsenate, As (V) and arsenite, As (III). In the pH range of 4 to 10, neutral in charge As (III) compound is the predominant form of arsenic, as opposed to negatively charged As (V) species, therefore, removal efficiencies for As (III) are usually less than those of As (V).

Many techniques including chemical precipitation, co-precipitation, coagulation, evaporator recovery process, reverse osmosis, electrolytic recovery, and adsorption have been employed for the removal of heavy metal ions such as chromium [112]. The adsorption of pollutant metal cations such as As, Cr, Hg, or Pb from aqueous solutions as well as from biological fluids by silica functionalized with sulfur-containing silanes has

been previously reported in literature [35, 57, 113-116]. It has also been shown that in aqueous matrices at neutral conditions metals like chromium or arsenic which exist in anionic form can be trapped by cationic species through electrostatic interaction[40].

In this study, APDMMS functionalized mesoporous silica nanoparticles (MSN) were used to adsorb anionic species (arsenate, chromate) from aqueous medium via electrostatic interaction between protonated amines on the surface of nanomaterials and metal anions. The adsorption process for toxic contaminants (chromate anions) on the surface of amine-functionalized MSN is shown schematically in Figure 6.1. However, surface chemistry of adsorbate materials modified with organic functional groups is not well understood. So the application of this method for biological systems, for example, could be impeded by complicated interactions of introduced sorbents with complex biological matrices. Due to the lack of highly effective methods to elucidate surface chemistry occurring between functionalities and adsorbed toxins, the development of extraction systems for toxic metals might be a very challenging task. In this study, the adsorption of chromate ($\text{Cr}_2\text{O}_7^{2-}$) and arsenate (HAsO_4^{2-}) ions on the surface of amine (APDMMS) grafted mesoporous silica nanoparticles in aqueous solution have been studied by ^1H solution NMR spectroscopy.

6.3 Experimental Methods

6.3.1 Chromate Adsorption Experiments

Samples with free APDMMS/dichromate in D_2O were prepared as following: 0.036 mmol of APDMMS MSN was added to 0.6 mL of 4500 ppm solution prepared from sodium dichromate ($\text{Na}_2\text{Cr}_2\text{O}_7$) in D_2O and controlled at a desired pH ranging from 2 to 12 with HNO_3 or NaOH . Then APDMMS/dichromate solutions were stirred overnight at

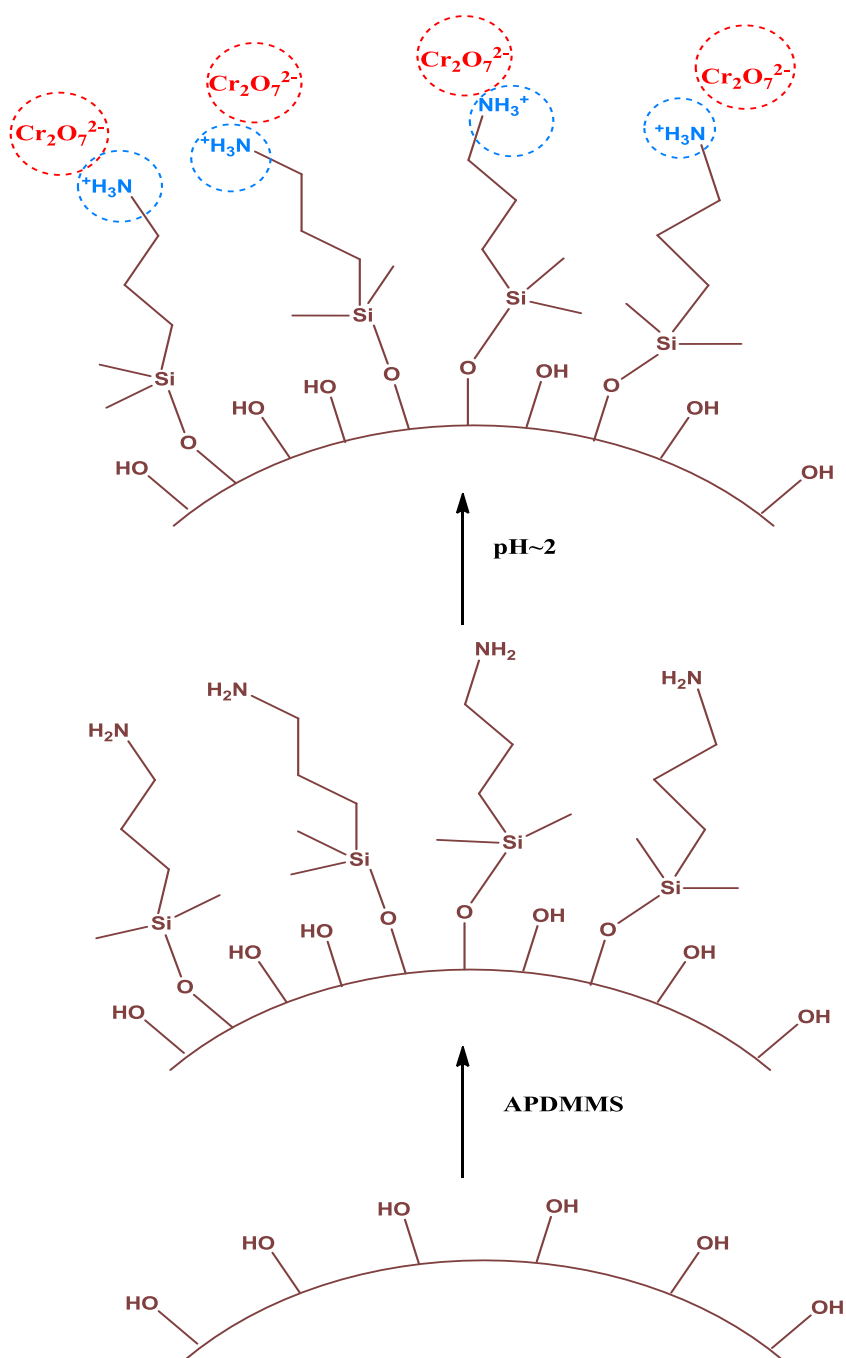


Figure 6.1 Schematic representation of the toxic contaminants (chromate anions) adsorption process on the surface of APDMMMS functionalized MSN.

room temperature. For samples with APDMMS functionalized MSN: 6 mg of APDMMS functionalized MSN was added to 0.6 mL of 4500 ppm solution prepared from potassium dichromate ($\text{K}_2\text{Cr}_2\text{O}_7$) in D_2O and controlled at a desired pH ranging from 2 to 12 with HNO_3 or NaOH . The functionalized MSN/chromate solution was stirred overnight at room temperature.

6.3.2 Arsenate Adsorption Experiments

Samples with free APDMMS/arsenate in D_2O were prepared as following: 0.036 mmol of APDMMS MSN was added to 0.6 mL of 4500 ppm solution prepared from sodium arsenate NaHAsO_4 in D_2O and controlled at a desired pH ranging from 2 to 12 with HNO_3 or NaOH . Then APDMMS/arsenate solutions were stirred overnight at room temperature. For samples with APDMMS functionalized MSN: 6 mg of APDMMS functionalized MSN was added to 0.6 mL of 4500 ppm solution prepared from KHAsO_4 in D_2O and controlled at a desired pH ranging from 2 to 12 with HNO_3 or NaOH . The functionalized MSN/arsenate solution was stirred overnight at room temperature.

6.3.3 NMR Experiments

6 mL of functionalized MSN /dichromate (or functionalized MSN/arsenate) solution was placed in an NMR tube and analyzed using solution state NMR spectroscopy. Acetone was used as an internal standard for all NMR experiments. The pH was measured before and after the NMR experiment using a Corning 320 pH meter and the average of the two values was used in subsequent data analysis. The pH reading obtained before and after each NMR experiment differed by <0.1 pH units. The NMR samples were sonicated for approximately 0.5 hour immediately before the NMR experiments. The proton NMR experiments were conducted on a Bruker DRX-400

Instrument operating at 400 MHz. Single pulse ^1H and 2D NOESY and 2D DOSY NMR experiments were performed. For 2D NOESY and 2D DOSY NMR experiments solution pH was adjusted to be ~ 11.6 . Single pulse experiments were performed with a pulse width of 7 μs and a recycle delay of 0.01 s with 128 scans.

6.3.4 Experimental Parameters for Pulse Field Gradient

Spin-echo (PGSE) NMR Experiments.

The Diffusion ordered spectroscopy (DOSY) experiments were conducted on a Bruker DRX-400 Instrument operating at 400 MHz. All diffusion measurements were made using the stimulated echo pulse sequence with bipolar gradient pulses. The diffusion delay (Δ) varied from 20 to 300 ms, and the gradient pulse duration (δ) from 1.6 to 3 ms and were optimized in order to obtain 1-5% residual signal with maximum gradient strength. The recycle delay was adjusted to 4s. Rectangular shapes were used for the gradients and a linear gradient ramp with 16 increments between 2% and 95% was applied for the diffusion relevant gradients. The strength of the gradient (56.0 Gauss/cm at a current of 10A) was calibrated by measuring the self-diffusion of the residual HDO signal in a 100% D_2O sample at 298K ($1.90 \times 10^{-9} \text{m}^2 \text{s}^{-1}$). Diffusion coefficients were obtained by integrating the resonances of interest and fitting the data to the Stejskal–Tanner equation.

6.3.5 Experimental Parameters for

2D NOESY NMR Spectroscopy

2D nuclear Overhauser effect spectroscopy (NOESY) experiments were recorded on a Bruker Avance 500 spectrometer that was equipped with a 5 mm triple resonance inverse Z-gradient probe. All of the samples were prepared in D_2O . 2D NOESY spectra

were recorded using a ^1H spectral width of 7.00 ppm. Typically 150 t_1 increments, consisting of 16 scans of 2048 sampled data points each, were recorded with a 4 s relaxation delay. ^1H spectral widths and 90° pulse widths are optimized for each sample. A recycle delay (D_1) of 4.0s was used in all the 2D experiments. An optimal range of mixing times for NOESY experiments was determined using the one dimensional version of spin-lattice relaxation measurements. 2D NOESY with mixing times of 200, 500, 1000, and 1500 ms were recorded. All NMR data were processed with TOPSPIN 1.3 or 2.1 suites of software programs. The 2D NMR data were processed with the zero-filling to 2,048 points and 1,024 points in acquisition and second dimension, respectively.

6.4 Results and Discussion

6.4.1 ^1H Solution NMR Studies

The proton chemical shifts for free as well as for surface bound APDMMS molecules vary with pH with the protons closest to the functional group exhibiting the largest chemical shift alteration as shown in Figures 6.2-6.5, where the proton NMR spectral assignments for APDMMS protons are shown on the inset molecule. This downfield chemical shift displacement is due to a change in the amine group electron configuration, namely its protonation. The protons closest to the amine functionality in APDMMS experience different electronic environments depending on whether the amine is neutral or protonated. Protonation typically takes place on the time scale of diffusion; therefore in the NMR spectrum, the resonance observed will be a weighted average of the chemical shifts for the protonated and nonprotonated forms for both surface bound and free functionalities in the solution. Though, as it can be seen from Figures 6.3 and 6.5, electrostatic interactions induced by the $\sim\text{NH}_3^+$ group and chromate (or arsenate) ions for

APDMMS molecules attached to MSN surface being split and/or shifted. This observation can be attributed to the different electron environment of the protonated amine functionalities that interact with contaminant anions compared with those that do not. As a matter of fact, only protonated amine groups can attract metal anions electrostatically. Some protonated functionalities are stabilized by anionic species and, consequently, prevent their deprotonation with increasing pH. As a result, two different resonances for the group of protons in the same structural position are observed: one is assigned to those molecules with adsorbed metal anions; another one is assigned to species without bound anions. It can be also seen that one resonance signal changes as a function of pH, while another one stays the same. It can be interpreted such that the NMR signal that experiences chemical shift displacement is a weighted average of the chemical shifts for the protonated and nonprotonated amines with no bound anions, while another one represents adsorbed metal anions. It is interesting to note, that the observations of peak shifting were found only for APDMMS molecules on the surface of nanomaterials and not for free APDMMS in the presence of chromate (or arsenate). For instance, peaks 3^A and 3^B that can be seen from Figure 6.3 and 6.5 are coming from protons that are closest to the functional groups and represent ligands interacting with anions and those that are without adsorbed contaminants, respectively. This chemical shift difference is much greater for hydrogens on C3 (in close vicinity to amine groups) than for other protons (C2, C1, and C5) that are further away from the functionalities (Figure 6.3 and 6.5, peaks 3^A and 3^B).

The intensities of two parts of peak 3: 3^A and 3^B observed in spectra for chromate/APDMMS-functionalized MSN in D₂O (shown in Figure 6.3) were found to

vary with pH. It can be interpreted as the relative number of protonated and unprotonated amine groups is pH dependent, and, consequently, the number of functionalities interacting with contaminants in the solution also changes with pH.

There are no double peaks observed for organic species that are free in the solution (Figure 6.2 and 6.4). Further experiments with functional groups with adsorbed ions could clarify observed phenomena and help interpret obtain results.

6.4.2 2D NOESY NMR Spectroscopy

The NOESY spectrum for chromate/APDMMS-functionalized MSN in D₂O is shown in Figure 6.6. It can be observed from the spectrum that the cross peaks and the diagonal peaks in the NOESY spectrum exhibit the same sign indicating a bound APDMMS surface group. There was no NOE signal found for the additional triplet at 2.91 ppm that might be assigned to protons from the functional groups interacting with anions, since its chemical shift does not vary with pH.

6.4.3 DOSY/Diffusion Coefficient Measurements

However, NOESY experiments suggest that the APDMMS molecules are bound to the MSN surface. As can be seen from Table 6.1 the diffusion coefficients measured by DOSY for chromate/APDMMS-functionalized MSN in D₂O are close to those for free APDMMS in solution $\sim 6.1 \times 10^{-10} \text{ m}^2/\text{s}$. However, since the negative NOEs are observed in the NOESY data indicating surface bound APDMMS, the DOSY data is interpreted as being indicative of a fast exchange between APDMMS and surface bound APDMMS and the presence of anionic species in solution did not change neither 2D NOESY NMR nor DOSY results and similar with spectra obtained for APDMMS-functionalized MSN in D₂O with no metal ions present.

6.5 Conclusions

The adsorption of toxic contaminants (chromate and arsenate anions) on the surface of mesoporous silica nanoparticles has been studied by ^1H solution NMR spectroscopy. With this method, the surface bound contaminants were detected. The sensitivity of solution NMR spectroscopy to the electronic environment and structure of the surface functional groups on porous nanomaterials was demonstrated.

NMR spectroscopy was utilized for the characterization of APDMMS functionalized mesoporous silica nanoparticles with adsorbed chromate or arsenate anions. Adsorption of the contaminants occurred via electrostatic interaction of protonated free or MSN surface bound amine functionalities with anionic toxic species in D_2O . The variation in the proton chemical shift for the alkyl group protons closest to the amine group with pH has been observed for both systems. The additional peaks appeared on the spectra for the functional groups bound to the surface of nanoparticles.

DOSY and NOESY spectroscopy were used as NMR techniques that enable bound ligands to be distinguished from free ligands, and tightly bound ligands from dynamic ligands in a rapid adsorption/desorption equilibrium. DOSY was used to measure the diffusion coefficients of the surface bound organic ligands with adsorbed anions. The NOESY spectra confirmed that the organic functional groups were bound to the nanoparticles.

Table 6.1: Diffusion Coefficients (m^2/s) obtained from DOSY experiments for Pure APDMMS, MSN-APDMMS, and chromate/APDMMS-functionalized MSN in D_2O at $\text{pH}=11.6$. Proton solution state NMR spectra for chromate/APDMMS-functionalized MSN in D_2O at various pH are shown in Figure 6.3.

	Peak 1 @0.55 ppm	Peak 2 @1.6 ppm	Peak 2 ^A @1.4 ppm	Peak 3 ^B @ 2.9 ppm	Peak 3 ^A @ 2.72 ppm	Peak 4 @3.25 ppm	Peak 5 @0.1 ppm
Pure APDMMS	6.11×10^{-10}	6.12×10^{-10}		6.11×10^{-10}		1.37×10^{-9}	6.11×10^{-10}
MSN-APDMMS	6.49×10^{-10}	6.26×10^{-10}		6.67×10^{-10}		-	6.46×10^{-10}
MSN- APDMMS/Chromate	5.16×10^{-10}	6.04×10^{-10}	5.17×10^{-10}	3.23×10^{-10}	1.4×10^{-9}	-	5.39×10^{-10}

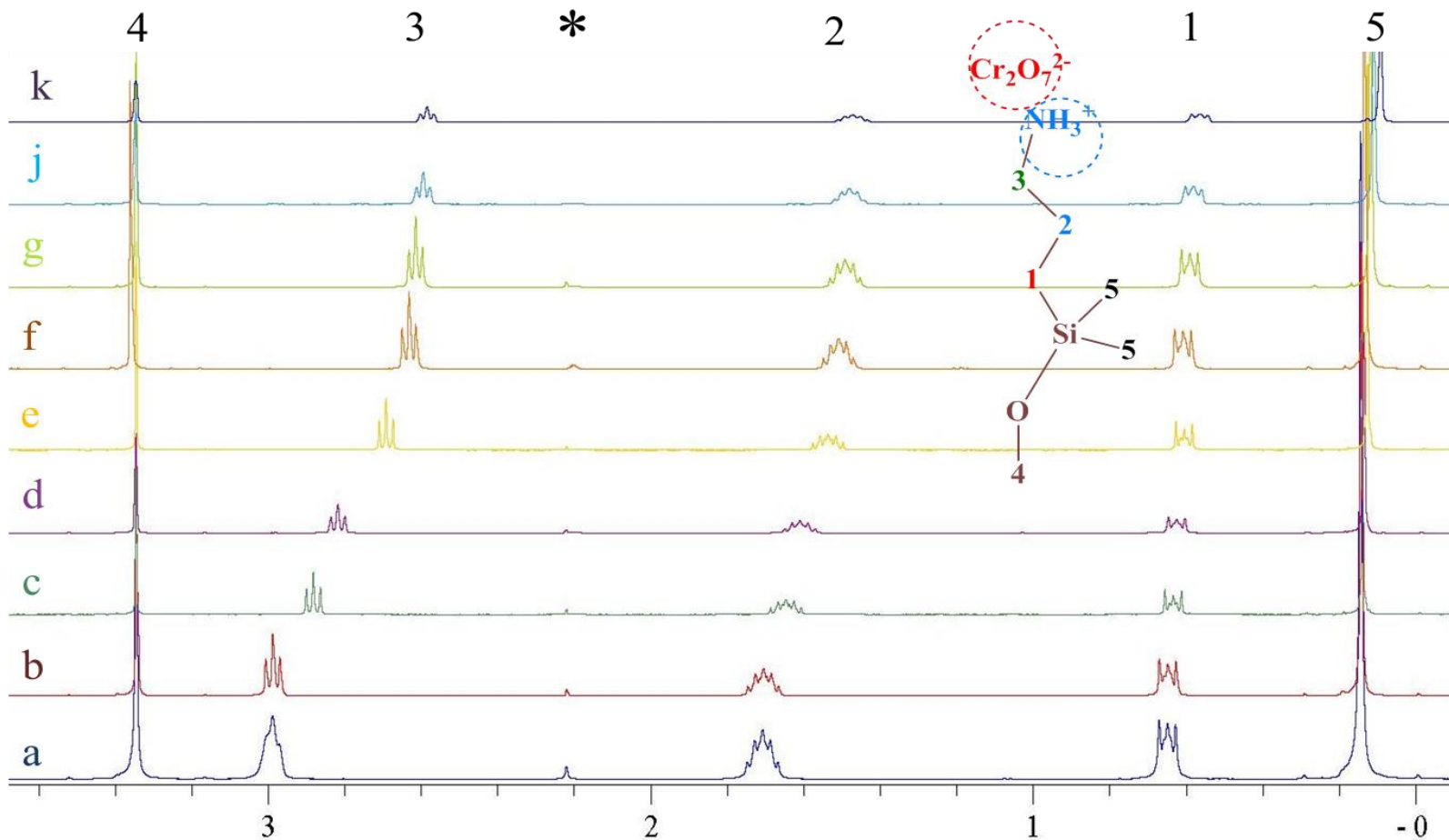


Figure 6.2 Proton solution state NMR spectra for chromate / free APDMMS in D_2O at varying pH's: a) 2.3, b) 8.6, c) 10.4, d) 10.8, e) 11.2, e) 11.4, g) 11.5, j) 12.7, k) 12.7. * is a peak for acetone (used as an internal standard), 1, 2, 3 and 5 are peaks due to the protons in the functional group on the inset molecule.

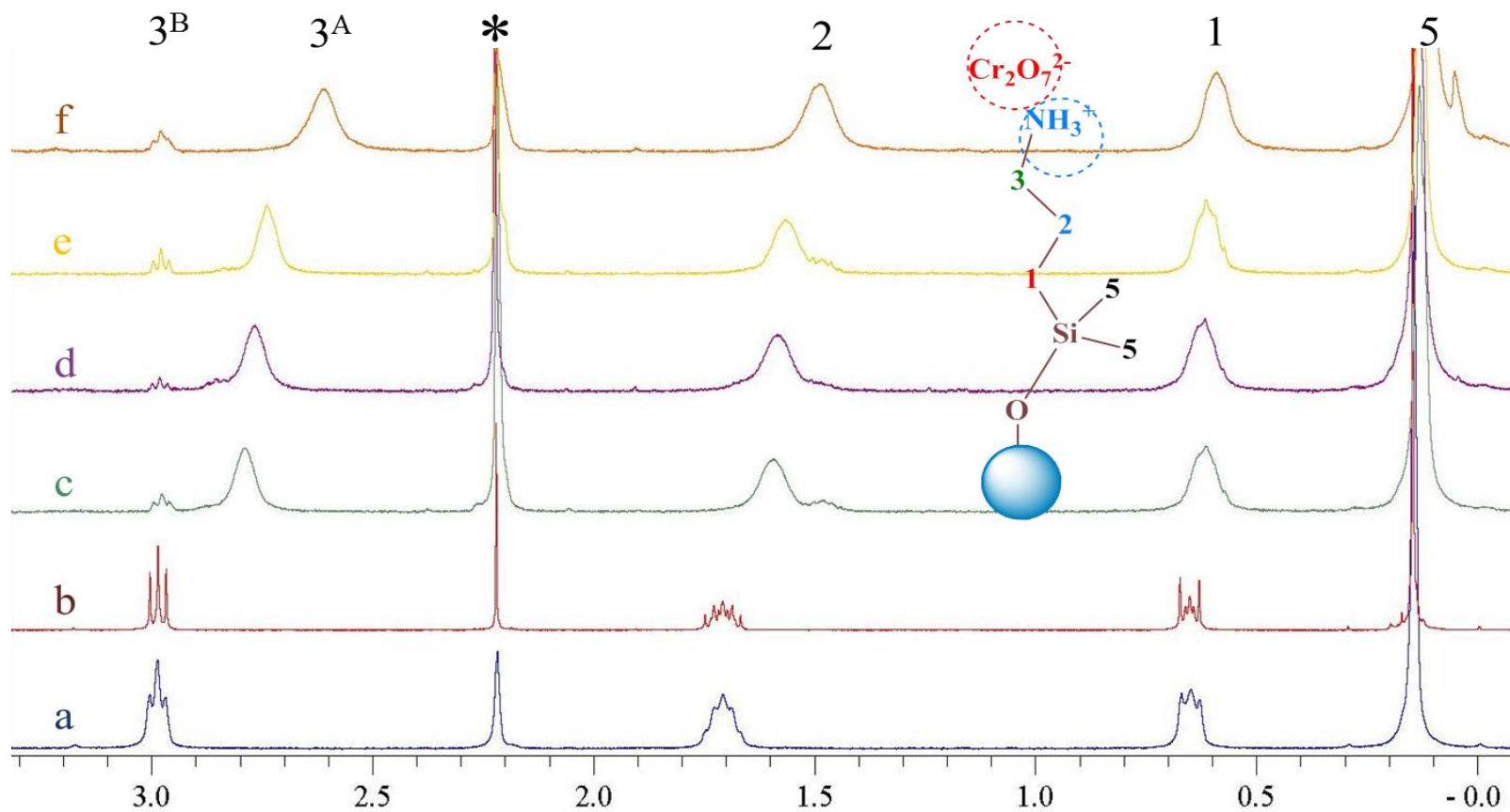


Figure 6.3 Proton solution state NMR spectra for chromate/APDMMS-functionalized MSN in D_2O at varying pH's: a) 7.8, b) 8.5, c) 10.8, d) 11.0, e) 11.2, f) 11.8. * is a peak for acetone (used as an internal standard), 1, 2, 3 and 5 are peaks due to the protons in the functional group on the inset molecule.

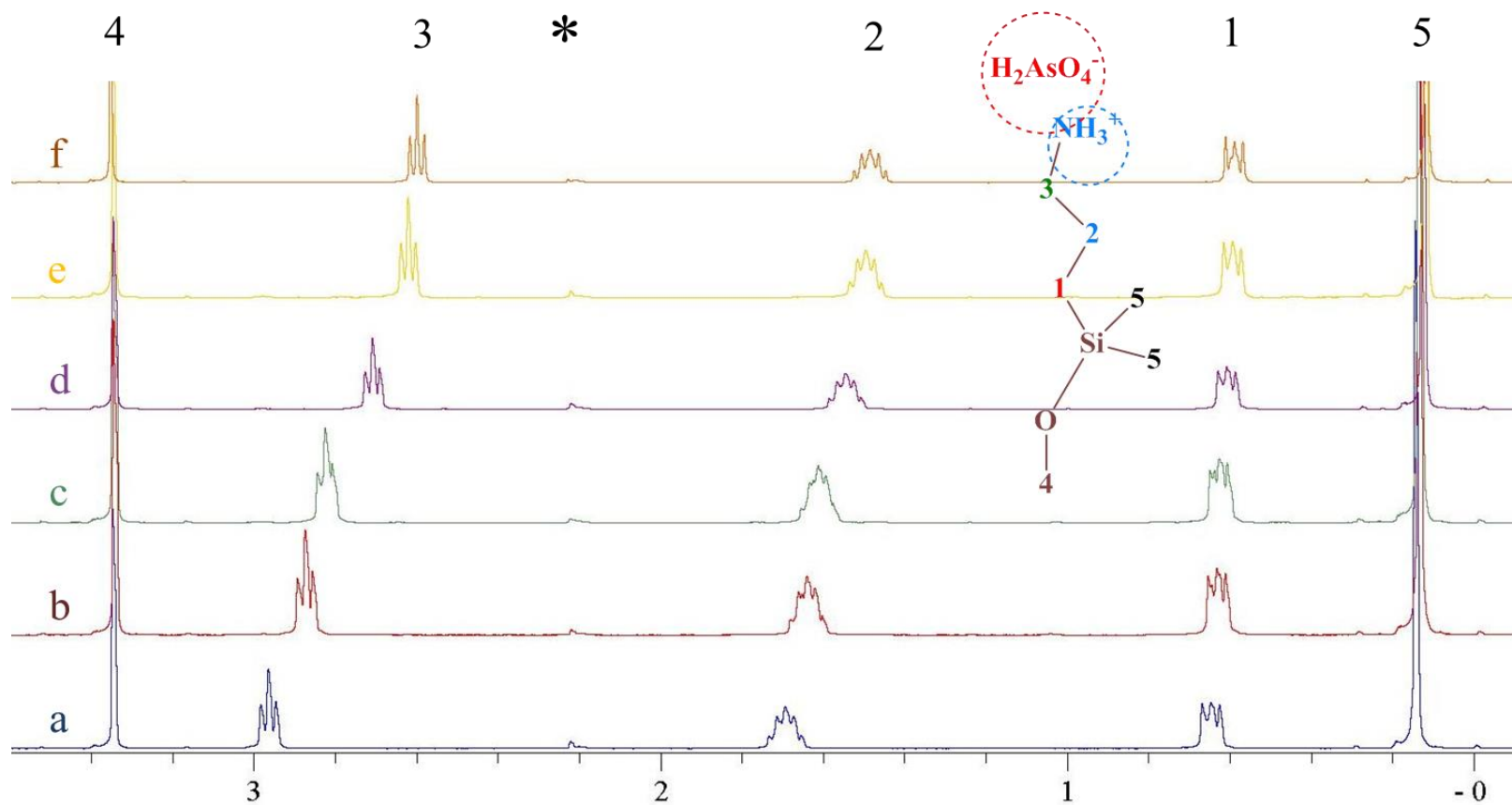


Figure 6.4 Proton solution state NMR spectra for arsenate / free APDMMS in D_2O at varying pH's: a) 9.9, b) 10.64, c) 10.8, d) 11.1, e) 11.6, e) 11.5, g) 12.0. * is a peak for acetone (used as an internal standard), 1, 2, 3 and 5 are peaks due to the protons in the functional group on the inset molecule.

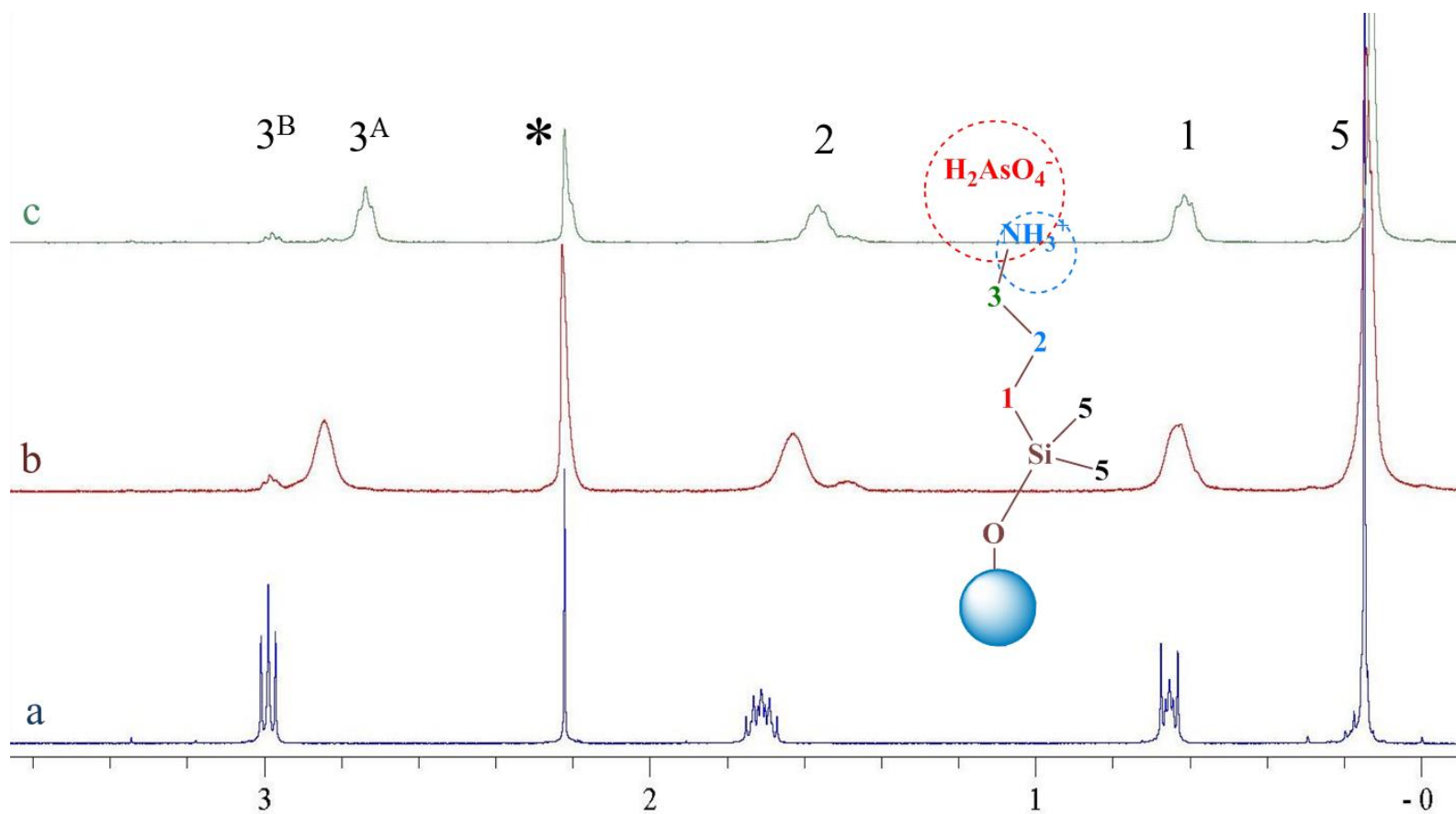


Figure 6.5 Proton solution state NMR spectra for arsenate/APDMMS-functionalized MSN in D₂O at varying pH's: a) 7.3, b) 10.8, c) 11.4. * is a peak for acetone (used as an internal standard), 1, 2, 3 and 5 are peaks due to the protons in the functional group on the inset molecule.

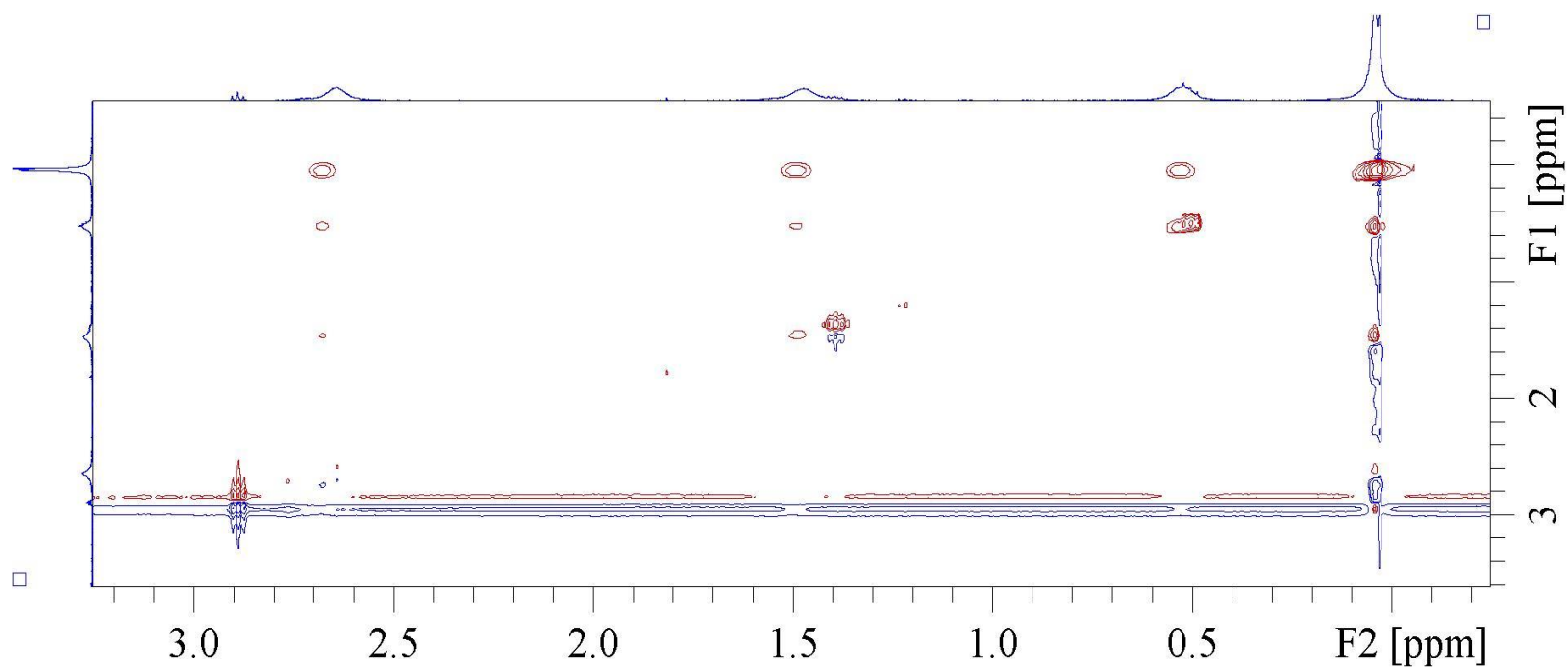


Figure 6.6 The NOESY spectra for chromate/APDMMS-functionalized MSN in D₂O at pH=11.6 (with mixing time 200 ms).

CHAPTER 7

CONCLUSIONS AND FUTURE WORK

Nanocrystalline silicalite and mesoporous silica nanoparticles with sizes of 35 and 52 nm respectively, were synthesized and functionalized with various organosilanes: APDMMS, APTES, and MPTMS. The functionalized nanomaterials were characterized by powder XRD, solid state ^{29}Si , ^{13}C , ^1H MAS NMR, TGA, FTIR, TEM, SEM, zeta potential, and ^1H solution state NMR. Obtained results demonstrate that the external surface of nanocrystals can be tailored through functionalization in order to achieve desired properties.

Specific functional groups that can be used to absorb heavy metals from the solution or target disease cells, such as cancer cells were synthesized on the external surface of silicalite nanoparticles, while for MSN functionalization took place on both external surface and inside of pores. In these studies, three main issues related to functionalized nanomaterials were addressed through the application of nuclear magnetic resonance (NMR) techniques including: 1) surface composition and structure of functionalized nanocrystalline particles; 2) chemical properties of the guest molecules on the surface of nanomaterials, and 3) adsorption and reactivity of surface bound functional groups.

We used nuclear magnetic resonance (NMR) spectroscopy for the characterization of molecular structure and conformational dynamics with atomic level detail of functionalized nanomaterials in an aqueous environment. The application of ^1H solution state NMR allowed us to understand the aqueous phase behavior of functionalized nanomaterials which is a key factor in the design and development of safe

nanomaterials because their interactions with living systems are mediated through the aqueous phase. The use of solution NMR spectroscopy results in high-resolution NMR spectra. This technique is selective for protons on the surface organic functional groups due to their motional averaging in solution. In this study, ^1H solution NMR spectroscopy was used to investigate the interface of the organic functional groups in D_2O and to obtain fundamental and essential knowledge in interfacial chemical and physical phenomena that occur on the surface of nanoparticles.

For the first time, the solution NMR toolbox has been applied to covalently modified zeolite and mesoporous silica nanoparticles. ^1H solution NMR spectroscopy was utilized to elucidate the interface of the organic functional groups of APDMMS (APTES, or MPTMS) functionalized silicalite (~35 nm) and mesoporous silica nanoparticles (MSN) (~52 nm) in D_2O . The pKa for the amine group of APDMMS (APTES) and the thiol group (-SH) of MPTMS functionalized silicalite nanoparticles and MSN in D_2O was determined using an NMR-pH titration method based on the variation in the proton chemical shift for the alkyl group protons closest to the amine (or thiol) group with pH. The pKa for these functional groups covalently bound to the surface of nanoparticles was determined using an NMR-pH titration method based on the variation in the proton chemical shift for the alkyl group protons closest to the amine group with pH.

Diffusion ordered (DOSY) and nuclear Overhauser effect spectroscopy (NOESY) were used as NMR techniques that enable bound ligands to be distinguished from free ligands, and tightly bound ligands from dynamic ligands in a rapid adsorption/desorption equilibrium. Diffusion ordered spectroscopy was used to measure the diffusion

coefficients of the surface bound organic ligands. The NOESY spectra confirmed that the organic functional groups were bound to the nanoparticles. Using APDMMS functionalized nanomaterials, where the ligands are tightly bound to the substrate, we demonstrated that bound and free functional groups had strongly different NOE spectra, where only bound ligands rapidly developed strong and negative NOEs that can be generated only while the ligand is bound to the nanocrystal surface. On the basis of 1D ^1H and DOSY and NOESY spectroscopy, we found that APDMMS molecules present interacted with the nanomaterial surface, although the APDMMS ligands resonances and diffusion coefficient resembled those of free molecules. These observations suggest that these NMR observables are a weighted average of a free and a bound state of organic functional groups and can be interpreted in terms of fast exchange between bound and free functional groups.

The adsorption of toxic contaminants (chromate and arsenate anions) on the surface of mesoporous silica nanoparticles has been studied by ^1H solution NMR spectroscopy. With this method, the surface bound contaminants are detected. The sensitivity of solution NMR spectroscopy to the electronic environment and structure of the surface functional groups on porous nanomaterials was demonstrated.

Future development of solution state NMR techniques as a surface selective probe for functionalized nanomaterials could improve on the characterization methods of nanoparticles in aqueous environments, attempt to address qualitative and quantitative analysis of those materials and their surfaces, or look at the structure, properties and surface chemistry of bound ligands. Improvements in the analytical toolbox for the structure elucidation would very be beneficial for a better understanding and appropriate

utilization of these materials in a wide range of applications including catalysis, drug delivery, environmental remediation, and many others.

REFERENCES

1. Vallet-Regi, M., et al., *A New Property of MCM-41: Drug Delivery System*. Chemistry of Materials, 2000. **13**(2): p. 308-311.
2. Tosheva, L. and V.P. Valtchev, *Nanozeolites: Synthesis, Crystallization Mechanism, and Applications*. Chemistry of Materials, 2005. **17**(10): p. 2494-2513.
3. Bhatia, S., *Zeolite catalysis: Principles and Applications*. CRC Press: Boca Raton, 1990.
4. Habuda-Stanić, M., et al., *Quality of groundwater in eastern Croatia. The problem of arsenic pollution*. Desalination, 2007. **210**(1-3): p. 157-162.
5. Klinowski, J., Chem. Rev., 1991. **91**(7): p. 1459-1479.
6. Gutiérrez-Alejandre, A., et al., *Hydroconversion of Hydrocarbons over HZSM5 and Mo-HZSM5 Catalysts: A FTIR and Flow Reactor Study*. Industrial & Engineering Chemistry Research, 2001. **40**(16): p. 3484-3494.
7. Krogh, A., et al., *Re/HZSM-5: a new catalyst for ethane aromatization with improved stability*. Catalysis Communications, 2003. **4**(12): p. 627-630.
8. Lu, R., et al., *Properties and Characterization of Modified HZSM-5 Zeolites*. Journal of Natural Gas Chemistry, 2003. **12**(1): p. 56-62.
9. Romotowski, T., et al., *Some observations of HZSM-5 zeolite dehydroxylation*. Reaction Kinetics and Catalysis Letters, 1992. **46**(1): p. 193-197.
10. Sigl, M., et al., *Characterization of the acid properties of [Al]-, [Ga]- and [Fe]-HZSM-5 by low-temperature FTIR spectroscopy of adsorbed dihydrogen and ethylbenzene disproportionation*. Catalysis Letters, 1997. **45**(1-2): p. 27-33.
11. Richer, R., *Direct synthesis of functionalizedmesoporous silica by non-ionic alkylpolyethyleneoxide surfactant assembly*. Chemical Communications, 1998: p. 1775-1777.
12. Haggerty, G.M. and R.S. Bowman, *Sorption of chromate and other inorganic anions by organo-zeolite*. Environmental Science & Technology, 1994. **28**(3): p. 452-458.
13. White, M.A. and M. Lumsden, *Bonding of Organic Amino, Vinyl, and Acryl Groups to Nanometer-Sized NaX Zeolite Crystal Surfaces*. Langmuir, 2003. **19**(10): p. 4205-4210.

14. http://izasc.ethz.ch/fmi/xsl/IZA-SC/ftc_main_image.xsl?-db=Atlas_main&-lay=fw&STC=MFI&-find.
15. http://www.analyticalspectroscopy.net/ap7_html_3bdb944c.jpg.
16. Tataurova, Y., et al., *Surface-Selective Solution NMR Studies of Functionalized Zeolite Nanoparticles*. The Journal of Physical Chemistry Letters, 2012. **3**(3): p. 425-429.
17. Donkers, R.L., Y. Song, and R.W. Murray, *Substituent effects on the exchange dynamics of ligands on 1.6 nm diameter gold nanoparticles*. Langmuir, 2004. **20**(11): p. 4703-4707.
18. Guo, R., et al., *Does core size matter in the kinetics of ligand exchanges of monolayer-protected Au clusters?* Journal of the American Chemical Society, 2005. **127**(8): p. 2752-7.
19. Fritzinger, B., et al., *Utilizing Self-Exchange To Address the Binding of Carboxylic Acid Ligands to CdSe Quantum Dots*. Journal of the American Chemical Society, 2010. **132**(29): p. 10195-10201.
20. Fritzinger, B., et al., *In Situ Observation of Rapid Ligand Exchange in Colloidal Nanocrystal Suspensions Using Transfer NOE Nuclear Magnetic Resonance Spectroscopy*. Journal Of The American Chemical Society, 2009. **131**(8): p. 3024-3032.
21. Hassinen, A., et al., *Nuclear Magnetic Resonance Spectroscopy Demonstrating Dynamic Stabilization of CdSe Quantum Dots by Alkylamines*. Journal of Physical Chemistry Letters, 2010. **1**(17): p. 2577-2581.
22. Hens, Z., I. Moreels, and J.C. Martins, *In situ H-1 NMR study on the trioctylphosphine oxide capping of colloidal InP nanocrystals*. Chemphyschem, 2005. **6**(12): p. 2578-2584.
23. Kralj, M., *Biomedical and environmental potential of nanoporous materials*. Periodicum Biologorum, 2003. **105**(2): p. 99-107.
24. Kralj, M. and K. Pavelic, *Medicine on a small scale*. EMBO Reports, 2003. **4**: p. 1008-1012.
25. Pavelic, K., et al., *Natural Zeolite Clinoptilolite: New Adjuvant in Anticancer Therapy*. J. Mol. Med., 2001. **78**: p. 708-720.
26. Larsen, S.C., *Nanocrystalline zeolites and zeolite structures: Synthesis, characterization, and applications*. J. Phys. Chem. C, 2007. **111**(50): p. 18464-18474.

27. Li, G.H., et al., *Selective catalytic reduction of NO₂ with urea in nanocrystalline NaY zeolite*. Journal of Catalysis, 2005. **234**(2): p. 401-413.
28. Pearce, M.E., et al., *Silicalite Nanoparticles That Promote Transgene Expression*. Nanotechnology, 2008. **19**: p. 175103-175109.
29. Trewyn, B.G., et al., *Mesoporous silica nanoparticle based controlled release, drug delivery, and biosensor systems*. Chemical Communications, 2007(31): p. 3236-3245.
30. Tsai, C.P., et al., *High-Contrast Paramagnetic Fluorescent Mesoporous Silica Nanorods as a Multifunctional Cell-Imaging Probe*. Small, 2008. **4**(2): p. 186-191.
31. Matheoud, R., et al., *The use of molecular sieves to simulate hot lesions in F-18-fluorodeoxyglucose - positron emission tomography imaging*. Physics in Medicine and Biology, 2008. **53**(8): p. N137-N148.
32. Li, W.S., et al., *Zeolites Mn²⁺-NaY as oral gastrointestinal tract contrast agents in magnetic resonance imaging*. Acta Chimica Sinica, 2007. **65**(18): p. 2029-2033.
33. Lin, Y.S., et al., *Gadolinium(III)-incorporated nanosized mesoporous silica as potential magnetic resonance imaging contrast agents*. J. Phys. Chem. B, 2004. **108**(40): p. 15608-15611.
34. Balkus, K.J. and J.M. Shi, *A study of suspending agents for gadolinium(III)-exchanged hectorite. An oral magnetic resonance imaging contrast agent*. Langmuir, 1996. **12**(26): p. 6277-6281.
35. Yantasee, W., et al., *Functionalized Nanoporous Silica for the Removal of Heavy Metals from Biological Systems: Adsorption and Application*. ACS Applied Materials & Interfaces, 2010. **2**(10): p. 2749-2758.
36. Galownia, J., J. Martin, and M.E. Davis, *Aluminophosphate-based, microporous materials for blood clotting*. Microporous and Mesoporous Materials, 2006. **92**(1-3): p. 61-63.
37. Tsotsalas, M.M., et al., *Encapsulating In-111 in Nanocontainers for Scintigraphic Imaging: Synthesis, Characterization, and In Vivo Biodistribution*. ACS Nano, 2010. **4**(1): p. 342-348.
38. Tsotsalas, M., et al., *Functionalized nanocontainers as dual magnetic and optical probes for molecular imaging applications*. Chem. Mat., 2008. **20**(18): p. 5888-5893.
39. Lerouge, F., et al., *Towards thrombosis-targeted zeolite nanoparticles for laser-polarized Xe-129 MRI*. J. Mater. Chem., 2009. **19**(3): p. 379-386.

40. Barquist, K. and S.C. Larsen, *Chromate adsorption on amine-functionalized nanocrystalline silicalite-I*. Microporous and Mesoporous Materials, 2008. **116**(1-3): p. 365-369.
41. Chutia, P., et al., *Adsorption of As(V) on surfactant-modified natural zeolites*. Journal of Hazardous Materials, 2009. **162**(1): p. 204-211.
42. Chen, X.Q., et al., *Synthesis of Highly Selective Magnetic Mesoporous Adsorbent*. Journal of Physical Chemistry C, 2009. **113**(22): p. 9804-9813.
43. Velma, V., S.S. Vutukuru, and P.B. Tchounwou, *Ecotoxicology of hexavalent chromium in freshwater fish: a critical review*. Rev Environ Health, 2009. **24**(2): p. 129-45.
44. Li, Y., et al., *Removal of hexavalent chromium in soil and groundwater by supported nano zero-valent iron on silica fume*. Water Sci Technol, 2011. **63**(12): p. 2781-7.
45. Lim, S.-F., et al., *Uptake of arsenate by an alginate-encapsulated magnetic sorbent: Process performance and characterization of adsorption chemistry*. Journal of Colloid and Interface Science, 2009. **333**(1): p. 33-39.
46. Song, W., et al., *Synthesis, Characterization, and Adsorption Properties of Nanocrystalline ZSM-5*. Langmuir, 2004. **20**(19): p. 8301-8306.
47. Mintova, S. and V. Valtchev, *Synthesis of nanosized FAU-type zeolite*, in *Studies in Surface Science and Catalysis*, G.P.-B.J.B.N. I. Kiricsi and H.G. Karge, Editors. 1999, Elsevier. p. 141-148.
48. Song, W., et al., *Microscopic and Macroscopic Characterization of Organosilane-Functionalized Nanocrystalline NaZSM-5*. Langmuir, 2005. **21**(15): p. 7009-7014.
49. Bowman, R.S., *Applications of surfactant-modified zeolites to environmental remediation*. Microporous and Mesoporous Materials, 2003. **61**(1-3): p. 43-56.
50. Li, Z., Y. Zou, and R.S. Bowman, *Long-Term Chemical and Biological Stability of Surfactant-Modified Zeolite*. Environmental Science & Technology, 1998. **32**(17): p. 2628-2632.
51. Lim, M.H. and A. Stein, *Comparative Studies of Grafting and Direct Syntheses of Inorganic–Organic Hybrid Mesoporous Materials*. Chemistry of Materials, 1999. **11**(11): p. 3285-3295.
52. Rosenholm, J.M. and M. Lindén, *Wet-Chemical Analysis of Surface Concentration of Accessible Groups on Different Amino-Functionalized Mesoporous SBA-15 Silicas*. Chemistry of Materials, 2007. **19**(20): p. 5023-5034.

53. Stein, A., B.J. Melde, and R.C. Schroden, *Hybrid Inorganic–Organic Mesoporous Silicates—Nanoscopic Reactors Coming of Age*. Advanced Materials, 2000. **12**(19): p. 1403-1419.
54. Song, W., et al., *Size-Dependent Properties of Nanocrystalline Silicalite Synthesized with Systematically Varied Crystal Sizes*. Langmuir, 2004. **20**(11): p. 4696-4702.
55. Möller, K., J. Kobler, and T. Bein, *Colloidal Suspensions of Nanometer-Sized Mesoporous Silica*. Advanced Functional Materials, 2007. **17**(4): p. 605-612.
56. Pecharsky, V.K. and P.Y. Zavalij, *Fundamentals Of Powder Diffraction And Structural Characterization Of Materials*. 2004: Springer.
57. Liu, A.M., et al., *A new class of hybrid mesoporous materials with functionalized organic monolayers for selective adsorption of heavy metal ions*. Chemical Communications, 2000(13): p. 1145-1146.
58. Zheng, H., C. Gao, and S. Che, *Amino and quaternary ammonium group functionalized mesoporous silica: An efficient ion-exchange method to remove anionic surfactant from AMS*. Microporous and Mesoporous Materials, 2008. **116**(1–3): p. 299-307.
59. Maria Chong, A.S. and X.S. Zhao, *Functionalization of SBA-15 with APTES and Characterization of Functionalized Materials*. The Journal of Physical Chemistry B, 2003. **107**(46): p. 12650-12657.
60. Suzuki, T.M., et al., *Direct synthesis of amino-functionalized monodispersed mesoporous silica spheres and their catalytic activity for nitroaldol condensation*. Journal of Molecular Catalysis A: Chemical, 2008. **280**(1–2): p. 224-232.
61. Hamoudi, S., A. El-Nemr, and K. Belkacemi, *Adsorptive removal of dihydrogenphosphate ion from aqueous solutions using mono, di- and tri-ammonium-functionalized SBA-15*. Journal of Colloid and Interface Science, 2010. **343**(2): p. 615-621.
62. Fomitchev, D., et al., *Colloidal Silica Particles for Toners: Treatment Chemistry*. NIP & Digital Fabrication Conference, 2007. **2007**(1): p. 283-287.
63. Du, F., et al., *Structure elucidation of nanoparticle-bound organic molecules by ¹H NMR*. TrAC Trends in Analytical Chemistry, 2009. **28**(1): p. 88-95.
64. Gunn, J., R.K. Paranj, and M.Q. Zhang, *A Simple and Highly Sensitive Method for Magnetic Nanoparticle Quantitation Using ¹H-NMR Spectroscopy*. Biophysical Journal, 2009. **97**(9): p. 2640-2647.

65. Zhou, H.Y., et al., *Characterization of Organic Molecules Attached to Gold Nanoparticle Surface Using High Resolution Magic Angle Spinning H-1 NMR*. Journal of Physical Chemistry C, 2008. **112**(49): p. 19360-19366.
66. Zhang, B. and B. Yan, *Analytical strategies for characterizing the surface chemistry of nanoparticles*. Analytical and Bioanalytical Chemistry, 2010. **396**(3): p. 973-982.
67. Szakacs, Z., M. Kraszni, and B. Noszal, *Determination of microscopic acid-base parameters from NMR-pH titrations*. Analytical and Bioanalytical Chemistry, 2004. **378**(6): p. 1428-1448.
68. King, E., *Acid-Base Equilibria*. 1965, Oxford: Pergamon.
69. André, I., S. Linse, and F.A.A. Mulder, *Residue-Specific pKa Determination of Lysine and Arginine Side Chains by Indirect 15N and 13C NMR Spectroscopy: Application to apo Calmodulin*. Journal of the American Chemical Society, 2007. **129**(51): p. 15805-15813.
70. Kakehashi, R., et al., *Hydrogen ion titration of alkyltrimethylamine oxides by 13C and 1H NMR and conventional methods*. Journal of Colloid and Interface Science, 2005. **289**(2): p. 498-503.
71. Orfi, L., C. Larive, and S. LeVine, *Physicochemical characterization of psychosine by 1H nuclear magnetic resonance and electron microscopy*. Lipids, 1997. **32**(10): p. 1035-1040.
72. Kumar, J.K. and J.S. Oliver, *Proximity effects in monolayer films: Kinetic analysis of amide bond formation at the air-water interface using H-1 NMR spectroscopy*. Journal Of The American Chemical Society, 2002. **124**(38): p. 11307-11314.
73. Davis, M.E., *Ordered porous materials for emerging applications*. Nature, 2002. **417**(6891): p. 813-821.
74. Hoffmann, F., et al., *Silica-based mesoporous organic-inorganic hybrid materials*. Angew. Chem. Int. Ed. Engl., 2006. **45**(20): p. 3216-3251.
75. Raman, N.K., M.T. Anderson, and C.J. Brinker, *Template-based approaches to the preparation of amorphous, nanoporous silicas*. Chem. Mat., 1996. **8**(8): p. 1682-1701.
76. Hens, Z. and J.C. Martins, *A Solution NMR Toolbox for Characterizing the Surface Chemistry of Colloidal Nanocrystals*. Chemistry of Materials, 2013. **25**(8): p. 1211-1221.

77. Gomes, R., et al., *Binding of Phosphonic Acids to CdSe Quantum Dots: A Solution NMR Study*. The Journal of Physical Chemistry Letters, 2011. **2**(3): p. 145-152.
78. Bonenfant, D., et al., *Advances in principal factors influencing carbon dioxide adsorption on zeolites*. Science and Technology of Advanced Materials, 2008. **9**(1).
79. Balkus, K.J. and I. Bresinska, *Molecular-Sieve Based Mri Contrast Agents*. Journal of Alloys and Compounds, 1994. **207**: p. 25-28.
80. Bhering, D.L., A. Ramirez-Solis, and C.J.A. Mota, *A density functional theory based approach to extraframework aluminum species in zeolites*. Journal of Physical Chemistry B, 2003. **107**(18): p. 4342-4347.
81. Huh, S., et al., *Tuning of particle morphology and pore properties in mesoporous silicas with multiple organic functional groups*. Chem. Commun., 2003(18): p. 2364-2365.
82. Trebosc, J., et al., *Studies of organically functionalized mesoporous silicas using heteronuclear solid-state correlation NMR spectroscopy under fast magic angle spinning*. Journal of the American Chemical Society, 2005. **127**(20): p. 7587-7593.
83. Trebosc, J., et al., *Solid-state NMR study of MCM-41-type mesoporous silica nanoparticles*. Journal of the American Chemical Society, 2005. **127**(9): p. 3057-3068.
84. Kumar, R., et al., *Template removal and thermal stability of organically functionalized mesoporous silica nanoparticles*. Chemistry of Materials, 2006. **18**(18): p. 4319-4327.
85. Wiench, J.W., et al., *Characterization of covalent linkages in organically functionalized MCM-41 mesoporous materials by solid-state NMR and theoretical calculations*. Journal of Physical Chemistry B, 2007. **111**(15): p. 3877-3885.
86. Rapp, J.L., et al., *A solid-state NMR investigation of the structure of mesoporous silica nanoparticle supported rhodium catalysts*. Solid State Nuclear Magnetic Resonance, 2009. **35**(2): p. 82-86.
87. Mao, K., et al., *Conformations of Silica-Bound (Pentafluorophenyl)propyl Groups Determined by Solid-State NMR Spectroscopy and Theoretical Calculations*. Journal of the American Chemical Society, 2010. **132**(35): p. 12452-12457.
88. Ghindes-Azaria, L., et al., *Conformation and Dynamics of Organic Tethers Bound to MCM41-Type Surfaces from Solid State NMR Measurements*. The Journal of Physical Chemistry C, 2012. **116**(13): p. 7442-7449.

89. Hara, K., et al., *Selective and Efficient Silylation of Mesoporous Silica: A Quantitative Assessment of Synthetic Strategies by Solid-State NMR*. The Journal of Physical Chemistry C, 2012. **116**(12): p. 7083-7090.
90. Babonneau, F., et al., *Solid state NMR characterisation of encapsulated molecules in mesoporous silica*. Journal of Sol-Gel Science and Technology, 2004. **31**(1-3): p. 219-223.
91. Bonhomme, C., et al., *Advanced Solid State NMR Techniques for the Characterization of Sol-Gel-Derived Materials*. Accounts of Chemical Research, 2007. **40**(9): p. 738-746.
92. Azais, T., et al., *Solid-state NMR characterization of drug-model molecules encapsulated in MCM-41 silica*. Pure and Applied Chemistry, 2009. **81**(8): p. 1345-1355.
93. Sharma, R., et al., *NMR Characterization of Ligand Binding and Exchange Dynamics in Triphenylphosphine-Capped Gold Nanoparticles*. Journal of Physical Chemistry C, 2009. **113**(37): p. 16387-16393.
94. Sinnaeve, D., *The Stejskal-Tanner equation generalized for any gradient shape—an overview of most pulse sequences measuring free diffusion*. Concepts in Magnetic Resonance Part A, 2012. **40A**(2): p. 39-65.
95. Li, X.A. and D.F. Shantz, *PFG NMR Investigations of Heated Tetrapropylammonium-Silica Mixtures*. Journal of Physical Chemistry C, 2010. **114**(34): p. 14561-14570.
96. Li, X. and D.F. Shantz, *PFG NMR Investigations of Tetraalkylammonium-Silica Mixtures*. Journal of Physical Chemistry C, 2010. **114**(18): p. 8449-8458.
97. Rivas-Cardona, A. and D.F. Shantz, *Pulsed Field Gradient NMR Investigations of Alkyltripropylammonium-Silica Mixtures*. J. Phys. Chem. C, 2010. **114**(47): p. 20178-20188.
98. Li, X.A. and D.F. Shantz, *PFG NMR Investigations of TPA-TMA-Silica Mixtures*. Langmuir, 2011. **27**(7): p. 3849-3858.
99. Rivas-Cardona, A. and D.F. Shantz, *In Situ PFG NMR of Silicalite-1 Synthesis Mixtures*. J. Phys. Chem. C, 2011. **115**(26): p. 13016-13026.
100. Rao, Y., et al., *Organic Solvent-Dispersed TiO₂ Nanoparticle Characterization*. Langmuir, 2009. **25**(21): p. 12713-12720.
101. Major, R.H., Johns Hopkins Hosp Bull, 1922. **33**: p. 56-61.
102. Terrill, P.J. and J.P. Gowar, *Chromic acid burns; beware, be aggressive, be watchful*. Br J Plast Surg, 1990. **43**(6): p. 699-701.

103. Matey, P., et al., *Chromic acid burns: early aggressive excision is the best method to prevent systemic toxicity*. J Burn Care Rehabil, 2000. **21**(3): p. 241-5.
104. Wang, X.W., et al., *Chromic acid burns and acute chromium poisoning*. Burns Incl Therm Inj, 1985. **11**(3): p. 181-4.
105. ATSDR. *Toxicological profile for cadmium; Department of Health and Human Services: Washington, DC. 1999.*
106. UNEP DTIE Chemicals Branch and WHO Department of Food Safety, Z., and Foodborne Disease. *Guidance for identifying populations at risk for mercury exposures*, Geneva, Switzerland. 2008.
107. Satarug, S., et al., *Cadmium, environmental exposure, and health outcomes*. Environ Health Perspect, 2010. **118**(2): p. 182-90.
108. Wiggers, G.A., et al., *Low mercury concentrations cause oxidative stress and endothelial dysfunction in conductance and resistance arteries*. Am J Physiol Heart Circ Physiol, 2008. **295**(3): p. H1033-H1043.
109. Toscano, C.D. and T.R. Guilarte, *Lead neurotoxicity: from exposure to molecular effects*. Brain Res Brain Res Rev, 2005. **49**(3): p. 529-54.
110. Kilivelu, G. and A. Yatimah, *Synthesis and Characterization of Novel Dimeric Ionic Liquids by Conventional Approaches*. International Journal of Molecular Sciences, 2008. **9**(7): p. 1207-1213.
111. Lin, C.C., et al., *Acute Severe Chromium Poisoning After Dermal Exposure to Hexavalent Chromium* J Chin Med Assoc, 2009. **72**: p. 219-221.
112. Waters, R., et al., *EDTA chelation-cadmium, calcium, chromium, cobalt, copper, lead, magnesium and zinc*. Biol Trace Element Res, 2001. **83**: p. 207-221.
113. Feng, X., et al., *Functionalized Monolayers on Ordered Mesoporous Supports*. Science, 1997. **276**(5314): p. 923-926.
114. Mercier, L. and T.J. Pinnavaia, *Heavy Metal Ion Adsorbents Formed by the Grafting of a Thiol Functionality to Mesoporous Silica Molecular Sieves: Factors Affecting Hg(II) Uptake*. Environmental Science & Technology, 1998. **32**(18): p. 2749-2754.
115. Antochshuk, V. and M. Jaroniec, *1-Allyl-3-propylthiourea modified mesoporous silica for mercury removal*. Chemical Communications, 2002(3): p. 258-259.
116. Meeks, N.D., S. Rankin, and D. Bhattacharyya, *Sulfur-Functionalization of Porous Silica Particles and Application to Mercury Vapor Sorption*. Industrial & Engineering Chemistry Research, 2010. **49**(10): p. 4687-4693.